12-2003

Theoretical and Experimental Study of Degradation Monitoring of Steam Generators and Heat Exchangers

Xuedong Huang
University of Tennessee - Knoxville

To the Graduate Council:

I am submitting herewith a thesis written by Xuedong Huang entitled "Theoretical and Experimental Study of Degradation Monitoring of Steam Generators and Heat Exchangers." I have examined the final electronic copy of this thesis for form and content and recommend that it be accepted in partial fulfillment of the requirements for the degree of Master of Science, with a major in Nuclear Engineering.

Belle R. Upadhyaya, Major Professor

We have read this thesis and recommend its acceptance:

J. Wesley Hines, Laurence F. Miller

Accepted for the Council:
Carolyn R. Hodges

Vice Provost and Dean of the Graduate School

(Original signatures are on file with official student records.)

To the Graduate Council:

I am submitting herewith a thesis written by Xuedong Huang entitled "Theoretical and Experimental Study of Degradation Monitoring of Steam Generators and Heat Exchangers." I have examined the final electronic copy of this thesis for form and content and recommend that it be accepted in partial fulfillment of the requirements for the degree of Master of Science, with a major in Nuclear Engineering.

Belle R. Upadhyaya
Major Professor

We have read this thesis
and recommend its acceptance:

J. Wesley Hines

_____

Laurence F. Miller

_____

Acceptance for the Council:

Anne Mayhew

_____

Vice Provost and Dean of Graduate Studies

(Original signatures are on file with official student records.)

Theoretical and Experimental Study of Degradation Monitoring of Steam Generators and Heat Exchangers

A Thesis

Presented for the

Master of Science Degree

The University of Tennessee, Knoxville

Xuedong Huang

December 2003

Dedication

This thesis is dedicated to my beloved wife, son and parents

for their love, patience, understanding and encouragement.

Acknowledgments

I wish to thank all those who helped me in completing my Master of Science degree in Nuclear Engineering. First I would like to thank my major professor, Dr. Belle R. Upadhyaya, for his invaluable guidance, suggestions, encouragement, and financial support. Without these, I would not be able to finish my thesis.

I owe special thanks to Dr. J. W. Hines for his valuable suggestions during the research.

I want to extend my thanks to the Head of the Nuclear Engineering Department, Dr. H. L. Dodds, who gave me much needed help and support.

Sincere thanks also go to my committee members, Dr. J. W. Hines and Dr. L. F. Miller, for their comments on my research and thesis.

I want to thank Mr. Gary Graves and Mr. Richard Bailey for their help during the laboratory experiments.

I am grateful for DOE-NEER project support during my thesis research.

Finally, I want to thank my family and friends for their understanding, encouragement, and help.

Abstract

The objective of this research is focused on the modeling, analysis, and experimental study of steam generator and heat exchanger degradation monitoring and fault diagnosis. Experimental and analytical studies of tube fouling are performed and the system-level degradations are monitored using data-driven modeling of heat exchanger measurements. Initially, a comprehensive literature study was made on the steam generator and heat exchanger degradation types and mechanisms, including fouling and corrosion.

Based on the mass balance, energy balance, and momentum balance and the moving-boundary method, a multi-node SIMULINK model of a U-tube steam generator (UTSG) has been developed so as to simulate the UTSG dynamics or responses to various defects, including fouling. UTSG responses to different events, such as reduced heat transfer area, change in heat transfer coefficient at different axial nodes, change in tube material conductivity, and the change of steam valve coefficients have been simulated and studied using the SIMULINK model. A mathematical model is established and implemented in MATLAB based on a systematic literature review of steam generator and heat exchanger fouling.

The fouling model and the UTSG SIMULINK model are both used to study the progression of tube fouling and the effects on UTSG thermal performance. The simulation results show the fidelity and validity of the developed models. The

developed models can be used to predict the time behavior of UTSG thermal performance. This could provide guidance for plant maintenance planning. The simulation results of fouling and its effect on UTSG thermal performance are presented.

Based on an existing heat exchanger laboratory system, an experimental study of the particulate fouling progression in a heat exchanger has been performed. The results show the particulate fouling in heat exchangers also exhibits an asymptotic behavior, and the model-based method for fouling monitoring and diagnosis is successful and efficient.

Finally a theoretical heat exchanger model is developed and coded using MATLAB. This model is then used to generate data representative of normal conditions. With these normal data and the fouling data collected from the experimental loop, the Group Method of Data Handling (GMDH) method is then used to monitor and diagnose the fouling problem in the heat exchanger. The GMDH results show that the residuals of both hot-side and cold-side outlet temperatures follow the same pattern as the overall thermal resistance obtained from the experiment. Also, the UTSG SIMULINK model is used to generate data and the GMDH method is used to establish a data-driven model. The results again show that the GMDH approach can appropriately model the UTSG system behavior and can be used for fouling monitoring and diagnosis and also model the effect of tube plugging on UTSG steam pressure.

These results demonstrate that an appropriately developed GMDH model can be used to monitor and diagnose the fouling, and possibly other degradation problems in both the heat exchanger and steam generator systems.

Table of Contents

Chapter 1 ---------- 1
Introduction ---------- 1
1.1 Background and Motivation 1
1.2 Problem Statement 2
1.3 Contributions of the Research 4
1.4 Organization of the Thesis 5

Chapter 2 ---------- 6
Literature Review ---------- 6
2.1 Introduction 6
2.2 Review of Steam Generator Modeling 8
2.3 Review of SG Degradation Mechanisms 9
2.4 Review of Fouling in Heat Exchangers and Steam Generators 20
2.5 Review of SG and Heat Exchanger Tube Corrosion and Water Chemistry 33
2.6 Remarks 48

Chapter 3 ---------- 50
Multi-node Modeling and Simulation of a UTSG and Its Responses to Various System-Level Degradations ---------- 50
3.1 Introduction 50
3.2 Methodology 52
3.3 Assumptions 55
3.4 Mathematic Equations for UTSG Multi-node Simulation Model 56
3.5 UTSG Three-Element Controller Model 65
3.6 UTSG SIMULINK Model 67
3.7 Simulation of UTSG Responses to Various System-Level Degradations 68
3.8 Remarks 76

Chapter 4 ---------- 79
Particulate Fouling Model of a UTSG and Simulation of the Effects of Fouling on Thermal Performance ---------- 79
4.1 UTSG Particulate Fouling Model 79
4.2. Effects of UTSG Fouling on Thermal Performance 84
4.3 Remarks 88

Chapter 5 ---------- 90
Experimental Study of Particulate Fouling in a Heat Exchanger ---------- 90
5.1 Introduction 90
5.2 Review of Experimental Study of Particulate Fouling in Heat Exchangers 90
5.3 Current Experimental Setup for Particulate Fouling Tests 94
5.4 Calculation of Overall Thermal Resistance and Experimental Results 97
5.5 Overall Thermal Resistance after Removal of the Fouling Deposition Layer 101
5.6 Remarks 101

Chapter 6 ---------- 105
Monitoring and Diagnosis of Fouling Using the GMDH Method ---------- 105
6.1 Introduction 105
6.2 GMDH Methodology 106
6.3 Data Generation 110
6.4 Monitoring and Diagnosis of Fouling in the Heat Exchanger 111
6.5 Monitoring and Diagnosis of Fouling in the Steam Generator 118
6.6 Remarks 123

Chapter 7 ---------- 125
Summary, Conclusions, and Recommendations for Future Research ---------- 125
7.1 Summary 125
7.2 Conclusions 126
7.3 Recommendations for Future Research 128

References ---------- 130

Appendices ---------- 137

Appendix A ---------- 138
Derivation of the Equations for UTSG Lumped Primary Coolant Nodes ---------- 138

Appendix B ---------- 145
Derivation of the Equations for UTSG Tube Wall Lumped Metal Nodes ---------- 145

Appendix C ---------- 149
The MATLAB Code for UTSG Particulate Fouling Model ---------- 149

Appendix D ---------- 151
The MATLAB Code Used to Process the Fouling Experimental Data and Calculate the Overall Thermal Resistance ---------- 151

Appendix E ---------- 153
The MATLAB Code Used to Generate Normal Data for Heat Exchanger ---------- 153

Appendix F ---------- 156
The MATLAB Code for Monitoring and Diagnosis of Fouling in the Heat Exchanger Using GMDH Method ---------- 156

Appendix G ---------- 162
The MATLAB Code for Monitoring and Diagnosis of Fouling in the Steam Generator Using GMDH Method ---------- 162

Vita ---------- 169

List of Figures

Figure 2.1. Simplified Schematic of a Recirculating Type Nuclear Steam Generator ----- 7
Figure 2.2. Illustration Showing the Typical Locations for SCC Occurring at Dents -----12
Figure 2.3. Illustration Showing the Typical Locations for SCC Occurring in the Roll Expansion Regions at the Tube Sheet ----------13
Figure 2.4. Illustration Showing the Intergranular Attack of SG Tubes Starting at the Surface on the Secondary Side ----------15
Figure 2.5. Illustration Showing Pitting Degradation ----------16
Figure 2.6. Different Cases of Fouling Rate----------25
Figure 2.7. A Basic Corroding System ----------35
Figure 2.8. Relative Corrosion Rate versus pH ----------38
Figure 3.1. A Schematic Illustrating Mass Balance in a Node ----------53
Figure 3.2. The Schematic of the UTSG Model with Four Axial Tube Nodes----------57
Figure 3.3. The Block Diagram of the Three-element UTSG Controller----------66
Figure 3.4. An Overview of the Top-level Layout of UTSG SIMULINK Model ---------67
Figure 3.5. Steam Pressure Change for the Case of 5% Decrease in the Number of Tubes ----------69
Figure 3.6. Steam Pressure Change for the Case of 10% Decrease in the Tube Metal Conductivity ----------69
Figure 3.7. Steam Pressure Change When Decreasing the Overall Heat Transfer Coefficient by 50% in the Metal-to-Secondary Side Sub-cooled Heat Transfer Nodes (MTL1 and MTL8) ----------70
Figure 3.8. Steam Pressure Change When Decreasing the Overall Heat Transfer Coefficient by 50% in the Primary-to-Metal Side Sub-cooled Heat Transfer Nodes (PRL1 and PRL8)----------70
Figure 3.9. Steam Pressure Change When Decreasing the Overall Heat Transfer Coefficient by 50% in the Metal-to-Secondary Side Boiling Heat Transfer Nodes (MTL2 and MTL7)----------71
Figure 3.10. Steam Pressure Change When Decreasing the Overall Heat Transfer Coefficient by 50% in the Primary-to-Metal Side Boiling Heat Transfer Nodes (PRL2 and PRL7)----------71
Figure 3.11. Steam Pressure Change When Decreasing the Overall Heat Transfer Coefficient by 50% in the Metal-to-Secondary Side Boiling Heat Transfer Nodes (MTL3 and MTL6)----------72
Figure 3.12. Steam Pressure Change When Decreasing the Overall Heat Transfer Coefficient by 50% in the Primary-to-Metal Side Boiling Heat Transfer Nodes (PRL3 and PRL6)----------72
Figure 3.13. Steam Pressure Change When Decreasing the Overall Heat Transfer Coefficient by 50% in the Metal-to-Secondary Side Boiling Heat Transfer Nodes (MTL4 and MTL5)----------73

Figure 3.14. Steam Pressure Change When Decreasing the Overall Heat Transfer Coefficient by 50% in the Primary-to-Metal Side Boiling Heat Transfer Nodes (PRL4 and PRL5)---73
Figure 3.15. Steam Pressure Variation for a 10% Decrease in the Steam Valve Coefficient (Decreased Steam Flowrate)---74
Figure 3.16. SG Water Level Variation for a 10% Decrease in the Steam Valve Coefficient ---74
Figure 3.17. Steam Pressure Variation for a 10% Increase in the Steam Valve Coefficient (Increased Steam Flowrate)---75
Figure 3.18. SG Water Level Variation for a 10% Increase in the Steam Valve Coefficient ---75
Figure 4.1. Fouling Deposit Mass Variation versus Time---85
Figure 4.2. Fouling Thermal Resistance Variation versus Time ---85
Figure 4.3. Steam Pressure Variation versus Time---87
Figure 4.4. Average Heat Flux (on Outer SG Tube Surface) Variation versus Time ---87
Figure 5.1. Configuration of the Heat Exchanger Experimental Set-up for Particulate Fouling Tests---95
Figure 5.2. An Overview of the Experimental Setup---96
Figure 5.3. Experimental Results—The Measured Raw Signals From the Experiment 100
Figure 5.4. Experimental Results—The Overall Thermal Resistance Variation vs. Experimental Running Time--- 100
Figure 5.5. Change in Overall Thermal Resistance of the Heat Exchanger before and after Removal of the Fouling Deposition Layers --- 102
Figure 5.6. Change in Overall Thermal Resistance of the Heat Exchanger before and after Removal of the Fouling Deposition Layers --- 103
Figure 6.1. The GMDH Network Structure--- 107
Figure 6.2. The Training Output and the GMDH Predicted Values of the Tube-side/Hot-side Outlet Temperature--- 113
Figure 6.3. The Testing Output and the GMDH Predicted Values of the Tube-side/Hot-side Outlet Temperature--- 113
Figure 6.4. The GMDH Predictions of the Hot-side Outlet Temperatures of the Heat Exchanger versus the Real Experimental Data--- 114
Figure 6.5. The Residual between the GMDH Predictions of the Hot-side Outlet Temperatures of the Heat Exchanger and the Real Experimental Data --- 114
Figure 6.6. The Training Output and the GMDH Predicted Values of the Shell-side/Cold-side Outlet Temperature --- 116
Figure 6.7. The Testing Output and the GMDH Predicted Values of the Shell-side/Cold-side Outlet Temperature --- 116
Figure 6.8. The GMDH Predictions of the Cold-side Outlet Temperatures of the Heat Exchanger versus the Real Experimental Data--- 117
Figure 6.9. The Residual between the GMDH Predictions of the Cold-side Outlet Temperatures of the Heat Exchanger and the Real Experimental Data --- 117
Figure 6.10. The Training Steam Pressure and the GMDH Predicted Values --- 119
Figure 6.11. The Testing Steam Pressure and the GMDH Predicted Values --- 119

Figure 6.12. The GMDH Predictions of the UTSG Steam Pressure versus the Simulations of the UTSG SIMULINK Model (with Different Hot-side Inlet Temperature)---------- 121
Figure 6.13. The Residual Between the GMDH Predictions of the UTSG Steam Pressure and the Simulations of the UTSG SIMULINK Model (with Different Hot-side Inlet Temperature)---------- 121
Figure 6.14. The GMDH Predictions of the UTSG Steam Pressure versus the Simulations of the UTSG SIMULINK Model (with a Single Hot-side Inlet Temperature)---------- 122
Figure 6.15. The Residual Between the GMDH Predictions of the UTSG Steam Pressure and the Simulations of the UTSG SIMULINK Model (with a Single Hot-side Inlet Temperature)---------- 122
Figure 6.16. The GMDH Predictions of the UTSG Steam Pressure versus the Simulations of the UTSG SIMULINK Model (with Decreasing Number of Heat Transfer Tubes) - 124
Figure 6.17. The Residual Between the GMDH Predictions of the UTSG Steam Pressure and the Simulations of the UTSG SIMULINK Model (with Decreasing Number of Heat Transfer Tubes)---------- 124

List of Acronyms

AVB: Anti-Vibration Bar

BWR: Boiling Water Reactor

DOE: Department of Energy

FDI: Fault Detection and Isolation

GMDH: Group Method of Data Handling

HX: Heat Exchanger

IGA: Intergranular Attack

IGSCC: Intergranular Stress Corrosion Cracking

NEER: Nuclear Engineering Education and Research

ODE: Ordinary Differential Equation

ODSCC: Outer Diameter Stress Corrosion Cracking

OTSG: Once-Through Steam Generator

PWR: Pressurized Water Reactor

PWSCC: Primary Water Stress Corrosion Cracking

SCC: Stress Corrosion Cracking

SG: Steam Generator

SGTR: Steam Generator Tube Rupture

UTK-NE: University of Tennessee at Knoxville, Nuclear Engineering

UTSG: U-Tube Steam Generator

Chapter 1

Introduction

1.1 Background and Motivation

It is well known that steam generators and heat exchangers are among the most important components in pressurized water reactor (PWR) nuclear power plants. The integrity of steam generators and heat exchangers is directly associated with the plant economy, safety, reliability, and availability. In a typical steam generator, there are generally thousands of heat transfer tubes. For example, the U-tube steam generator (UTSG) in a typical four-loop, 1,300 MWe PWR, consists of about 3600 tubes. Hence a steam generator or a heat exchanger in a nuclear power plant is a complex system and its performance is influenced by many factors.

For instance, in a steam generator or a heat exchanger, tube degradation can occur due to thermal and mechanical stresses, fouling and deposits, fatigue and creep, wear and fretting, stress corrosion cracking and intergranular attack, etc. [11]-[14]. Depending on the plant operating conditions, one or more of the above factors may cause tube damage. The degradation of tubes in a steam generator or heat exchanger is the primary cause that results in structural deterioration and degraded performance. The remedial measure generally taken by the industry is to plug the damaged and leaking tubes. This will certainly results in decreased operational efficiency with time. The cost of replacement

of a large UTSG in a 1,300 MWe four-loop PWR is about $150 million. In U.S. utilities, some PWR units have either replaced steam generators or are seriously considering some measures. Therefore we can clearly see that it is of great significance to develop a system for continuous on-line monitoring of the structural integrity and incipient fault detection and isolation.

A research project, *On-line Monitoring and Diagnostics of Integrity of Nuclear Plant Steam Generators and Heat Exchangers*, funded by the DOE-NEER program, is being carried out in the Nuclear Engineering Department of The University of Tennessee. For details, refer to Upadhyaya et al (2001, 2002, 2003) [1,2,3,4,5]. The goal of this project is to integrate the new, innovative, and existing technologies to develop an automated structural fault diagnostics and characterization system for nuclear plant heat exchangers and steam generators. As part of the essential tasks included in the above project, this thesis work aims to review the degradation mechanisms, develop a good first-principle model for a UTSG, study the mechanisms, model the behavior of fouling, and finally use the GMDH method to monitor and diagnose the fouling in both heat exchanger and steam generator systems.

1.2 Problem Statement

In general, a steam generator or heat exchanger can malfunction due to various system-level degradations such as corrosion, fouling, or material degradation. In order to monitor and diagnose the defects or degradations that may occur in a UTSG or in a heat exchanger, one of the main tasks included in this project is to develop a high-fidelity

process model to simulate the dynamic performance and the response of a UTSG to various defects, and to study particulate fouling behavior in a heat exchanger by laboratory experiment, so as to provide a reliable first-principle model for monitoring and diagnostics of integrity of steam generators and heat exchangers. The following main tasks are developed in order to accomplish the objectives of this research.

- A comprehensive literature study. The goal is to achieve a good understanding of the types of degradation and their mechanisms in a steam generator or a heat exchanger.

- Development of a multi-nodal MATLAB SIMULINK model for UTSG and simulation of UTSG behavior using the developed model. This model should be able to reliably simulate the dynamics or responses of UTSG to various defects, including fouling.

- Investigation of the fouling mechanism and development of a mathematical model for simulation of the time-progress of fouling in a SG or a heat exchanger. This model should reflect the fouling mechanism and its characteristics as a function of time.

- Verification of the theoretical model of fouling progress and collection of experimental data. A laboratory experimental setup is used to accomplish this. This experimental setup can also be used to study the effects of various factors, such as flow velocity, temperature, particle concentration, etc, on particulate

fouling. In addition, experimental data can be collected for normal operation and operation with a fouling problem in a heat exchanger. These data, and the data that are generated from the UTSG model can be used for monitoring and fault diagnosis of a steam generator or a heat exchanger.

- Using the GMDH (Group Method of Data Handling) method to monitor and diagnose the fouling problem in both a heat exchanger and a steam generator.

1.3 Contributions of the Research

The main accomplishments of this research include the successful development of a multi-node UTSG SIMULINK model, experimental simulation of the fouling progress in a heat exchanger, and monitoring and diagnosing the fouling using the GMDH method. The following are the contributions of this thesis research.

- A comprehensive literature review of steam generator/heat exchanger degradation mechanisms, fouling, corrosion, and experimental study and theoretical modeling of fouling.

- Development of a multi-nodal UTSG SIMULINK model and simulation of the UTSG responses to various defects.

- Experimental study of fouling in a heat exchanger so as to verify the fouling model and diagnose the fouling deposition behavior using the related measurements and the first-principle model.

- Use of the GMDH method and the theoretical and experimental data to monitor and diagnose the fouling problem in both heat exchangers and the steam generators.

1.4 Organization of the Thesis

A comprehensive literature review of steam generator/heat exchanger degradation mechanisms, fouling, corrosion and water chemistry is given in Chapter 2.

In Chapter 3, detailed description and derivation of the UTSG mathematical model equations and the SIMULINK model are given, and the results of simulation of UTSG dynamics and responses to various defects are presented.

Chapter 4 is focused on UTSG particulate fouling model and simulation of the effects of fouling on thermal performance.

Chapter 5 details the experimental study of particulate fouling of heat exchanger tubing, including a review on experimental study of fouling, a description of current experimental setup and the experimental results.

Chapter 6 briefly describes the GMDH method and the use of the physics model to generate data, and presents the results of monitoring and diagnosis of fouling in both the heat exchanger and the steam generator using the GMDH method.

Summary, conclusions and recommendations for future research are presented in Chapter 7.

Chapter 2

Literature Review

2.1 Introduction

Steam generators (SGs) are used in pressurized water reactors (PWRs) to convert water in the secondary side into steam and thus safely remove the heat produced in the reactor core (primary side). Figure 2.1 shows a simplified schematic of a recirculating-type nuclear steam generator [6]. The steam generators are large components, which measure up to 70 feet in height and weigh as much as 800 tons. Hot primary water circulates through thousands of feet of tubing in the steam generator -- each steam generator can contain anywhere from 3,000 to 10,000 tubes, each about three-quarters of an inch in diameter (the number of tubes depends on the type of SG, U-tube or once-through) -- under high pressure. The water flowing within the tubes heats non-radioactive water on the outside of the tubes and converts the secondary water into steam. The steam (saturated or superheated) flows into several stages of a turbine that is coupled to electrical generators. The steam from the last stage of the turbine is subsequently condensed into water and is pumped back to the steam generator.

These SG tubes have an important safety role because they constitute one of the primary barriers between the radioactive and non-radioactive sides of the plant. For this reason, the integrity of the tubing is essential in minimizing the leakage of water between the two sides of the plant. If a tube rupture occurs while a plant is operating, it is highly probable that the radioactivity from the primary loop could escape directly into the

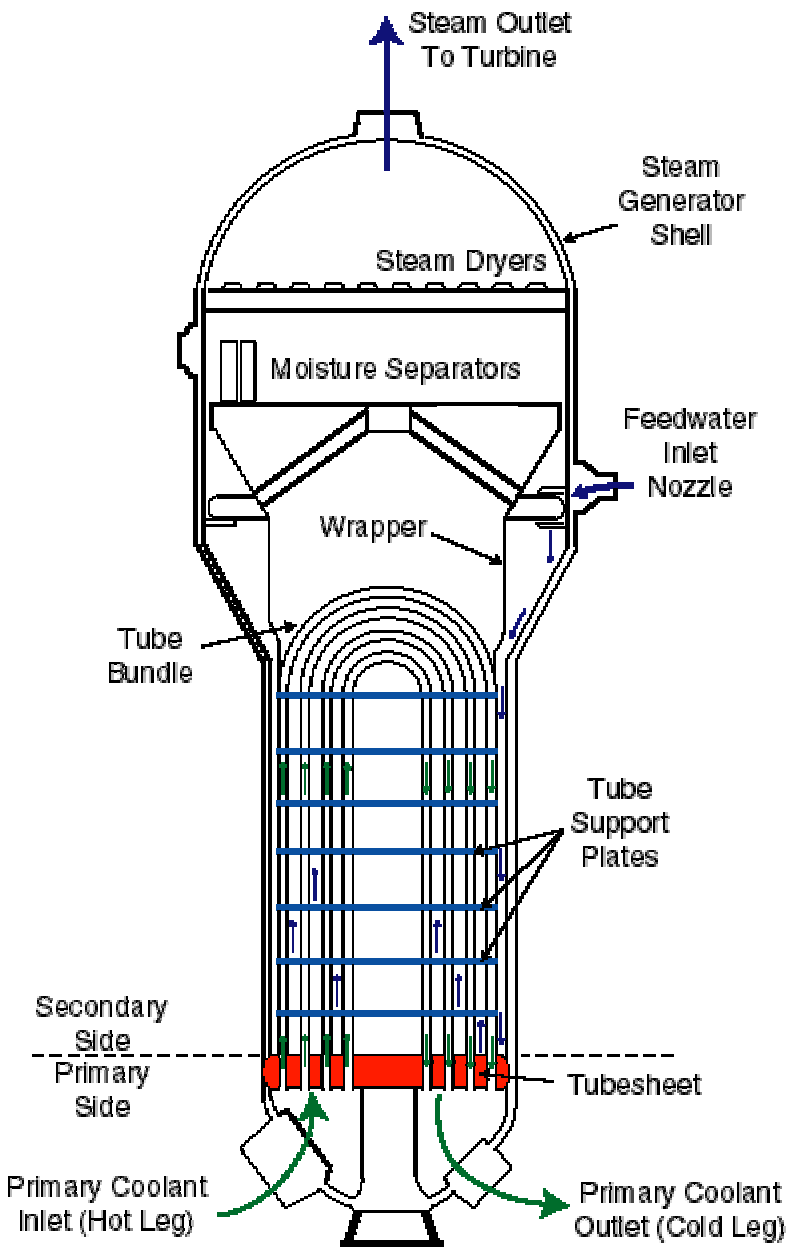

Figure 2.1. Simplified Schematic of a Recirculating Type Nuclear Steam Generator

[From Ref. 6]

atmosphere along with the steam.

Operating results show that about one-half of the PWR nuclear power plants in the world have plugged or sleeved steam generator tubes in any given year during the first half of 1990s. The total number of steam generator tubes plugged per year has ranged from about 10,000 to 12,000 tubes. Moreover, more than 48,000 steam generator tubes were sleeved as of December 1994. This indicates that it is of great significance to maintain the structural integrity of SG for efficient power generation and for the safe operation of nuclear power stations. To achieve this goal, it is necessary to get a good understanding of steam generator flaws and degradation mechanisms.

In this chapter, we present a detailed review of literature on steam generator modeling, steam generator/ heat exchanger defect or degradation mechanisms, fouling in heat exchangers and steam generators, and steam generator and heat exchanger tube corrosion and water chemistry.

2.2 Review of Steam Generator Modeling

Extensive research has been conducted in steam generator modeling. Some of the steam generator simulation models, such as those incorporated in the well-known software RELAP (see Allison et al (1989) [7], Putney et al (1993) [8] and SCDAP/RELAP5 Development Team (1998) [9]), are quite detailed. These are commercial software systems, and thus are not readily available. At UTK-NE, Naghedolfeizi and Upadhyaya (1991) [10] developed a dynamic model for a PWR for diagnostics and control. The model is established based on the mass balance, energy

balance, and momentum balance. The UTSG heat transfer tubes are axially divided into two sections, namely the sub-cooled boiling region and the saturated boiling region. Thus using this model, we cannot study in detail the effect of fouling at different axial locations along the tubes. Therefore, it is necessary to further develop and improve this model.

The new model may not be necessarily very complex, but it must be precise enough to provide us a fairly "good" tool and can be used to simulate various processes that may occur in a steam generator. Especially this model should enable us to selectively change the various heat transfer coefficients or add an additional thermal resistance and change the heat transfer area so as to simulate degradations such as tube fouling, plugging, and tube property changes.

2.3 Review of SG Degradation Mechanisms [6] [11] [12]

An extensive literature review on SG defects and degradation mechanisms has been made. The discussion in this section is mainly adapted and taken from Ref. [6] [11] [12].

Generally, there are several degradation modes associated with steam generators (mainly for the tubing). The degradation modes are somewhat different for UTSG and OTSG systems. According to studies by MacDonald et al (1996) [11] and Wade (1995) [12], the following modes are among the most common: (a) Stress Corrosion Cracking (SCC), (b) Intergranular attack (IGA), (c) Denting, (d) Pitting, (e) Fretting, Wear, and Thinning, (f) High-cycle Fatigue and Wastage. Fouling is often not regarded as a

degradation mode of tubing. It may be regarded as a degradation cause, which is influenced by other sources (water chemistry, impurities, etc). Fouling will be further discussed in the following section. From the point of view of SG integrity and heat transfer, fouling mainly results in SG performance degradation by changing the heat transfer. Almost all other degradation mechanisms lead to loss of structural integrity of the SG and also the degradation in the SG thermal performance. If they are severe enough they may initiate an accident, such as steam generator tube rupture (SGTR). Hence it is of great importance to monitor both the structural and process integrity of steam generators.

Steam generator (SG) defects mainly involve SG material discontinuity, or loss of SG structural integrity and capability of normal heat transfer and steam generation. Major SG degradation forms have changed with time. From the early time to mid-1970s, thinning of steam generator tube walls due to water chemistry was the dominant cause of tube degradation. Since then, all plants have changed their water chemistry control programs, hence almost completely eliminated the problem of tube thinning.

Tube denting became a primary concern later. Denting generally results from the corrosion of the carbon steel support plates and the buildup of corrosion products in the crevices between tubes and tube support plates. Measures have been taken to control denting, including changes in the chemistry of the secondary side, the non-radioactive side of the plant. But other phenomena continue to cause tube cracking.

Some of the newer steam generators are improved with features that make the tubes less susceptible to corrosion [6] [11] [12]. These include using stainless steel tube support plates to minimize the likelihood of denting; using new fabrication techniques to minimize mechanical stresses on tubes; and using more corrosion-resistant tube materials, such as thermally treated Alloy 600 and Alloy 690. Although for different types of SGs, there exist some differences and characteristics in their degradation mechanisms, the following typical categories of SG degradation mechanisms have been identified.

2.3.1. Stress Corrosion Cracking (SCC)

Stress corrosion cracking occurs under the combined action of corrosion and stress, which is either applied or residual. Depending on the metal and corrosive medium, the cracking may be either intergranular or transgranular. SCC can occur on both the primary side (tube-side) and secondary side (shell-side) of SG tubes, which are named respectively as PWSCC (Primary Water Stress Corrosion Cracking) and ODSCC (Outer Diameter Stress Corrosion Cracking). The frequency of occurrence of SCC and the speed of crack growth increase as stresses increase, as the environment becomes more severe (higher temperature, more aggressive chemical environment, etc.), and as the material susceptibility increases. Typical locations for SCC are at dents (see Figure 2.2), in the roll expansion regions at the tube sheet (see Figure 2.3), and in areas with concentrated impurities [6].

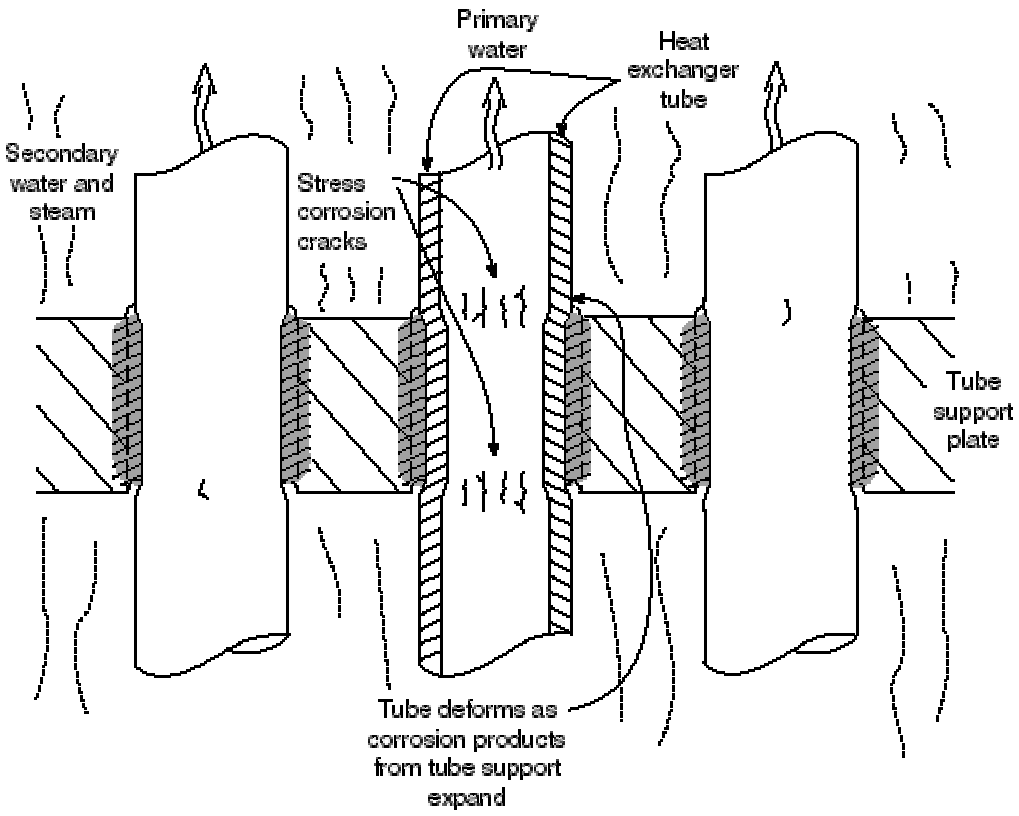

Figure 2.2. Illustration Showing the Typical Locations for SCC Occurring at Dents

[From Ref. 6]

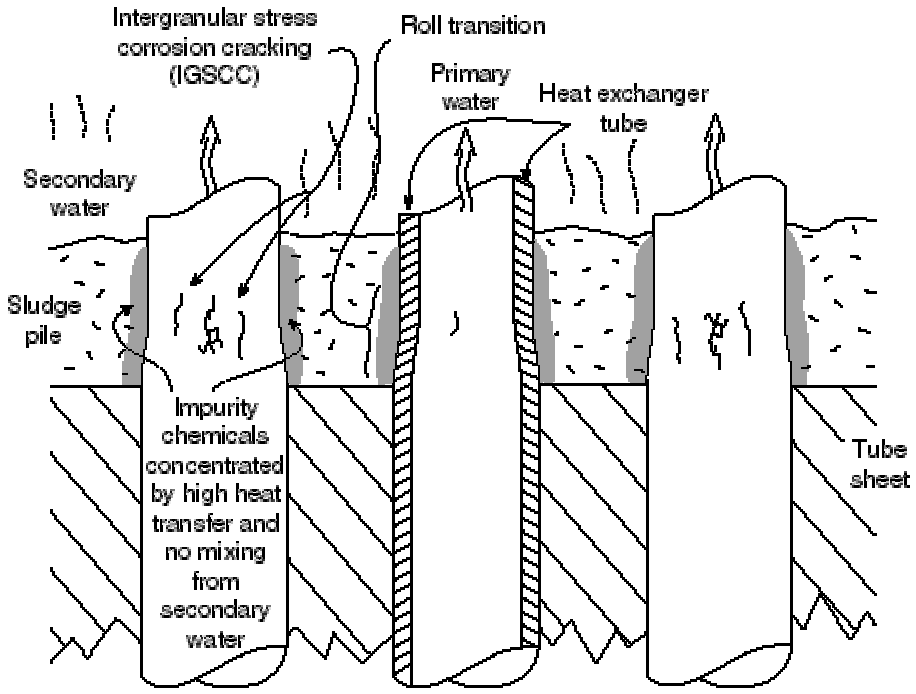

Figure 2.3. Illustration Showing the Typical Locations for SCC Occurring in the Roll Expansion Regions at the Tube Sheet
[From Ref. 6]

2.3.2. Intergranular Attack (IGA)

Intergranular attack of SG tubes proceeds along the grain boundaries of the metal, starting at the surface on the secondary side (see Figure 2.4) [6]. It also occurs to a smaller extent on the primary side. This form of corrosion proceeds in the absence of stress, but may be accelerated by stress. IGA can occur both in sludge piles (see Figure 2.3) and in tube support regions, and it may be a precursor to subsequent intergranular stress corrosion cracking (IGSCC) [6].

2.3.3. Denting

Denting is a process in which the SG tubes are squeezed inward and deformed at a carbon steel tube support plate intersection or within the tube sheet as a result of the corrosion of carbon steel supports, which produces a buildup of corrosion products between the tube support structure and the outer surface of the tube. Stresses are introduced and can lead to stress corrosion cracking and other types of tube failures (see Figure 2.2) [6].

2.3.4. Pitting

Pitting corrosion essentially acts like a chemical drill and is not focused on structural features such as grain boundaries (see Figure 2.5) [6]. This degradation has been observed on the secondary side of SG tubes in both the hot and cold legs, primarily on tube surfaces in the sludge piles in the cold leg. Pitting occurs because of the presence of oxidizing impurities (oxygen and copper) and acidic forming impurities

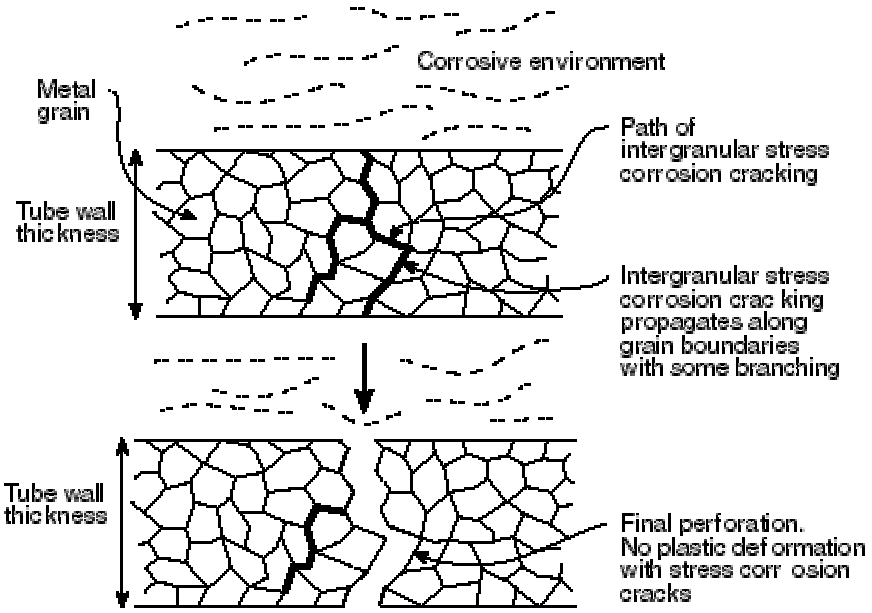

Figure 2.4. Illustration Showing the Intergranular Attack of SG Tubes Starting at the Surface on the Secondary Side

[From Ref. 6]

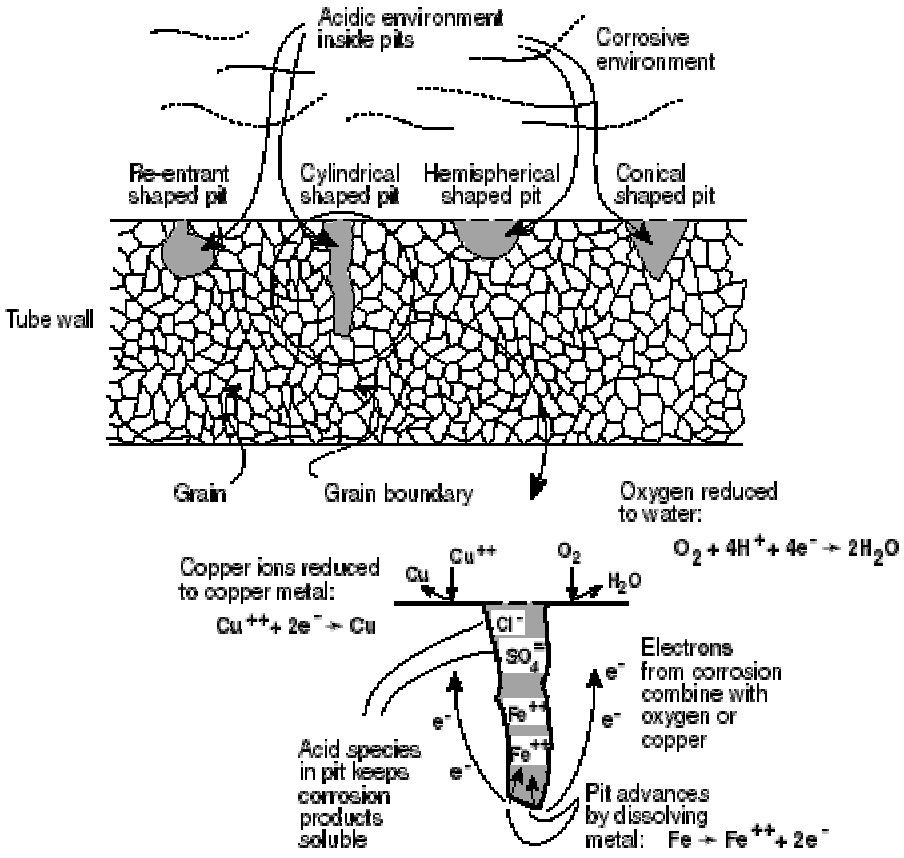

Figure 2.5. Illustration Showing Pitting Degradation

[From Ref. 6]

(chloride and sulfate). Any barriers to diffusion such as sludge accumulation on tube wall will accelerate the pitting process by enhancing the chemical concentrations [6].

2.3.5. Fretting, Wear, and Thinning

These steam generator degradation types are also broadly characterized as mechanically induced or aided degradation mechanisms. Degradation from small amplitude, oscillatory motion, between continuously rubbing surfaces, is generally termed as fretting. Tube vibration of relatively large amplitude, resulting in intermittent sliding contact between tube and support, is called sliding wear, or wear. Concurrent effects of vibration and corrosion generally cause thinning. However, thinning occurs at some locations where flow-induced vibrations are not expected, so it is not certain that tube motion is required for this mechanism; in some cases it may simply be the result of corrosion wastage.

The major stressor in fretting and wear is the flow-induced vibration. When anti-vibration bars (AVBs) are used in the U-bend regions of tube bundles of recirculating steam generators to stiffen the tubes and limit vibration amplitudes, the anti-vibration bar fretting/wear can occur [6].

2.3.6. High-cycle Fatigue

The combination of high vibration amplitude and low strength may lead to catastrophic fatigue failures. Vibration occurs in steam generators with high recirculation flow factors (causing flow-induced vibrations in the U-bend region) and improper AVB

support. A high mean stress (e.g. residual stress) or a tube defect (fretting mark or crack) significantly reduces the fatigue strength. Therefore, tubes with dents, fret marks, or cracks at the top tube support plate in U-bend region of the recirculating SGs are susceptible to high-cycle fatigue failure.

Wastage of the peripheral tubes near the lower support plates on the cold leg sides of recirculating SGs in a few plants might also have been caused by acidic sulfates. Resin leakage from the condensate polisher beds could have produced the acidic sulfate environment. The phosphate corrosion or wastage is transgranular and may lead to significant thinning and, ultimately, to local ductile rupture and leakage. Phosphate wastage was the major cause of tube failures in PWR SGs until around 1976. However, it is no longer an active degradation mechanism in most of the PWR plants since phosphate water chemistry is no longer used in most plants [6].

2.3.7. Wastage

Wastage is the relatively uniform corrosion and thinning of a SG tube on its outside surface (secondary side of the SG). This degradation tends to occur in relatively stagnant regions in recirculating SGs with secondary-side phosphate water chemistry. These regions include the tube-to-tube sheet crevices, the tube-to-tube support plate annuli, and the sludge pile on the tube sheet, or the short radius U-bends in the vicinity of AVBs.

Table 2.1 presents a summary of PWR recirculating steam generator tube degradation mechanisms [11].

Table 2.1. Summary of PWR recirculating steam generator tube degradation processes (from Ref. [11])

Rank[a]	Degradation Mechanism	Stressor	Degradation Sites	Potential Failure Mode	ISI Method
1	ODSCC	Tensile stresses, impurity concentrations, sensitive materials	• Tube-to-tubesheet crevices • Sludge Pile • Tube support plate • Free span	Axial or circumferential crack Circumferential crack Axial crack Axial crack	MRPC[b] MRPC/Cecco 5 Bobbin coil/ Cecco 5 Bobbin coil (in absolute mode)
2	PWSCC	Temperature, residual tensile stresses, sensitive materials (low mill anneal temperature)	• Inside surface of U-bend • Roll transition w/o kiss rolling • Roll transition with kiss rolling • Dented tube regions	Mixed Crack Mixed Crack Axial Crack Circumferential crack	MRPC[b] MRPC MRPC Bobbin coil or MRPC
3	Fretting, Wear	Flow induced vibration, aggressive chemicals	• Contact points between tubes and the AVBs, or tubes and the preheater baffles • Contact Between tubes and loose parts • Tube-to-tube contact	Local wear Depends on loose part geometry Axial Wear	Bobbin coil Bobbin coil Bobbin coil
4	High-cycle fatigue	High mean stress level and flow induced vibration, initiating defect (crack, dent, pit)	At the upper support plate if the tube is clamped	Transgranular circumferential cracking	Leak detection or by detection of precursor
5	Denting	Oxygen, copper oxide, chlorides, temperature, PH, crevice condition, deposits	At the tube support plates, in the sludge pile, in the tubesheet crevices	Flow blockage in tube, may lead to circumferential cracking (see PWSCC), decreases in fatigue resistance	Profilometry, Bobbin coil
6	Pitting	Brackish water, chlorides, sulfates, oxygen, copper oxides	Cold leg in sludge pile or where scale containing copper deposits is found, under deposit pitting in hot leg	Local attack and tube thinning, may lead to a hole	Bobbin coil, ultrasonics
7	Wastage	Phosphate chemistry, chloride concentration, resin leakage	Tubesheet crevices, sludge pile, tube support plates, AVBs	General thinning	Bobbin coil

[a] Based on operating experience and number of defects (as of 1993).
[b] Multi-frequency rotating pancake coil probe.

2.4 Review of Fouling in Heat Exchangers and Steam Generators [13]-[28]

There is an extensive amount of literatures on tube fouling [13-28]. Over the past several years, an increasing number of pressurized water reactor (PWR) plants have begun to experience degradation in steam generator thermal performance, which is often manifested as a decrease in SG steam pressure during operation. Such degradation can result in costly reductions in the electrical generating capacity of the plant. Even a 1% decrease in electrical generation approximately results in $2 million in lost revenues per year for a typical PWR. Numerous causes of SG thermal performance degradation have been identified, including primary and secondary tube fouling, dryer clogging, and flow resistance due to scaling, tube plugging and sleeving. Hence, fouling-related degradation is one of the major problems in steam generators as well as in heat exchangers. Therefore in this research, we focus part of our effort on the study of fouling, including a literature review, modeling, experimental study, and monitoring and diagnosis of fouling using the GMDH method.

2.4.1. Definition of Fouling [13] [14]

Fouling is generally defined as the accumulation of unwanted material onto the surfaces of the process equipment. It has been widely identified as an important

problem in design and operation of the process equipment since it often negatively affects the operation of equipment, mainly due to the following two effects :

- Since the fouling layer has a low thermal conductivity, it increases the thermal resistance to heat transfer and leads to a reduction in the effectiveness of heat exchangers and steam generators.

- While the fouling deposition occurs, the cross-sectional area is reduced and this results in an increase in pressure drop across the flow path.

Therefore, heat exchangers or steam generators are generally designed with certain amount of excess heat transfer capacity so as to offset the losses in efficiency resulting from fouling. That is, the thermal resistance due to fouling, R_f, is included in the equation for the overall heat transfer coefficient as follows [14]:

$$\frac{1}{U_o A_o} = \frac{1}{\alpha_o A_o} + \frac{R_{f,i}}{A_i} + \frac{R_w}{A_w} + \frac{R_{f,o}}{A_o} + \frac{1}{\alpha_i A_i} \qquad (2.1)$$

U_o= overall heat transfer coefficient based on outside area of tube wall

A = tube wall area

A_w = mean wall area

R_f = thermal resistance due to fouling

R_w = thermal resistance of wall

α = convective heat transfer coefficient.

U_o decreases as the deposit thickness or R_f increases with time. The thermal fouling resistance, R_f, is defined as:

$$R_f = \frac{1}{U_{o,dirty}} - \frac{1}{U_{o,clean}} \qquad (2.2)$$

The overall heat transfer coefficient determines how much heat can be transferred between the hot and the cold fluid in a given heat exchanger. When it falls below a tolerable value, the heat exchanger has to be serviced.

2.4.2. Fouling Mechanisms [14]

According to the mechanism of fouling deposit generation, fouling can be generally classified into crystallization fouling, particulate fouling, chemical reaction fouling, corrosion fouling, and biological fouling (bio-fouling) [14].

- Crystallization fouling: The deposition of a solid fouling layer on a heat transfer surface. This type of fouling occurs mainly due to the presence of dissolved inorganic salts in the flowing fluid, which becomes supersaturated under process conditions.

- Particulate fouling: The accumulation of solid particles suspended in a fluid

onto a heat transfer surface. The suspended particles can be ambient pollutants (sand, silt, clay), upstream corrosion products, or products of chemical reactions occurring within the fluid.

- Chemical reaction fouling: This involves deposits that are formed due to the chemical reactions on the heat transfer surface. The heat exchanger surface material may not react itself, but it may act as a catalyst.

- Corrosion fouling: This kind of fouling occurs when the heat exchanger material reacts with the fluid to form corrosion products on the heat transfer surface.

- Biological fouling: This involves the development and deposition of organic films consisting of micro-organisms and their products (microbial fouling) and the attachment and growth of macro-organisms (macrobial fouling).

Several fouling mechanisms often occur simultaneously and they are almost always mutually reinforcing. Generally fouling occurs in five consecutive steps [14]:

- Initiation or delay period: When a new or cleaned heat exchanger is put into operation, the initially high heat transfer coefficients may remain unchanged for a certain period of time. This delay period varies from a few seconds to several days. Research results show that there is no delay period for particulate fouling.

- Mass transport: For a deposit layer to form on a heat transfer surface, the foulant

has to be transported to the surface from the bulk coolant flow. In most cases, this occurs by diffusion.

- Formation of the deposit: After the foulant has been transported to the heat transfer surface, it must stick to the surface.

- Removal or auto-retardation: Depending on the strength of the deposit, erosion may occur immediately after the first deposit sticks to the surface. Meanwhile several mechanisms may cause auto-retardation of the deposition process.

- Aging: Every deposit is subject to this period. This can increase the deposit strength by, for example, polymerization, re-crystallization, or dehydration. Nevertheless, biological deposits weaken with time due to contamination of organisms.

Depending on the process conditions and the dominant fouling mechanism, the fouling rate will either be constant or decrease with time, as shown in Figure 2.6 [14].

- Linear rate: R_f increases with time or the growth rate of deposit is constant. This is the result of hard and adherent deposit where removal and aging can be ignored.

- Falling rate: R_f increases with time, but with a progressively falling rate or the

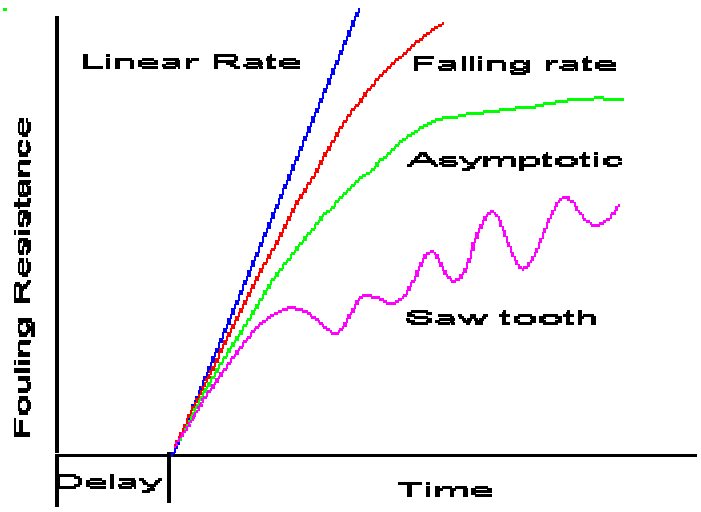

Figure 2.6. Different Cases of Fouling Rate

[From Ref. 14]

removal rate increases with time.

- Asymptotic rate: After a period of time, R_f reaches a constant value or the growth rate of deposit approaches zero.

- Saw-tooth fouling: Part of the deposit is detached after a critical residence time or once a critical deposit thickness has been reached. The fouling layer then builds up and breaks off again.

2.4.3. Mitigation or Control of Fouling [13] [14] [33]

Since fouling can cause high losses, various fouling mitigation strategies have been developed. Fouling is generally a function of many variables. For example,

fouling in a heat exchanger can be affected by the following variables: the amount of impurities and the concentration in the coolant flow, coolant temperature, system pressure, coolant flow rate, and surface temperature, etc. Therefore effective control of the variables may control or mitigate fouling. Generally the following fouling control methods are available:

- Preventing formation of the foulant
- Preventing foulant from attaching to heat transfer surfaces
- Removing the deposits from the heat transfer surfaces.

Experiences have shown that measures can be taken to prevent or mitigate the effect of fouling problems during the phases of plant design, construction, operation, and maintenance.

The techniques for mitigation and control of fouling generally include reduction of foulant concentration, use of chemical additives, mechanical on-line mitigation strategies, high flow rate and low surface temperature, chemical or mechanical cleaning of fouled process equipment, surface coatings and treatments, ultraviolet, acoustic, magnetic, electric and radiation treatment.

2.4.4 Heat Exchanger or SG Degradation Models

The degradation models are those that define the relationships between the characterization variable (for example, steam pressure change, tube wear rate, etc.) and the contributors or stressors (thermal fouling resistance, contact forces, contact time, coefficient of friction, etc.) of the defects. These models can be used to predict the reliability or residual lifetime of tubing in heat exchangers and SGs.

Even though there are various degradation models for SG residual lifetime prediction, which could be used by the nuclear industry, the Nuclear Regulatory Commission (NRC) has not yet approved any one of these as the standard method. This may be due to the fact that the SG degradations are so complex that up to now no single model can characterize all the degradation mechanisms very well.

Based on parametric study of the UTSG thermal-hydraulic model, Naghedolfeizi and Upadhyaya [15] determined that a quadratic function provides the best statistical fit to the trends of steam pressure variation as a function of the overall heat transfer coefficient.

$$\Delta P = a_0 + b_0 U_n + c_0 U_n^2 \qquad (2.3)$$

Where, ΔP is the SG steam pressure deviation from the set point and U_n is the

reduction in the heat transfer coefficient.

By combining the above equation with the fouling model (for example an exponential function), the following model may be obtained and applied to predict tube residual life [15].

$$\Delta P = \alpha_0 + \alpha_1 t + \alpha_2 t^2 \qquad (2.4)$$

Where, t is time.

One of the statistical techniques used by some engineers is the Weibull probability distribution, which has been successfully used to describe the statistics of material failure caused by fatigue and stress corrosion cracking. Reference [11] emphasized the Weibull distribution with two-parameter distribution given by

$$F(t) = 1 - \exp[-(t/t_\tau)^b] \qquad (2.5)$$

F(t) is the cumulative fraction of tubes "failed" by a given degradation mechanism, t is the time of operation, t_τ is the characteristic time of the Weibull probability distribution, and b is the slope of the distribution when plotted on a Weibull probability graph.

Kern and Seaton [16] were among the pioneer researchers to conduct a systematic

investigation of particulate fouling. From many experimental particulate fouling data from heat exchangers, they noticed that the fouling data all repeat the same type of asymptotic behavior. After Kern and Seaton, many researchers tried to develop a general model for particulate fouling on heat exchanger tubing surfaces, but there was little general agreement on the predictive model for particulate fouling.

Since the interaction between particulates and fluid flow is complicated, especially in the turbulent flow field, there has not been a general predictive model for particulate deposition until recently. In the heat exchangers or steam generators, the fact that there is a temperature gradient between the flow and the HX or SG surface makes the problem of developing a theoretical model for particulate deposition more complicated due to the thermophoresis effect.

In a more recent experimental investigation on particulate fouling in heat exchangers, a generalized model has been developed. The effect of operational variables such as flow, velocity, surface temperature, and fluid bulk temperature on particle deposition has been measured. Details of the models are as follows.

Kern and Seaton's model [16], which was based on the deposit removal rate concept, did not consider the thermal or particle size effects.

$$R_f(t) = \frac{K_1 UC}{K_2 \lambda_d \tau_W}(1 - e^{-K_2 \tau_W t}) = R_f^{*}(1 - e^{-bt}) \qquad (2.6)$$

Watkinson and Epstein introduced a sticking probability to the particles and modified Kern-Seaton model and led to the following model [19].

$$R_f(t) = \frac{K_3 C \beta e^{-E/RT_S}}{K_4 \lambda_d {\tau_W}^2}(1 - e^{-K_4 \tau_W t}) \tag{2.7}$$

$$\beta = \frac{U(f/8)^{1/2}}{11.8 {S_C}^{2/3}} \tag{2.8}$$

Muller-Steinhagen [19] took into account the effect of wall temperature and the fouling behavior in their equation, which is given as

$$R_f(t) = \frac{K_5 C \beta e^{-E/RT_S}}{K_6 \lambda_d \tau_W} \tag{2.9}$$

For adhesion controlled particles on heat transfer surfaces, the fouling resistance is given by [19]

$$R_f(t) = \frac{K_7 f C e^{-E/RT_S}}{K_8 \lambda_d \tau_W}(1 - e^{-K_8 \tau_W t}) \tag{2.10}$$

The thermophoretic effect is the effect of surface temperature on the deposition of submicron particles, which act in the direction of temperature gradients. This means that a hot surface will repel particles, while a cold surface will attract them [13].

Muller-Steinhagen [19] developed the following model for particle deposition rate:

$$m_d = (\beta - V_t / 2)C - (\beta + V_t / 2)C_W \qquad (2.11)$$

Where, V_t is the thermophoretic velocity and is defined as

$$V_t = \frac{0.26}{2\lambda_l + \lambda_p} * \frac{v_l q}{T} \qquad (2.12)$$

Within the limited range of experimental data, the general agreement between the data and the predictive model is fairly good. The nomenclatures are as follows [13]:

C = Bulk particle concentration kg/kg

C_W = Particle concentration near the solid-liquid interface kg/kg

E = Activation Energy, J/mol

f = Moody friction factor

m_d = Deposition flux, kg/m^2.S

q = Heat Flux, W/m^2

R_f = Fouling resistance, m^2.k/W

R_f* = Asymptotic fouling resistance m^2.K/W

R = Universal gas constant

Sc = Schmidt number = V_l/D

t = time, sec

T_s = Temperature at liquid-solid interface ˚C

U = Flow velocity, m/s

V_t = Thermophoretic velocity, m/s

β = Mass transfer coefficient, m/s

λ_d = Thermal conductivity of deposit

λ_l = Thermal conductivity of liquid W/m.K

λ_p = Thermal conductivity of particles W/m.K

v_l = Kinematic viscosity of liquid, m^2/s

τ_W = Wall shear stress, N/m^2

K1,...,K8 = Constants.

In the simulation of fouling in this study, we use the fouling factor to take into account the fouling effect. Generally the fouling factor must be obtained experimentally by determining the values of U for both clean and dirty conditions in the heat exchanger. The fouling factor is thus defined as:

$$R_f = 1/U_{dirty} - 1/U_{clean} \qquad (2.13)$$

According to Ref. [56] and the “Standard of Tubular Exchanger Manufacturers

Association," 4th ed., 1959, for treated boiler feed water above 125°F, the fouling factor is 0.001 $h \cdot ft^2 \cdot °F/Btu$ or 0.0002 $m^2 \cdot °C/W$.

2.5 Review of SG and Heat Exchanger Tube Corrosion and Water Chemistry

Corrosion is an important issue in SG and HX operations. In this section, we review the basics of corrosion and water chemistry. The discussion is mainly based on and adapted from Kuppan (2000) [33] and [29]-[46].

2.5.1 Corrosion Mechanisms [33] [29]-[46]

According to Kuppan [33], corrosion is defined as the deterioration of a metal caused by the reaction of the metal with the environment. Though other factors may also be important in certain cases, here the environment includes the following primary factors: (1) physical states: gas, liquid or solid; (2) chemical composition: constituents and concentrations; and (3) temperature.

According to electrochemical theory, the combination of anode, cathode, and aqueous solutions constitutes a small galvanic cell (Figure 2.7 [33]), and the corrosion reaction proceeds with a flow of current in a way similar to that of the current generated by chemical action in a primary cell or in a storage battery on discharge. The anode is dissolved because of the electrochemical action. A complete electrical circuit is

necessary for a current to flow. In a typical corroding system, as shown in Figure 2.7, the circuit is comprised of the following four components:

(1) Anode: The anode is the electrode at which the oxidation (corrosion) takes place and current in the form of positively charged metal ions enters the electrolyte. At the anode, the metal atom loses an electron, oxidizing to an ion.

(2) Electrolyte: The electrolyte is the solution or a solid layer e.g. a thick metal oxide scale) that surrounds or covers both the anode and the cathode. The conductivity of this solution is closely related to the corrosion speed. The lower the conductivity, the slower the corrosion reaction; and vice versa. If there is a total absence of an electrolyte, then little or no corrosion will occur.

(3) Cathode: The cathode is the electrode at which reduction takes place and current enters from the electrolyte.

(4) An external circuit: If there are two pieces of metal, they must either be in contact or have an external connection for corrosion to occur. The external circuit is a metallic path between the anode and the cathode that completes the circuit. If the anode and the cathode are on the metal surface, then this metal itself acts as the external circuit.

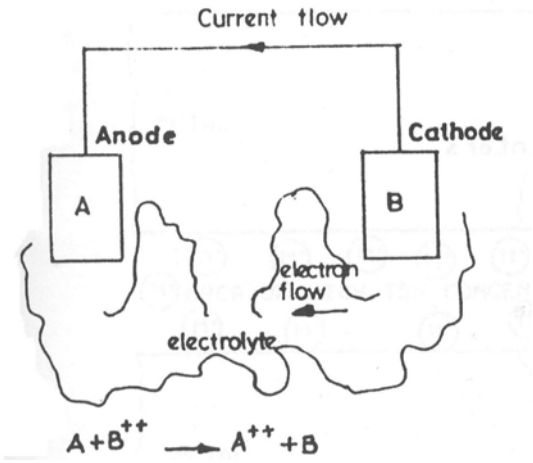

Figure 2.7. A Basic Corroding System

(From Ref. 33)

2.5.2 Forms of Corrosion [33] [29]-[46]

Corrosion attack on the metal surfaces can be either uniform or localized. In the latter, the major part of the metal surfaces remains unaffected but certain localized areas are corroded at a high rate. In contrast, the uniform corrosion occurs when a metal is corroded in an acid or alkali, or when the metal is exposed to natural environment such as air, soil, etc. Generally, uniform corrosion occurs when the metal and the environment system is homogeneous. When heterogeneities exist in the metal and/or variations in the environment, corrosion may be localized. For metals and alloys, factors that favor localized corrosion include grain boundaries, inter-metallic phases, inclusions, impurities, regions that differ in their mechanical or thermal treatments, discontinuities on metal

surfaces such as cut edges or scratches, discontinuities in oxide or passive films or in applied metallic or nonmetallic coatings, and geometrical factors such as crevices.

More specifically, the most common forms of corrosion include:

(1) Uniform corrosion

(2) Galvanic corrosion

(3) Crevice corrosion

(4) Pitting corrosion

(5) Intergranular corrosion

(6) Stress corrosion cracking

(7) Erosion-corrosion

(8) Dealloying corrosion

(9) Hydrogen damage

(10) Liquid-Metal Embrittlement, etc.

2.5.3 Effect of Some Important Variables on Corrosion [29]-[46]

The pH, electrochemical potential, and impurities in SG are the key factors that affect steam generator tube corrosion.

A. pH [33]

pH is a measure of the concentration of hydrogen ions and indicate whether and how strong the solution is acidic or basic. The stability of the oxide films on metal alloys in SG depends strongly on the pH. For many alloys, either very low (acidic) pH or very high (basic) pH causes unacceptable corrosion. As indicated above, depending on specific conditions, the corrosion can be general (or uniform, e.g. wastage) or localized (e.g. pitting or cracking). The pH of the bulk flow is controlled by the concentration of dissolved species in the solution, while the pH of local areas can be strongly affected by the electrochemical reactions occurring in the area. The stability of the oxide films is strongly affected by the oxygen concentration in the water or steam that the metal alloys are exposed to. The regions of stability depend on pH, electrochemical potential, temperature, other dissolved species, and the oxygen concentration. For high temperature water with very low levels of oxygen, stability of the oxide films on steel is increased as the pH increases, at least up to a pH of around 10. Figure 2.8 presents the corrosion rate versus pH. The general shape of this curve is typical for copper-base alloys. Such curves can be prepared for various metals and alloys and they may have

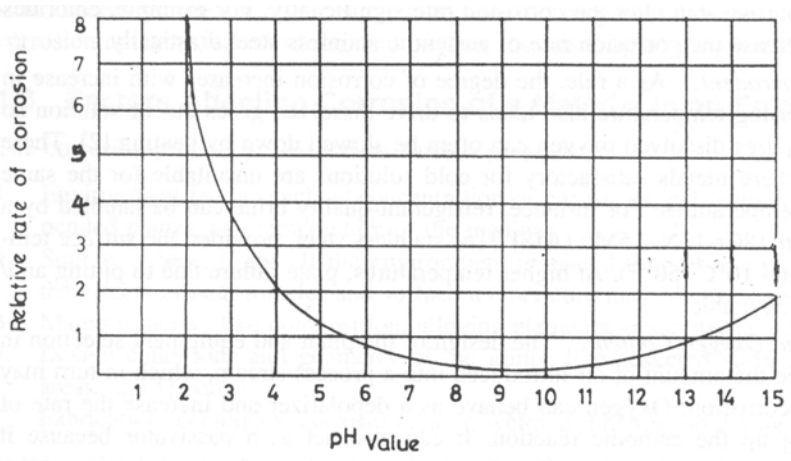

Figure 2.8. Relative Corrosion Rate versus pH

(From Reference [33])

their minima broadened or shortened. The slopes may vary considerably, depending upon the characteristics of the metal or alloy and the composition of the solution.

B. Electrochemical Potential [33]

The electrochemical potential of the surface is a measure of the galvanic force (voltage) available to cause electrochemical reactions to occur. This potential, together with other important variables such as temperature, pH, and the dissolved species, controls the form and extent of corrosion. The electrochemical potential is affected by the bulk and local solution chemistry, temperature, material, etc.

C. Impurities [35] [36] [37]

Many impurities that enter the secondary side of SG can aggravate corrosion of SG materials, especially tubes and tube support plates. The following impurities have been found to be especially harmful to SG integrity:

- Chloride: Since Inconel 600 is immune to chloride-induced SCC, it is chosen and used as SG structural material. However, chloride impurities have been found to be important causes for denting and pitting. The main source of chloride is condenser leakage, and the introduction of chloride by impurities in the makeup water.

- Sulfate: Concentrated sulfates can be aggressive to Inconel 600, and can cause IGA and IGSCC. They can also cause accelerated corrosion of carbon steel and thus lead to denting. The main sources of sulfates are condenser leakage and leakage of chemicals or resin fines from condensate polisher and makeup water demineralizers.

- Sodium: Concentrated sodium hydroxides are believed to be the major causes of IGA and IGSCC of SG tubes. The main sources of sodium are condenser leakage and leakage from condensate polisher and makeup water demineralizers.

- Copper: copper and copper oxides, together with other species such as chlorides, severely speed up denting and pitting in SGs and may also aggravate caustic IGSCC. Meanwhile, copper contributes to the total amount of sludge and deposits in SG. The main source of copper is the corrosion of copper containing alloys in secondary system heat exchanger tubes.

- Iron: Iron oxide tube deposits and sludge promote local boiling and concentration of impurities, and cause corrosive attacks such as IGA, IGSCC, and Pitting of SG tubes. In addition, iron oxide deposits in OTSGs have caused significant increases in pressure drop in the tube bundle and have led to plant power level reductions and extensive cleaning operations, including chemical cleaning.

- Organics: Organics have not been directly implicated in specific corrosion problems in SGs, but concerns remain because they may be introduced into SGs and then break down into aggressive species. Organics can be introduced by condenser leaks as impurities in the makeup water, resin fines, or lubricating oils.

2.5.4 Approaches for Corrosion Control [33] [29]-[46]

There are various techniques for corrosion control. These include the following.

- Proper engineering design

- Changing the characteristics of the corrosive environment
- Selecting the corrosion-resistant material
- Bimetal concept involving cladding and bimetallic tubes
- Application of protective coatings and inhibitors
- Providing electrochemical protection by cathodic and anodic protection
- Passivation.

From the point of view of water chemistry, the following main approaches are used to control corrosion of nuclear power plant materials, including steam generators [33] [35] [36] [37]:

(1) Maintenance of high purity

Since many corrosion processes in high temperature water system are aggravated by the presence of impurities, one of the main approaches to control corrosion is to control impurity concentrations to levels that result in tolerable corrosion during the expected lifetime.

To achieve a desired high purity, a number of requirements must be satisfied. These include use of high integrity condensers, use of makeup systems that can produce

water with very low impurity levels, continuous or periodic monitoring of makeup and system water purity, and continuous purification of all or portion of the system flow.

In locations such as crevices, sludge piles, or other occluded areas where boiling occurs, the concentration of impurities can increase by many orders of magnitude. This makes it difficult to prevent corrosion attack in such locations. In fact, corrosion attack at occluded locations continues to occur in the secondary side of many SGs over the past years, though great efforts have been made to reduce the impurity levels in the secondary coolant. Nevertheless, since the rate at which the impurities concentrate in occluded areas is directly proportional to their concentration in the bulk water, the reduction in impurity concentrations can help to delay or slow down the corrosion attack, if the attack cannot be prevented at all.

(2) Oxygen and pH control

Many materials used in power plants are thermodynamically unstable in high temperature water and tend to oxidize. However, under proper water chemistry conditions, stable thin films of protective oxides form on the metal surfaces and reduce the rate of oxidation to acceptable levels. Therefore the main objective of water chemistry is to maintain the integrity of these oxide films. Both neutral pH-high oxygen (for BWR) and high pH-low oxygen (for PWR) water treatment schemes have been

successfully used for this purpose.

PWRs have used high pH-low oxygen approach for both primary and secondary water chemistries. Low oxygen is achieved on the secondary side by combined use of mechanical de-aeration coupled with chemical scavenging using hydrazine; and it is obtained on the primary side by the use of a hydrogen overpressure, which results in scavenging of oxygen in the core. The pH is controlled using chemical additives like ammonia or lithium hydroxide.

Maintaining the desired pH value is very difficult in occluded areas due to the presence of concentrated impurities. The concentrated impurities can make the pH change widely. The occluded area pH can range from very low (strongly acidic) to very high (strongly basic), leading to a variety of corrosion problems. Some chemical additives have the potential to minimize these pH swings by a buffering action.

(3) Avoiding or reducing the deposits

Prevention of the formation of deposits and sludge piles on or around the heat transfer surfaces is another important aspect of water chemistry and corrosion control. This can minimize interference with heat transfer and avoid development of occluded areas where boiling can concentrate chemicals in the water to levels that can cause corrosive attack. Deposits in the primary system also need to be minimized so as to

reduce activation in the core and buildup of plant radiation levels. The following approaches may be used to avoid or reduce the occurrence of deposits:

- Minimizing the introduction of impurities into the system, e.g. by keeping the condensers leak-tight and controlling the purity of makeup water.

- Limiting the ingress of corrosion products into the SGs and reactor core by controlling the corrosion rate of system materials.

- Purification of bleed-off streams (primary coolant letdown and secondary coolant blowdown) to keep the concentrations of impurities and solids in the primary and secondary systems at acceptable levels.

- Full flow purification of the secondary system water.

2.5.5 Corrosion Monitoring [33] [34]

There are generally three approaches for corrosion monitoring:

- Local approach: This approach involves investigations of corrosion in terms of local conditions.

- Component approach: This approach involves investigating plant components and their corrosion phenomena that occur due to the complex environmental and

operational conditions.

- System approach: This approach considers the plant system as a whole. It deals with interrelations of phenomena occurring in different components of the system.

More specifically, the following techniques, generally classified as online monitoring or offline monitoring, are used in corrosion monitoring:

(1) Online monitoring techniques: Online corrosion monitoring is necessary for assessing the corrosivity of the process stream and for detecting the changes that may occur in operation. Online corrosion data are obtained from probes or sensors inserted into the system at accessible points that reproduce the specific area of interest. Online corrosion techniques include corrosion coupons, electrical resistance principle, pitting potential, linear polarization principle and Tafel plots, hydrogen test probe, galvanic measurements, pH measurements, dimensional changes through online ultrasonic testing, radiography, and acoustic emission technique, etc. [34].

Online monitoring of a cooling water system, including SG or heat exchanger, involves monitoring the calcium hardness, alkalinity, total solids, pH, dissolved oxygen and hydrogen, etc. Automatic analyzers continuously monitor the water and steam purities. Typical parameters monitored by online instruments include:

- Conductivity, pH (purity and acidity of the water)
- Ammonia, hydrazine phosphate (control of conditioning)
- Oxygen and Hydrogen (dissolved gases)
- Sodium, chloride, silica, etc. (harmful impurities in the system).

(2) Offline monitoring techniques: Offline corrosion monitoring mainly involves various nondestructive examination techniques to determine the thickness and integrity of SG or heat exchanger. The following nondestructive testing techniques are used [33]:

- Visual examination
- Eddy current testing
- Magnetic particle examination
- Liquid penetrant test
- Ultrasonic examination
- Radiography
- Thermography.

As stated above, corrosion monitoring of condensers is very important. It can be done through systematic examination of the state of the tubes. This involves extracting representative tubes and examining them in the laboratory. The following four aspects should be checked:

- Microscopic examination of the condition of the tube surfaces
- Residual wall thickness
- Weight of the surface layer
- Composition of the surface layer.

2.5.6 Steam Generator Program Guidelines [39]-[46]

Since it is of great importance to maintain the structural integrity of steam generators, a well-established steam generator program is important to achieve this goal. Nuclear Energy Institute issued the document NEI 97-06, *Steam Generator Program Guidelines*, which, along with the referenced EPRI guidelines [39-46], provide very good guidelines for steam generator and heat exchanger management. This is an industry self-imposed requirement on a number of steam generators, including water chemistry, and others. It establishes a framework for structuring and strengthening existing steam generator programs. It also provides the fundamental elements expected to be included

in a steam generator program. These elements incorporate a balance of prevention, inspection, evaluation, repair and leakage monitoring measures. This guideline refers licensees to EPRI guidelines or other documents that must be conformed with so as to meet the requirements. The intent of this document is to bring consistency in application of industry guidelines relative to managing steam generator programs.

Water chemistry control is one of the important elements in the steam generator program guidelines. In this aspect, EPRI issued the following two important guidelines [41-42]:

- PWR Secondary Water Chemistry Guidelines, EPRI Report TR-102134
- PWR Primary Water Chemistry Guidelines, EPRI Report TR-105714.

2.6 Remarks

From the above comprehensive literature review, we can make the following remarks:

- UTSG models can be either very detailed hence complex or comparatively simple. A model with complexity may be very time-consuming during both the development of the model and running of the computer code. A relatively simple one can be easier to be developed and implemented using various

computer environment or tools. Hence, in this study the first important task is to develop a simpler UTSG SIMULINK model with sufficiently high fidelity. This model will be based on a previous model and the emphasis will be on its improvement and its enhanced capability.

- There are various defects or degradations that may occur in a UTSG. They may occur independently or two or more of them may even take place simultaneously. This latter case will further complicate the problem. Therefore, it is very difficult to develop a model that can simulate all these defects. In our modeling, the focus is on simulation of the thermal-hydraulics and heat transfer process in a UTSG.

- There are various fouling models for heat exchanger, but only a few fouling models for steam generators. We will try to find an appropriate model to simulate fouling progress in SG and then use it and the UTSG SIMULINK model to study the effect of fouling on UTSG thermal performance.

- A literature review of experimental study of fouling progress in heat exchangers is given in Chapter 6.

Chapter 3

Multi-node Modeling and Simulation of a UTSG and Its Responses to Various System-Level Degradations

3.1 Introduction

Based on an existing model, a new multi-node simulation model has been developed for a typical recirculating U-tube steam generator (UTSG). As shown in Figure 2.1, in a typical UTSG, the primary coolant enters the steam generator through an inlet nozzle at the bottom of the inlet plenum. The coolant flows through the U-tube, first upward and then downward, and thus transfers heat to the secondary fluid on the shell side of the SG. The primary fluid leaves the outlet plenum through an outlet nozzle connected to the cold leg piping. The feedwater enters the downcomer shell at a level just above the U-tube region. It flows down through an annulus inside the shell and mixes with water coming from the drum section. The water enters the tube bundle region where heat is transferred to the fluid. As it flows over the outside of the U-tubes, a mixture of steam and water is formed. The mixture enters the riser region where the nozzle effect increases the natural driving force. As the flow passes through the separator region, water is removed from the steam and is returned to the drum section.

The steam leaving the separator passes through steam dryers and exits the steam generator with a quality of almost 100%.

A typical 1,300 MWe four-loop Westinghouse nuclear plant has about 3,400 U-tubes per SG. The Inconel stainless steel tubing has an outer diameter of 0.875 inch with a tube metal thickness of 0.05 inch. The height of U-tubes is ≈ 36 feet. The nominal steam pressure is 850 psia with a saturation temperature of 522 °F. The feed water has an inlet temperature of 434 °F and a flow rate of ≈ 3.73×10^6 *lbm/hr*.

One of the objectives of this new model is to divide the tube length into a number of axial nodes so as to simulate tube fouling at different axial locations. The simulation may be made by varying heat transfer areas, flow rates, and heat transfer coefficients. The latter include film heat transfer coefficient of primary water in tubes, film heat transfer coefficient of secondary sub-cooled water, film heat transfer coefficient of secondary boiling water, and metal tube conductivity.

In the following sections of this chapter, we will describe the detailed UTSG first-principle model. This model is developed based on the model previously established by Naghedolfeizi and Upadhyaya (1991) [10]. Here our focus is on improving this model by increasing the number of axial nodes for UTSG heat transfer tubes so as to take into account the effects of axial change in heat transfer coefficient due

to UTSG tube fouling. First we describe the methodology, the basic conservation laws, and derive the new model equations. The new model equations are implemented under MATLAB SIMULINK platform.

3.2 Methodology

To develop a first-principle model for UTSG and study the dynamic behavior, we first divide the UTSG structure into a certain number of control volumes or nodes. Then we apply the basic physical laws, such as mass balance, energy balance, and momentum balance, to each node so that we can derive the mathematical equations for each node. These equations and related constitutive relationships form the whole set of mathematical model equations for the UTSG.

In a fluid transport system with heat transfer, the first-principle model is developed generally based on three overall balance equations: (a) mass balance, (b) energy balance, and (c) momentum balance (rate of change of momentum and force). Generally these equations are quite complicated due to change in the phase of the fluid, such as due to boiling in a BWR or in a steam generator.

In our study, we use the lumped mass nodes so that the behavior of each node can be described by ordinary differential equations.

Figure 3.1. A Schematic Illustrating Mass Balance in a Node

Here we give a brief description of conservation principles. Our UTSG multi-node SIMULINK model developed later in this chapter will be based on these conservation laws.

(1) Overall mass balance

Figure 3.1 gives a block diagram illustrating mass balance in a node. The mass balance equation is given by

$$\frac{dM}{dt} = W_{in} - W_{out} \qquad (3.1)$$

Where, W_{in} = Mass flow rate into the control volume

W_{out} = Mass flow rate out of the control volume

M = Mass of control volume at time t.

(2) Overall energy (heat) balance

The simplified form of the overall energy balance is written in terms of the rate of

change of the internal energy of the control volume.

$$\frac{dU}{dt} = Q_{in} - Q_{out} \tag{3.2}$$

Where, U = Internal energy of the control volume at time t

Q_{in} = Energy (heat) into the control volume

Q_{out} = Energy (heat) out of the control volume.

(3) Overall momentum balance

The overall momentum balance involves changes in dynamic pressure, moving fluid boundaries (such as in steam generators) and changes in fluid velocities. For a control volume, considering a single direction:

Rate of change of momentum = Net forces acting in that direction

$$\frac{d}{dt}(mv) = F_p + F_d + F_g \tag{3.3}$$

Where, m= mass of control volume

v = Velocity of fluid

F_p = Forces due to pressure acting on the control volume

F_d = Drag, friction or shear force. This is parallel to the fluid flow.

F_g =Gravity force. This is zero if the direction of force (or flow) considered is horizontal.

3.3 Assumptions

The following assumptions are made in model development [10].

- Both water and steam are considered to be saturated.
- Density and specific heat capacity of the feed water, sub-cooled region, and the primary side are assumed to be constant.
- Heat transfer coefficients are constant.
- Steam leaving the steam generator is 100% saturated.
- Heat transfer between the downcomer and the tube bundle regions is negligible.

The thermodynamic properties of the saturated water and steam are assumed to be linear functions of the steam pressure for a range of ± 100 *psi* from the nominal operating point. The steam flow leaving the UTSG is considered to be a critical flow, meaning that the steam flow rate is dependent only on the upstream (SG) pressure and any

decrease in the downstream (turbine) pressure does not affect the steam flow rate from the SG any more. In this case, the steam flow rate is defined as

$$W_s = C_l P \qquad (3.4)$$

Where, W_s = steam flow rate, C_l = steam valve coefficient, P = steam pressure.

Figure 3.2 shows a schematic of the nodal model representation. The equations describing the nonlinear model of the UTSG are presented in Section 3.4.

3.4 Mathematic Equations for UTSG Multi-node Simulation Model

Some of the describing equations given below were derived with reference to those given by Naghedolfeizi and Upadhyaya (1991) [10].

1. Primary Side

a. Inlet Plenum (PRIN):

$$\frac{dT_{pi}}{dt} = \frac{W_{pi}}{M_{pi}}(\theta_i - T_{pi}) \qquad (3.5)$$

b. U-tube Primary Lumped Coolant Node Equations:

For the detailed derivation of the describing equations for the primary-side lumped coolant nodes, see Appendix A. These equations are presented here.

Node 1 (PRL1):

$$\frac{dT_{p1}}{dt} = \frac{W_{pi}}{\rho_{pi} A_p L_{s1}}(T_{pi} - T_{p1}) + \frac{U_{pm1} S_{pm1}}{M_{p1} C_{p1}}(T_{m1} - T_{p1}) \qquad (3.6)$$

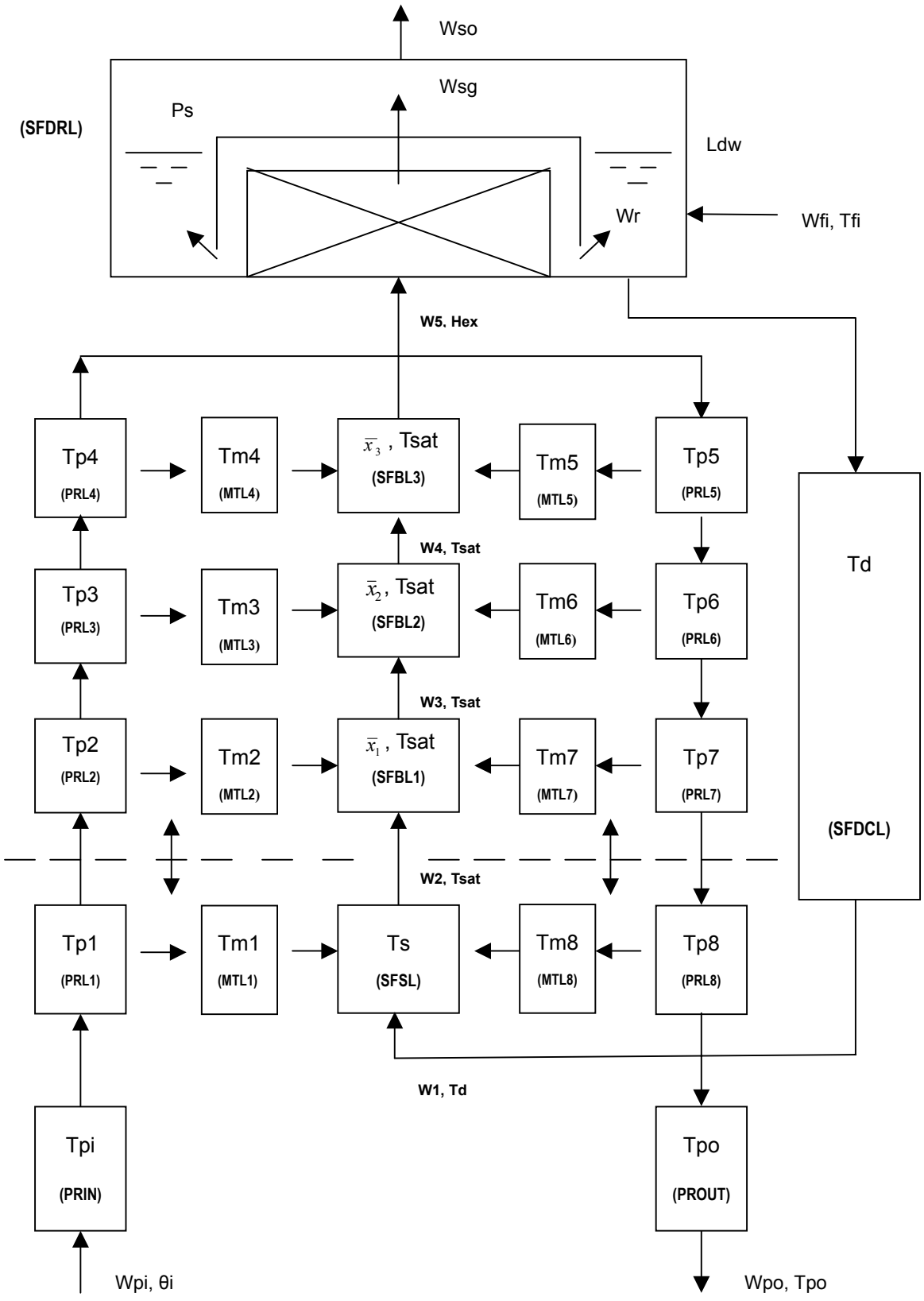

Figure 3.2. The Schematic of the UTSG Model with Four Axial Tube Nodes

Node 2 (PRL2):

$$\frac{dT_{p2}}{dt}=\frac{W_{pi}}{\rho_{pi}A_pL_{s2}}(T_{p1}-T_{p2})+\frac{U_{pm2}S_{pm2}}{M_{p2}C_{p2}}(T_{m2}-T_{p2})+\frac{T_{p2}-T_{p1}}{L_{s2}}\frac{dL_{s1}}{dt} \quad (3.7)$$

Where, $L_{s2}=(L_0-L_{s1})/3$

Node 3 (PRL3):

$$\frac{dT_{p3}}{dt}=\frac{W_{pi}}{\rho_{pi}A_pL_{s2}}(T_{p2}-T_{p3})+\frac{U_{pm3}S_{pm3}}{M_{p3}C_{p3}}(T_{m3}-T_{p3})+\frac{2(T_{p3}-T_{p2})}{3L_{s2}}\frac{dL_{s1}}{dt} \quad (3.8)$$

Node 4 (PRL4):

$$\frac{dT_{p4}}{dt}=\frac{W_{pi}}{\rho_{pi}A_pL_{s2}}(T_{p3}-T_{p4})+\frac{U_{pm4}S_{pm4}}{M_{p4}C_{p4}}(T_{m4}-T_{p4})+\frac{T_{p4}-T_{p3}}{3L_{s2}}\frac{dL_{s1}}{dt} \quad (3.9)$$

Node 5 (PRL5):

$$\frac{dT_{p5}}{dt}=\frac{W_{pi}}{\rho_{pi}A_pL_{s2}}(T_{p4}-T_{p5})+\frac{U_{pm5}S_{pm5}}{M_{p5}C_{p5}}(T_{m5}-T_{p5}) \quad (3.10)$$

Node 6 (PRL6):

$$\frac{dT_{p6}}{dt}=\frac{W_{pi}}{\rho_{pi}A_pL_{s2}}(T_{p5}-T_{p6})+\frac{U_{pm6}S_{pm6}}{M_{p6}C_{p6}}(T_{m6}-T_{p6})+\frac{T_{p5}-T_{p6}}{3L_{s2}}\frac{dL_{s1}}{dt} \quad (3.11)$$

Node 7 (PRL7):

$$\frac{dT_{p7}}{dt}=\frac{W_{pi}}{\rho_{pi}A_pL_{s2}}(T_{p6}-T_{p7})+\frac{U_{pm7}S_{pm7}}{M_{p7}C_{p7}}(T_{m7}-T_{p7})+\frac{2(T_{p6}-T_{p7})}{3L_{s2}}\frac{dL_{s1}}{dt} \quad (3.12)$$

Node 8 (PRL8):

$$\frac{dT_{p8}}{dt}=\frac{W_{pi}}{\rho_{pi}A_pL_{s1}}(T_{p7}-T_{p8})+\frac{U_{pm8}S_{pm8}}{M_{p8}C_{p8}}(T_{m8}-T_{p8})+\frac{T_{p7}-T_{p8}}{L_{s1}}\frac{dL_{s1}}{dt} \quad (3.13)$$

c. Outlet Plenum (PROUT):

$$\frac{dT_{po}}{dt} = \frac{W_{pi}}{M_{po}}(T_{p8} - T_{po}) \qquad (3.14)$$

2. Tube-wall Equations

For the detailed derivation of the describing equations for the lumped tube-wall nodes, please see Appendix B. These equations are presented here.

Node 1 (MTL1):

$$\frac{dT_{m1}}{dt} = \frac{U_{pm1}S_{pm1}}{M_{m1}C_m}T_{p1} - \frac{U_{pm1}S_{pm1} + U_{ms1}S_{ms1}}{M_{m1}C_m}T_{m1} + \frac{U_{ms1}S_{ms1}}{M_{m1}C_m}\cdot\frac{T_d + T_{sat}}{2} + \frac{T_{m2} - T_{m1}}{2L_{s1}}\cdot\frac{dL_{s1}}{dt} \qquad (3.15)$$

Node 2 (MTL2):

$$\frac{dT_{m2}}{dt} = \frac{U_{pm2}S_{pm2}}{M_{m2}C_m}(T_{p2} - T_{m2}) - \frac{U_{ms2}S_{ms2}}{M_{m2}C_m}(T_{m2} - T_{sat}) + \frac{T_{m2} + 2T_{m3} - 3T_{m1}}{2(L_0 - L_{s1})}\cdot\frac{dL_{s1}}{dt} \qquad (3.16)$$

Node 3 (MTL3):

$$\frac{dT_{m3}}{dt} = \frac{U_{pm3}S_{pm3}}{M_{m3}C_m}(T_{p3} - T_{m3}) - \frac{U_{ms3}S_{ms3}}{M_{m3}C_m}(T_{m3} - T_{sat}) + \frac{T_{m3} + T_{m4} - 2T_{m2}}{2(L_0 - L_{s1})}\cdot\frac{dL_{s1}}{dt} \qquad (3.17)$$

Node 4 (MTL4):

$$\frac{dT_{m4}}{dt} = \frac{U_{pm4}S_{pm4}}{M_{m4}C_m}(T_{p4} - T_{m4}) - \frac{U_{ms4}S_{ms4}}{M_{m4}C_m}(T_{m4} - T_{sat}) + \frac{T_{m4} - T_{m3}}{2(L_0 - L_{s1})}\cdot\frac{dL_{s1}}{dt} \qquad (3.18)$$

Node 5 (MTL5):

$$\frac{dT_{m5}}{dt} = \frac{U_{pm5}S_{pm5}}{M_{m5}C_m}(T_{p5} - T_{m5}) - \frac{U_{ms5}S_{ms5}}{M_{m5}C_m}(T_{m5} - T_{sat}) + \frac{T_{m5} - T_{m6}}{2(L_0 - L_{s1})}\cdot\frac{dL_{s1}}{dt} \qquad (3.19)$$

Node 6 (MTL6):

$$\frac{dT_{m6}}{dt} = \frac{U_{pm6}S_{pm6}}{M_{m6}C_m}(T_{p6} - T_{m6}) - \frac{U_{ms6}S_{ms6}}{M_{m6}C_m}(T_{m6} - T_{sat}) + \frac{T_{m5} + T_{m6} - 2T_{m7}}{2(L_0 - L_{s1})}\cdot\frac{dL_{s1}}{dt} \qquad (3.20)$$

Node 7 (MTL7):

$$\frac{dT_{m7}}{dt}=\frac{U_{pm7}S_{pm7}}{M_{m7}C_m}(T_{p7}-T_{m7})-\frac{U_{ms7}S_{ms7}}{M_{m7}C_m}(T_{m7}-T_{sat})+\frac{2T_{m6}+T_{m7}-3T_{m8}}{2(L_0-L_{s1})}\cdot\frac{dL_{s1}}{dt} \qquad (3.21)$$

Node 8 (MTL8):

$$\frac{dT_{m8}}{dt}=\frac{U_{pm8}S_{pm8}}{M_{m8}C_m}(T_{p8}-T_{m8})-\frac{U_{ms8}S_{ms8}}{M_{m8}C_m}(T_{m8}-\frac{T_d+T_{sat}}{2})+\frac{T_{m7}-T_{m8}}{2L_{s1}}\cdot\frac{dL_{s1}}{dt} \qquad (3.22)$$

3. Secondary Side Equations

a. Sub-cooled region (SFSL)

Mass Balance:

$$\frac{dL_{s1}}{dt}=\frac{W_1-W_2}{\rho_{s1}A_{fs}} \qquad (3.23)$$

Energy Balance:

$$\frac{d}{dt}(\rho_{s1}A_{fs}L_{s1}C_{psub}\frac{T_d+T_{sat}}{2})=P_{r2}L_{s1}[U_{ms1}(T_{m1}-\frac{T_d+T_{sat}}{2})+U_{ms8}(T_{m8}-\frac{T_d+T_{sat}}{2})]+W_1C_{psub}T_d-W_2C_{psub}T_{sat} \qquad (3.24)$$

b. Boiling region equations

Node 1 (SFBL1):

Mass Balance:

$$\frac{d}{dt}(\rho_{b1}A_{fs}L_{s2})=W_2-W_3 \qquad (3.25)$$

$$\frac{d}{dt}\rho_{b1}=-\frac{K_1+K_2\frac{X_{e1}}{2}}{(V_f+\frac{X_{e1}}{2}V_{fg})^2}\frac{dP}{dt}-\frac{V_{fg}}{2(V_f+\frac{X_{e1}}{2}V_{fg})^2}\frac{dX_{e1}}{dt} \qquad (3.26)$$

Energy Balance:

$$\frac{d}{dt}(\rho_{b1}A_{fs}L_{s2}h_{b1}) = P_{r2}L_{s2}[U_{ms2}(T_{m2}-T_{sat})+U_{ms7}(T_{m7}-T_{sat})]+W_2h_f-W_3h_{ex1} \qquad (3.27)$$

Node 2 (SFBL2):

Mass Balance:

$$\frac{d}{dt}(\rho_{b2}A_{fs}L_{s2}) = W_3-W_4 \qquad (3.28)$$

$$\frac{d}{dt}\rho_{b2} = -\frac{K_1+K_2\dfrac{X_{e1}+X_{e2}}{2}}{(V_f+\dfrac{X_{e1}+X_{e2}}{2}V_{fg})^2}\frac{dP}{dt}-\frac{V_{fg}}{2(V_f+\dfrac{X_{e1}+X_{e2}}{2}V_{fg})^2}(\frac{dX_{e1}}{dt}+\frac{dX_{e2}}{dt}) \qquad (3.29)$$

Energy Balance:

$$\frac{d}{dt}(\rho_{b2}A_{fs}L_{s2}h_{b2}) = P_{r2}L_{s2}[U_{ms3}(T_{m3}-T_{sat})+U_{ms6}(T_{m6}-T_{sat})]+W_3h_{ex1}-W_4h_{ex2} \qquad (3.30)$$

Node 3 (SFBL3):

Mass Balance:

$$\frac{d}{dt}(\rho_{b3}A_{fs}L_{s2}) = W_4-W_5 \qquad (3.31)$$

$$\frac{d}{dt}\rho_{b3} = -\frac{K_1+K_2\dfrac{X_{e2}+X_{e3}}{2}}{(V_f+\dfrac{X_{e2}+X_{e3}}{2}V_{fg})^2}\frac{dP}{dt}-\frac{V_{fg}}{2(V_f+\dfrac{X_{e2}+X_{e3}}{2}V_{fg})^2}(\frac{dX_{e2}}{dt}+\frac{dX_{e3}}{dt}) \qquad (3.32)$$

Energy Balance:

$$\frac{d}{dt}(\rho_{b3}A_{fs}L_{s2}h_{b3}) = P_{r2}L_{s2}[U_{ms4}(T_{m4}-T_{sat})+U_{ms5}(T_{m5}-T_{sat})]+W_4h_{ex2}-W_5h_{ex3} \qquad (3.33)$$

4. Drum Region Equations (SFDRL)

a. Riser/Separator Volume

$$\frac{d}{dt}(V_r\rho_r) = W_5-W_6 \qquad (3.34)$$

$$\frac{d}{dt}\rho_r = -\frac{K_1 + K_2 X_{e3}}{(V_f + X_{e3} V_{fg})^2}\frac{dP}{dt} - \frac{V_{fg}}{(V_f + X_{e3} V_{fg})^2}\frac{dX_{e3}}{dt} \tag{3.35}$$

b. Drum Water Volume

Mass Balance:

$$\frac{d}{dt}(\rho_{dw} A_{dw} L_{dw}) = W_{fi} + (1 - X_{e3}) W_6 - W_1 \tag{3.36}$$

Energy Balance:

$$\frac{d}{dt}(\rho_{dw} A_{dw} L_{dw} T_{dw}) = W_{fi} T_{fi} + (1 - X_{e3}) W_6 T_{sat} - W_1 T_{dw} \tag{3.37}$$

c. Drum Steam Volume

$$(V_{dr} - A_{dw} L_{dw})\frac{d\rho_g}{dt} - \rho_g A_{dw}\frac{dL_{dw}}{dt} = X_{e3} W_6 - C_l P \tag{3.38}$$

5. Downcomer Region Equations (SFDCL)

$$\frac{dT_d}{dt} = \frac{W_1}{M_d}(T_{dw} - T_d) \tag{3.39}$$

6. Constitutive Relations

$h_{bi}=h_f+0.5(Xe_{i-1}+Xe_i)h_{fg}$ (i= 1,2,3; $Xe_0=0$)

$h_{exi}=h_f+Xe_i h_{fg}$ (i= 1,2,3)

$h_f=X_4+K_3P$

$h_{fg}=X_5+K_4P$

$L_{s2}=(L_0-L_{s1})/3$

$T_{sat}=X_1+K_5P$

$V_f=X_2+K_1P$

$V_{fg}=X_3+K_2P$

$$\rho_b = \frac{1}{V_f + \frac{X_e}{2} V_{fg}}$$

$$\rho_r = \frac{1}{V_f + X_e V_{fg}}$$

$$\rho_g = X_6 + K_6 P$$

$$W_1 = \frac{C_1}{12}[\rho_d (L_{dw} + L_d - L_{s1}) - L_{s2}(\rho_{b1} + \rho_{b2} + \rho_{b3}) - L_r \rho_r]^{0.5}$$

The definitions of the parameters and variables are given below:

A_p= Primary-side coolant flow cross section

A_{fs} = Secondary flow area in the U-tube region

A_{dw} = Effective area of the drum water section

C_l = Effective pressure drop coefficient in the recirculating loop

$C_{\ l}$ = Steam valve coefficient

C_m = Specific heat capacity of the metal tubes

$C_{p1\text{-}8}$ = Specific heat capacity of the primary fluid

C_{psub} = Specific heat capacity of the secondary-side water in the sub-cooled region

$h_{b1\text{-}3}$ = Average enthalpy of the nodes in boiling region

h_f, h_{fg} = Saturated and latent enthalpies of water

$h_{ex1\text{-}3}$ = Exit enthalpy of the nodes in boiling region

$K_{1\text{-}6} = \frac{\partial v_f}{\partial P}, \frac{\partial v_{fg}}{\partial P}, \frac{\partial h_f}{\partial P}, \frac{\partial h_{fg}}{\partial P}, \frac{\partial T_{sat}}{\partial P}, \frac{\partial \rho_g}{\partial P}$

L = Effective height of U-tubes

L_d = Downcomer length

L_{dw} = Steam generator water level (drum section)

$L_{s1,2}$ = Lengths of subcooled and boiling nodes respectively

$M_{m1\text{-}8}$ = Metal mass in metal nodes

$M_{p1\text{-}8}$ = Water mass in primary nodes

M_{pi} = Water mass in the inlet plenum

P = Steam generator pressure

$P_{r1,2}$ = Inside and outside perimeters of the U-tubes

$S_{ms1\text{-}8}$ = Heat transfer areas from the U-tubes to the secondary side in each node

$S_{pm1\text{-}8}$ = Heat transfer areas from the primary side to the U-tubes in each node

T_d = Downcomer temperature

T_{dw} = Drum water temperature

$T_{m1\text{-}8}$ = Metal tube temperature in each node

$T_{p1\text{-}8}$ = Primary water temperature in each node

T_p = Water temperature in the inlet plenum

T_{po} = Water temperature in the outlet plenum

T_{sat} = Saturated temperature of the water and steam in the UTSG

$U_{pm1\text{-}8}$ = Heat transfer coefficient from the primary side to metal side in each node

$U_{ms1\text{-}8}$ = Heat transfer coefficient from the metal side to secondary side in each node

V_{dr} = Volume of the drum section

V_f, V_g = Specific volume of the saturated water and steam

$V_{fg} = V_g - V_f$

V_r = Volume of the riser region

$X_{1\text{-}6}$ = Constants

$Xe_{1\text{-}3}$ = Exit quality of the steam leaving the nodes in boiling region

ρ_b = Average density of the water in boiling region

ρ_g = Density of the saturated steam

ρ_r = Density of the water in riser region.

3.5 UTSG Three-Element Controller Model

To incorporate the control actions into the above UTSG model, we have adopted a three-element controller model, as given in Ref. [10]. This three-element controller controls the steam generator water level. The forcing functions of the isolated UTSG model are: primary inlet temperature, steam valve coefficient, feed water temperature, and SG level set point.

The controller is illustrated in Figure 3.3 [10]. It uses the water level, feed-water flow rate and steam flow rate as the control variables. The error signal between the set-point and measured water level is first processed by a low-pass filter so as to remove the noise in the measurements. Then the output signal feeds to the first PI controller and then summed with the feed-water flow and steam flow mismatch signal. The resultant signal then passes to the second PI controller and the output signal from G_3 governs the feed-water valve opening hence the feed-water flow rate. The feed-water valve has a second-order system characteristic.

For details, including the mathematical equations of this controller model, please see Naghedolfeizi and Upadhyaya (1991) [10].

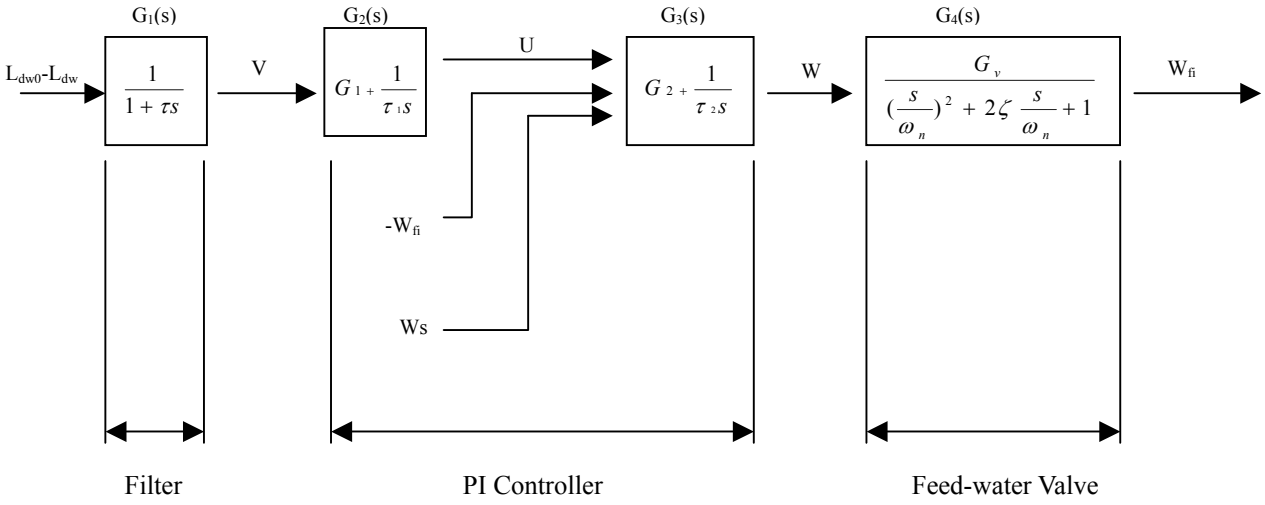

Figure 3.3. The Block Diagram of the Three-element UTSG Controller

(From Ref. [10])

3.6 UTSG SIMULINK Model

After we have derived and obtained the above set of ordinary differential equations (ODE) for UTSG, we can then simulate the process occurring in it by solving these equations. MATLAB SIMULINK provides a very good tool for this purpose. We have implemented the mathematical equations under SIMULINK in a very simple and easy way. That is, we directly input the mathematical expression of the first derivative of a dependent variable in the SIMULINK model, with the initial value appropriately defined. Figure 3.4 gives an overview of the top-level layout of this SIMULINK model.

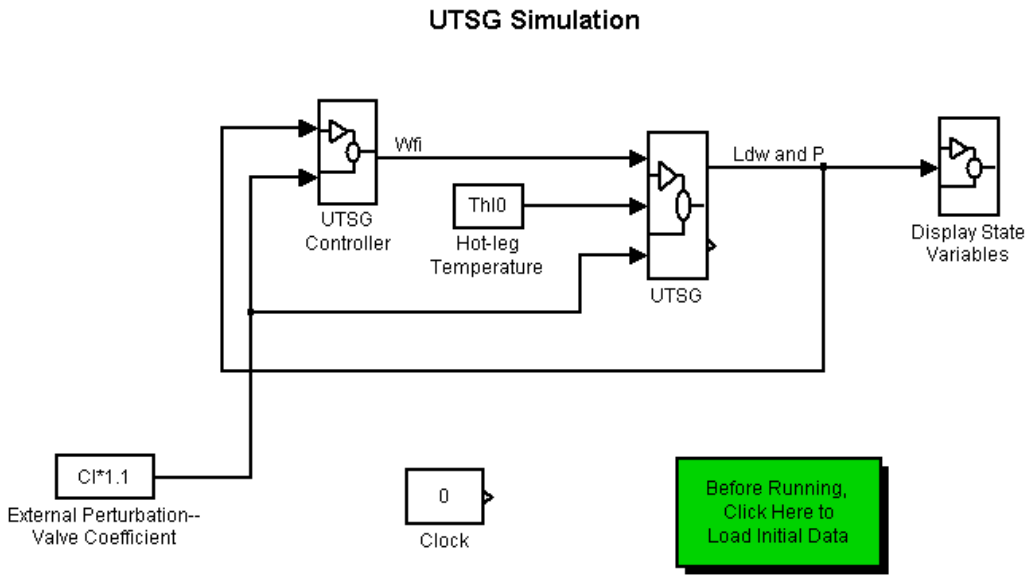

Figure 3.4. An Overview of the Top-level Layout of UTSG SIMULINK Model

3.7 Simulation of UTSG Responses to Various System-Level Degradations

Now that we have developed the mathematical equations and implemented them under MATLAB SIMULINK, we can now use this multi-nodal UTSG SIMULINK model to simulate the UTSG responses to various faults or defects that may occur in a UTSG. In our study, we have simulated the following defects or tube degradation mechanisms:

- Tube plugging by changing the heat transfer area.
- Tube fouling on the primary side (inner tube) by introducing an additional heat transfer resistance at different axial locations.
- Tube fouling on the secondary side (outer tube) by introducing an additional heat transfer resistance at different axial locations.
- Tube metal heat conductivity.

Figures 3.5 - 3.18 present the results of simulation for normal operation and for the cases of tube degradation. The latter include decreased heat transfer area (tube plugging), decreased heat transfer coefficients (fouling) and decreased tube metal conductivity (material property). In all these cases the steam pressure decreases from its nominal value. Figures 3.15 - 3.18 show the process dynamics during normal transients.

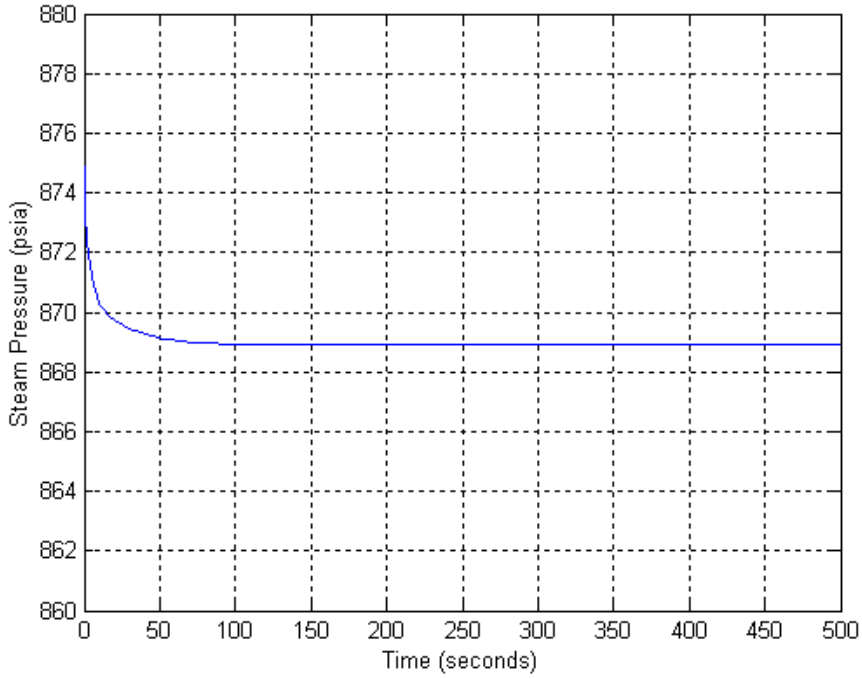

Figure 3.5. Steam Pressure Change for the Case of 5% Decrease in the Number of Tubes

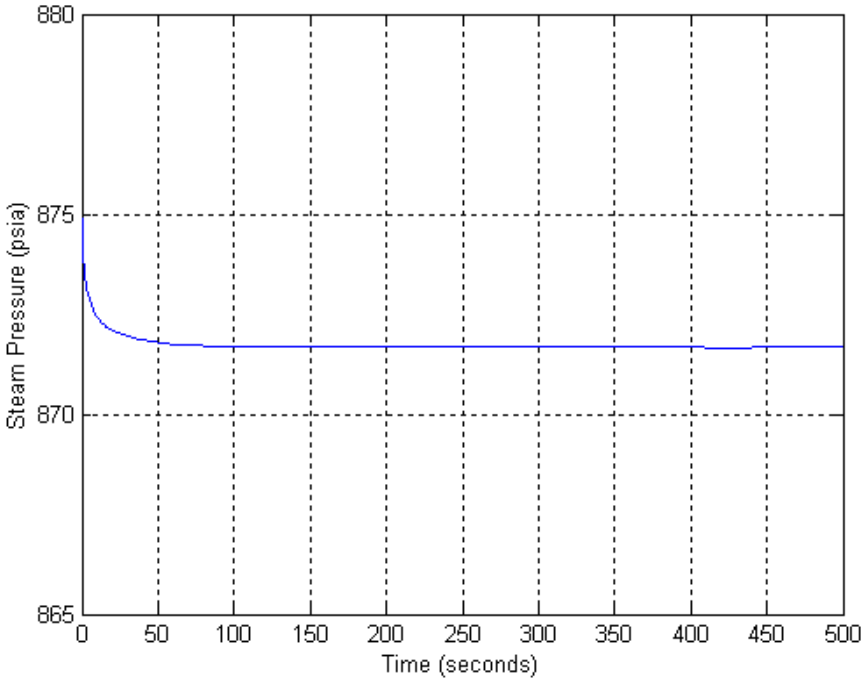

Figure 3.6. Steam Pressure Change for the Case of 10% Decrease in the Tube Metal Conductivity

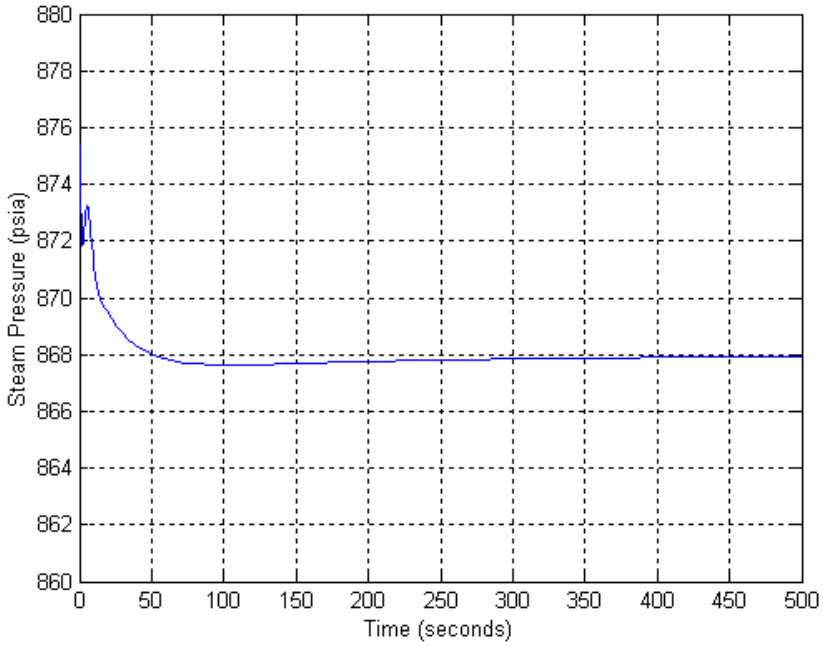

Figure 3.7. Steam Pressure Change When Decreasing the Overall Heat Transfer Coefficient by 50% in the Metal-to-Secondary Side Sub-cooled Heat Transfer Nodes (MTL1 and MTL8)

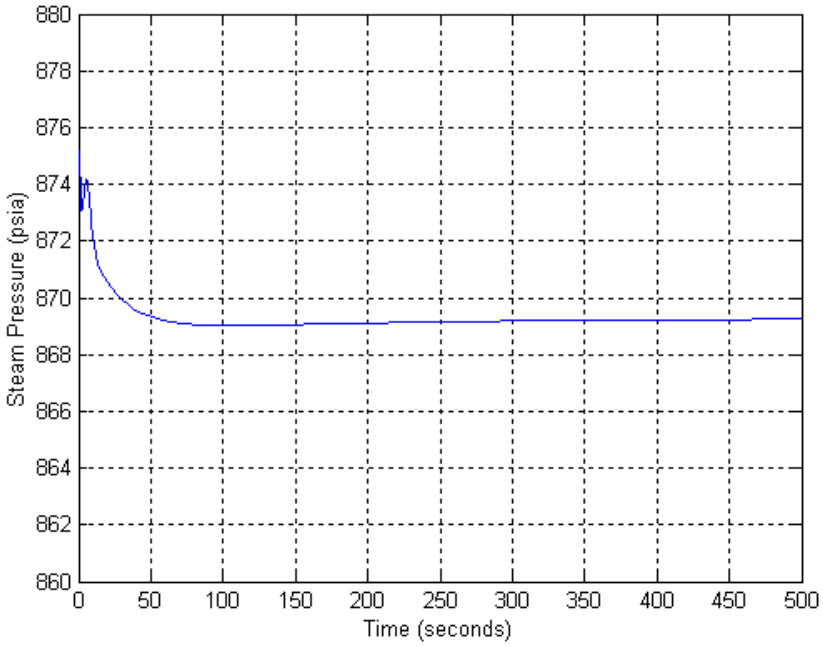

Figure 3.8. Steam Pressure Change When Decreasing the Overall Heat Transfer Coefficient by 50% in the Primary-to-Metal Side Sub-cooled Heat Transfer Nodes (PRL1 and PRL8)

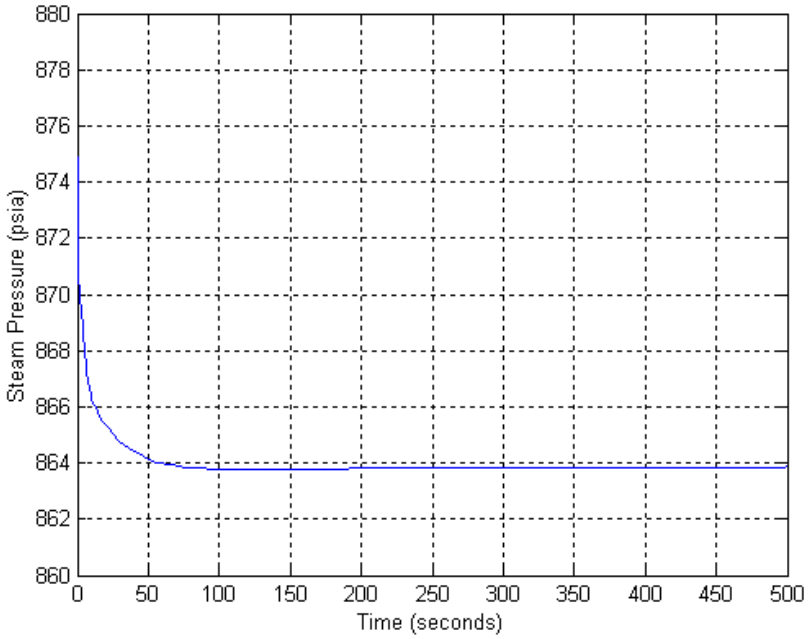

Figure 3.9. Steam Pressure Change When Decreasing the Overall Heat Transfer Coefficient by 50% in the Metal-to-Secondary Side Boiling Heat Transfer Nodes (MTL2 and MTL7)

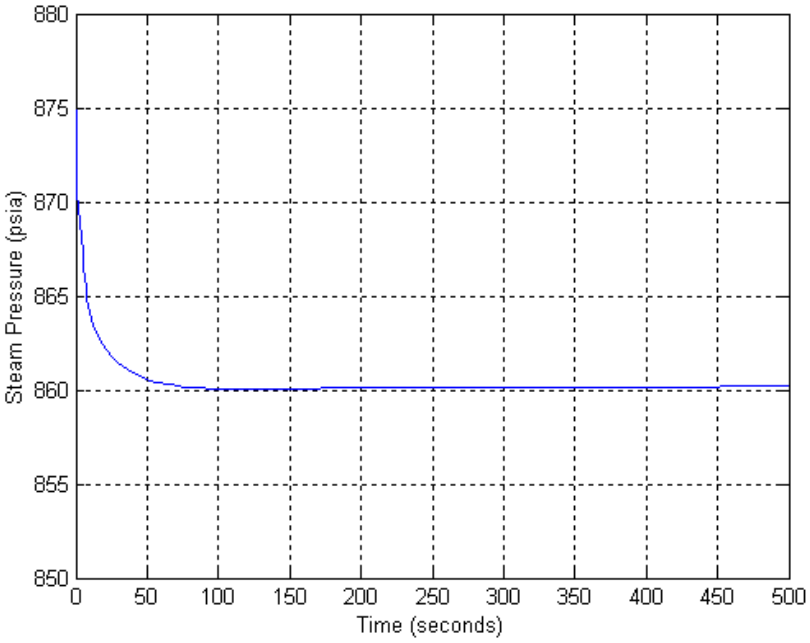

Figure 3.10. Steam Pressure Change When Decreasing the Overall Heat Transfer Coefficient by 50% in the Primary-to-Metal Side Boiling Heat Transfer Nodes (PRL2 and PRL7)

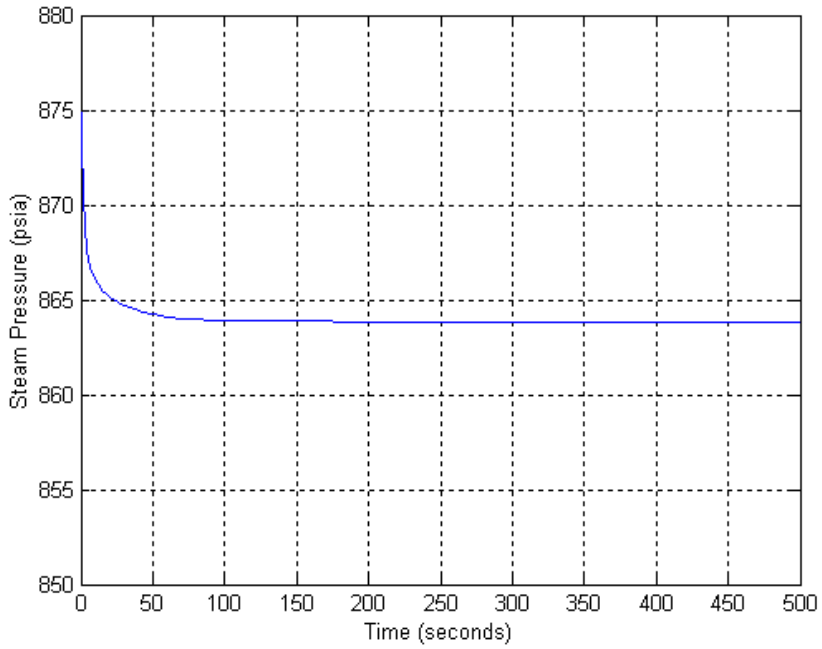

Figure 3.11. Steam Pressure Change When Decreasing the Overall Heat Transfer Coefficient by 50% in the Metal-to-Secondary Side Boiling Heat Transfer Nodes (MTL3 and MTL6)

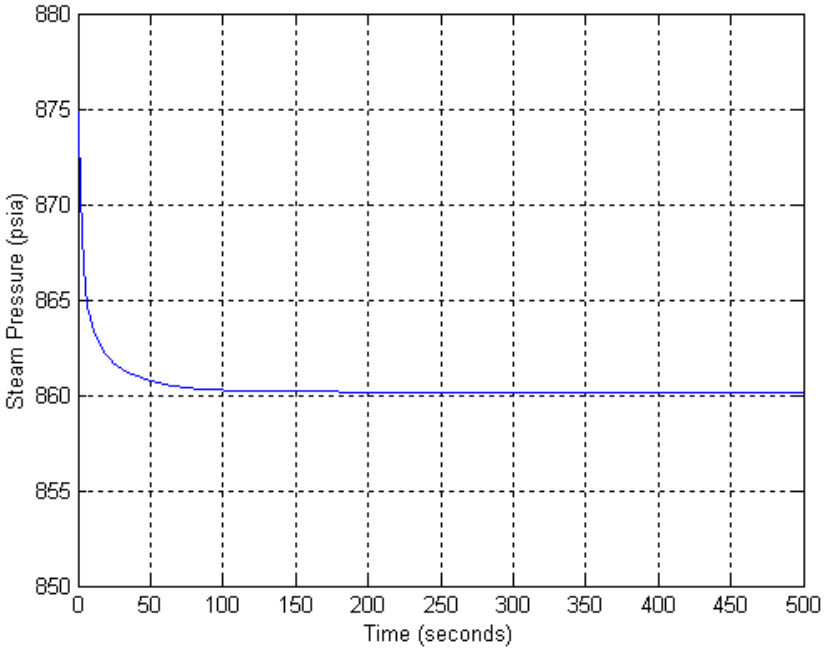

Figure 3.12. Steam Pressure Change When Decreasing the Overall Heat Transfer Coefficient by 50% in the Primary-to-Metal Side Boiling Heat Transfer Nodes (PRL3 and PRL6)

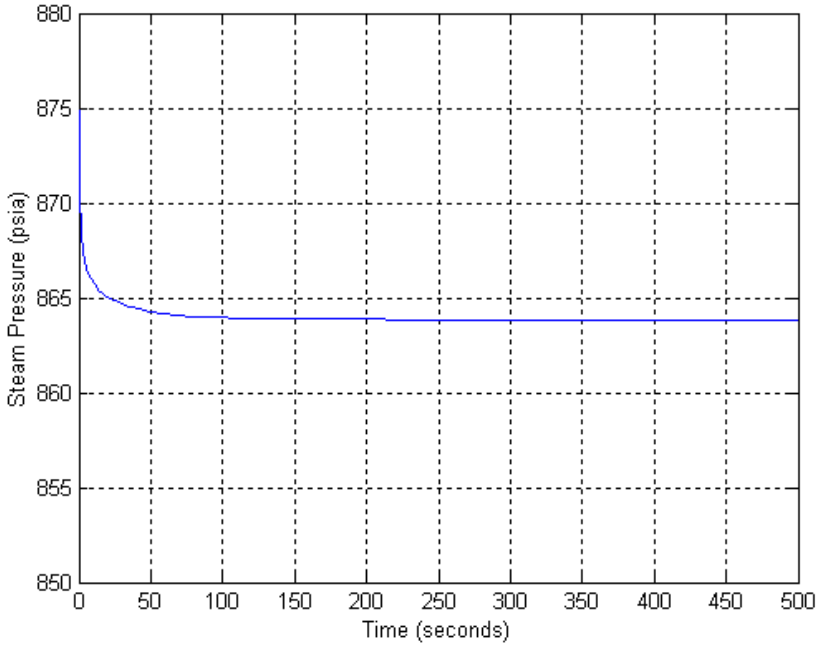

Figure 3.13. Steam Pressure Change When Decreasing the Overall Heat Transfer Coefficient by 50% in the Metal-to-Secondary Side Boiling Heat Transfer Nodes (MTL4 and MTL5)

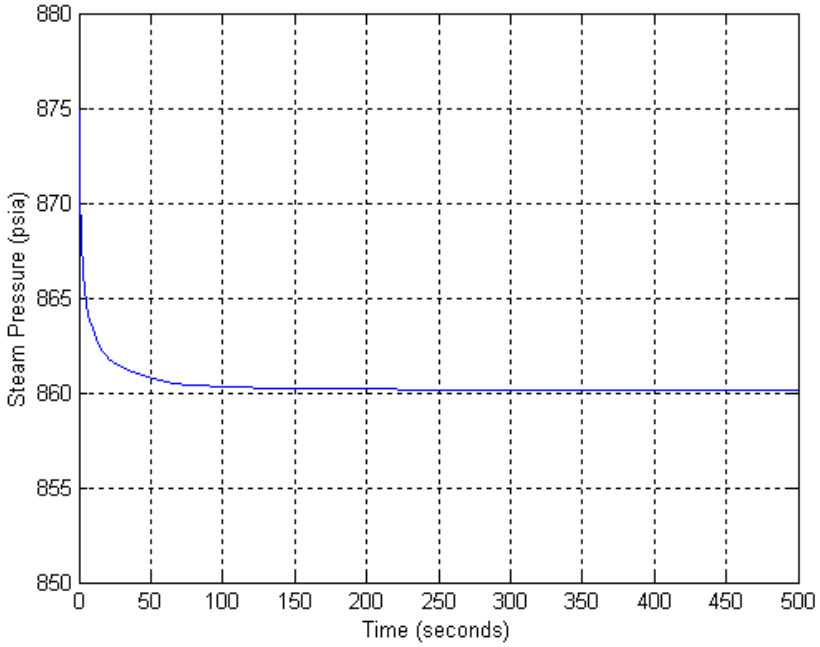

Figure 3.14. Steam Pressure Change When Decreasing the Overall Heat Transfer Coefficient by 50% in the Primary-to-Metal Side Boiling Heat Transfer Nodes (PRL4 and PRL5)

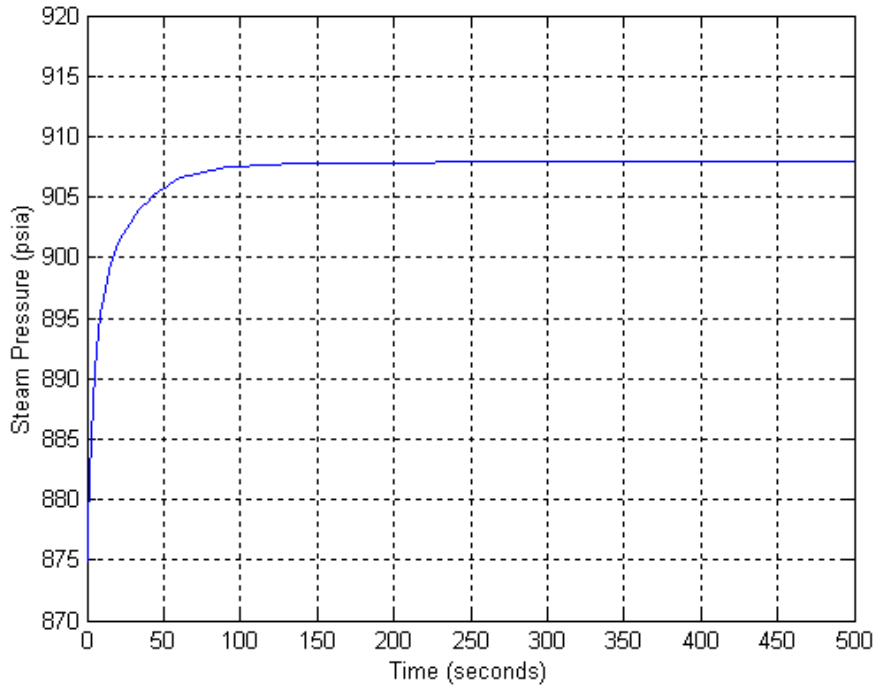

Figure 3.15. Steam Pressure Variation for a 10% Decrease in the Steam Valve Coefficient (Decreased Steam Flowrate)

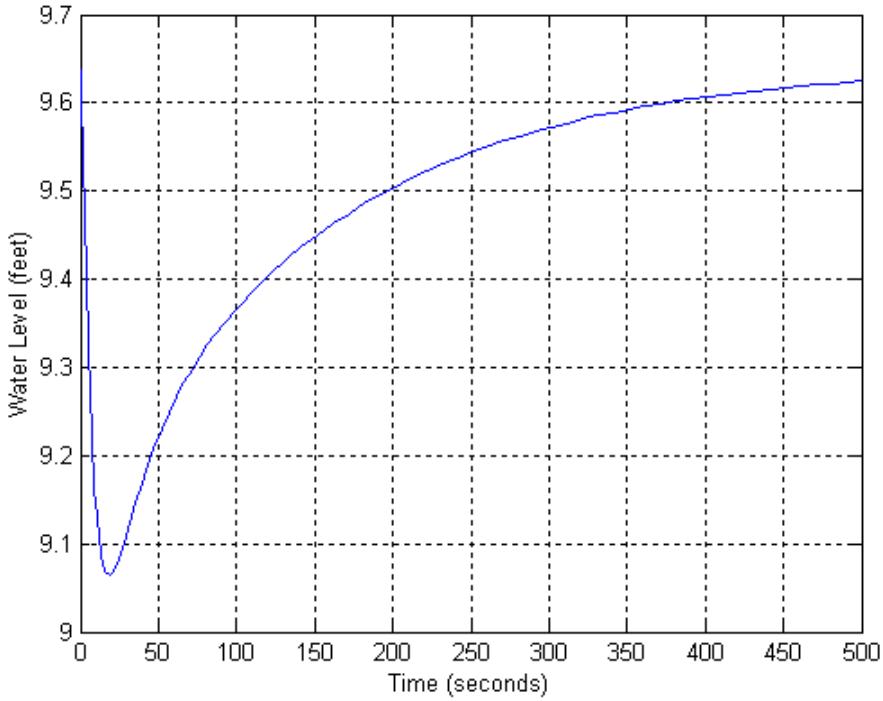

Figure 3.16. SG Water Level Variation for a 10% Decrease in the Steam Valve Coefficient

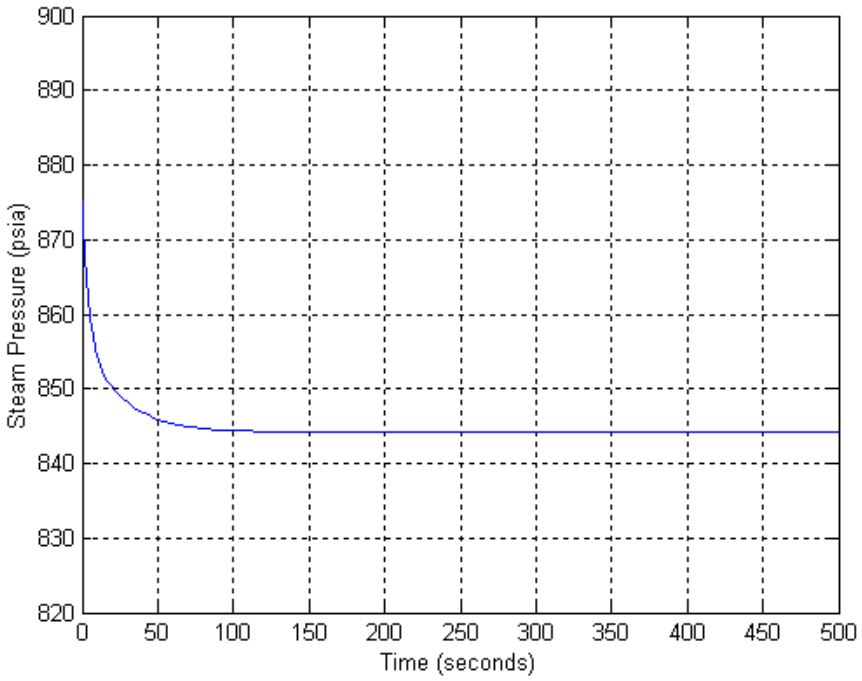

Figure 3.17. Steam Pressure Variation for a 10% Increase in the Steam Valve Coefficient (Increased Steam Flowrate)

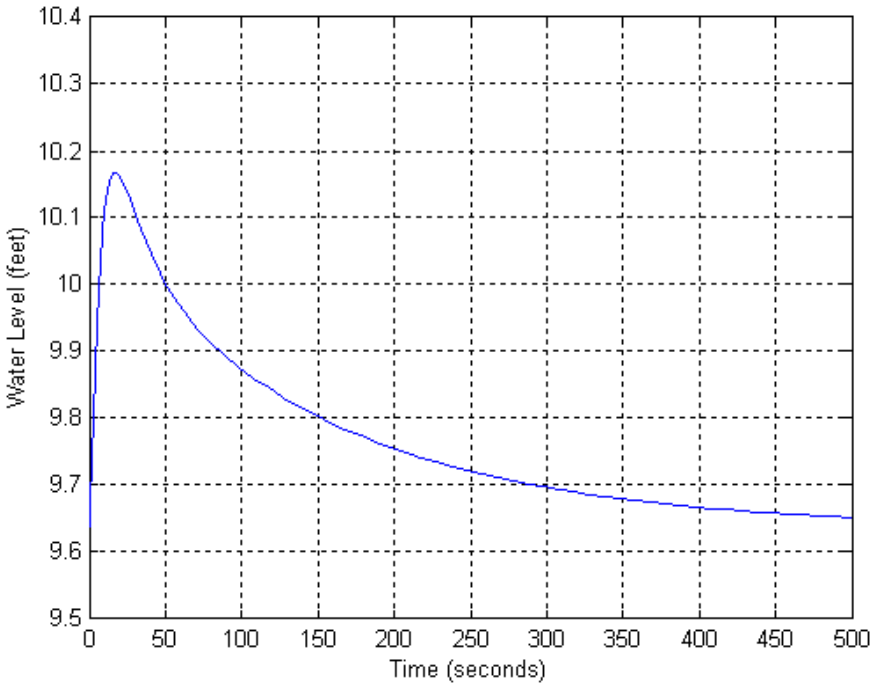

Figure 3.18. SG Water Level Variation for a 10% Increase in the Steam Valve Coefficient

Before we perform the simulations, we initially set the UTSG SIMULINK model system to balanced normal state. Then we simulate the UTSG responses to various parameter changes or defects by perturbing the related parameter(s) and then running the SIMULINK model system.

3.8 Remarks

The following observations are made from the above simulation results shown in Figures 3.5 - 3.18.

- For all the cases of decreased heat transfer area (tube plugging), decreased heat transfer coefficients (fouling) and decreased tube metal conductivity (material property), these always result in a decrease in the heat transferred from the primary coolant to the secondary coolant, which then leads to less steam production and therefore a decrease in the steam pressure.

- When we introduce an additional heat transfer resistance so as to decrease the overall heat transfer coefficient by 50% in the metal-to-secondary side sub-cooled heat transfer nodes (MTL1 and MTL8) or the primary-to-metal side sub-cooled heat transfer nodes (PRL1 and PRL8), the steam pressure decreases from 874.9 psia to 868 psia and 868.6 psia, respectively.

- When we introduce an additional heat transfer resistance so as to decrease the overall heat transfer coefficient by 50% in the metal-to-secondary side boiling heat transfer nodes or the primary-to-metal side boiling heat transfer nodes, the steam pressure decreases from 874.9 psia to about 863.8 psia and 860.1 psia respectively, and there is not much difference in the pressure changes caused by fouling at different axial locations within the boiling region.

- These results show that given the same percentage decrease in the overall heat transfer coefficient, we can differentiate the fouling in sub-cooled region and the boiling region. However, it seems difficult to identify the fouling at different axial locations within a specific heat transfer region.

- When there is either an increase or a decrease in the steam valve coefficient, we see the steam pressure quickly decreases or increases respectively and then reaches the respective new balanced value. However, the water level initially increases then under the action of the water level controller decreases and finally returns to the preset water level for the case of an increase in the steam valve coefficient. On the contrary, the water level initially decreases and then with the functioning of the water level controller increases and gradually returns to the preset water level for the case of a decrease in the steam valve coefficient. These are respectively due to the so-called swell and shrink phenomena, caused

by phase changes on the two-phase fluid flow.

- All the above simulation results for normal condition and for the cases of tube degradation are indicative of the high fidelity of the model. Hence the UTSG multi-node model can be used to appropriately simulate the UTSG dynamics and responses to certain defects or degradations, including the fouling problem. It can therefore be used to generate data for UTSG degradation monitoring and diagnosis.

Chapter 4

Particulate Fouling Model of a UTSG and Simulation of the Effects of Fouling on Thermal Performance

4.1 UTSG Particulate Fouling Model

As we determined from the review in Section 2, several mathematical models are available for simulation of fouling in simple tubing. However, very few models for steam generator fouling were developed. Liner et al (1992) [47] and Turner (1994) [48] developed a model for simulation of magnetite particulate fouling in nuclear steam generators. This model is described below.

The deposited mass per unit area is based on Cleaver et al's analysis (Cleaver et al (1976) [49]) of simultaneous deposition and re-entrainment of particles on a surface and is given by

$$M = (KC\rho\upsilon/(a(U^*)^2))(1-\exp(-a(U^*)^2 t/\upsilon)) \qquad (4.1)$$

According to Bowen et al (1979) [50] and Ruckenstein et al (1973) [51], the deposition rate, K, in the above equation is written as:

$$K = (1/K_t + 1/K_a)^{-1} \tag{4.2}$$

This equation basically means that particle deposition occurs by two steps in series: transport to the surface followed by attachment to the surface.

For a vertical surface (such as that of UTSG tubes), the transport coefficient K_t includes contributions from molecular plus eddy diffusion, inertial transport, thermophoresis, and boiling. These transport processes take place in parallel. Hence we have

$$K_t = K_d + K_i + K_{th} + K_b \tag{4.3}$$

The contribution to the particle transport by eddy plus molecular diffusion can be calculated from Cleaver et al (1975) [52]:

$$K_d = (Sc)^{-2/3} U^* / 11.9 \tag{4.4}$$

The inertial contribution to the particle transport rate is computed by

$$K_i = \frac{1}{500}\frac{U^* t_p^*}{5.23}\frac{\rho}{\rho_p}\exp(0.48 t_p^*) \qquad (4.5)$$

The dimensionless relaxation time t_p^* is given by

$$t_p^* = \frac{1}{18}\frac{\rho_p}{\rho}\left(\frac{U^* d_p}{\upsilon}\right)^2 \qquad (4.6)$$

The contribution from boiling to the particle transport rate can be estimated from the data of Asakura et al (1979) [53]:

$$K_b = bq/(h_{fg}\rho) \qquad (4.7)$$

The contribution from thermophoresis to the particle transport rate can be computed using the model by McNab et al (1973) [54]:

$$K_{th} = -\frac{0.26 h_c \upsilon (T_s - T_b)}{6(2k_f + k_p)T_b} \qquad (4.8)$$

The rate of particle attachment is given by

$$K_a = K_0 \exp(-E_a/(R * T_s)) \quad (4.9)$$

The unit thermal resistance (or fouling factor) caused by fouling is given by Kakac (1980) [55]:

$$R_f = M/(\rho_f k_f) \quad (4.10)$$

The various symbols are defined as follows:

C: Bulk particle concentration

d_p: Particle diameter

D: Diffusion coefficient

g: Acceleration due to gravity

h_c: Heat transfer coefficient

h_{fg}: Latent heat of vaporization

k_g: Thermal conductivity of liquid

k_p: Thermal conductivity of magnetite particles

k_f: Thermal conductivity of fouling deposit

K: Particle deposition coefficient

K_a: Attachment coefficient

K_b: Boiling deposition coefficient

K_d: Eddy diffusion coefficient

K_i: Inertial coasting coefficient

K_t: Transport coefficient

K_{th}: Thermophoresis coefficient

M: Deposited mass per unit area

q = Heat flux

R: Universal gas constant

Sc: Schmidt number

T_b: Bulk fluid temperature

T_s: Surface temperature

t: time

t_p^*: Dimensionless relaxation time

$U^* = \sqrt{\tau / \rho}$

τ : Surface shear stress

υ : Kinematic viscosity of liquid

R_f = Fouling resistance

Sc = Schmidt number = υ /D

ρ : Mixture density

ρ_p : Particle density

ρ_f : Density of fouling deposit

As experience has shown, the secondary side SG fouling is of a major concern (Stutzmann et al (2002) [30]), hence we have mainly simulated the secondary side SG tube surface fouling using the above mathematical model and related constants. The model has been implemented using MATLAB and simulations have been performed to simulate the progress of the secondary side SG tube surface fouling. The MATLAB code is given in Appendix C. The results are given in Figures 4.1 and 4.2. Comparing the results with those from [47] [48] and the typical heat exchanger fouling factor [56], we see that the results are comparable.

4.2. Effects of UTSG Fouling on Thermal Performance

In order to study the effect of secondary side tube fouling on UTSG thermal performance, we use the previously developed multi-node UTSG SIMULINK model for the simulation and use the above results for fouling simulation as part of the inputs. Finally the UTSG thermal performance variations versus time have been obtained.

The following important assumptions are made in the study:

- Only secondary side tube fouling on UTSG tubes is simulated.
- The distribution of fouling deposit along UTSG tube is uniform.
- The increase in pressure drop across the UTSG tube due to cross-sectional area

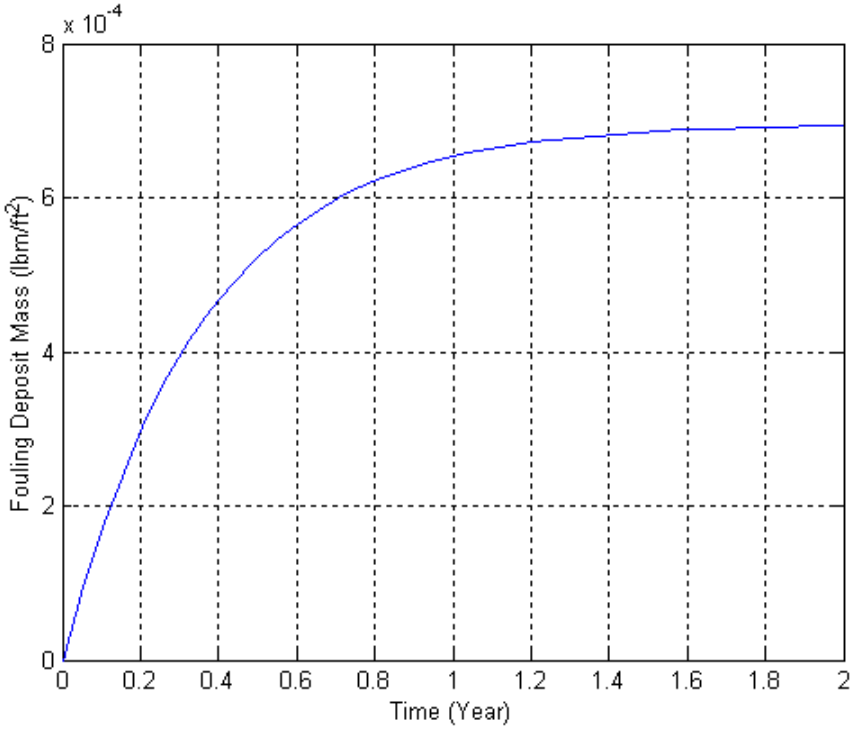

Figure 4.1. Fouling Deposit Mass Variation versus Time

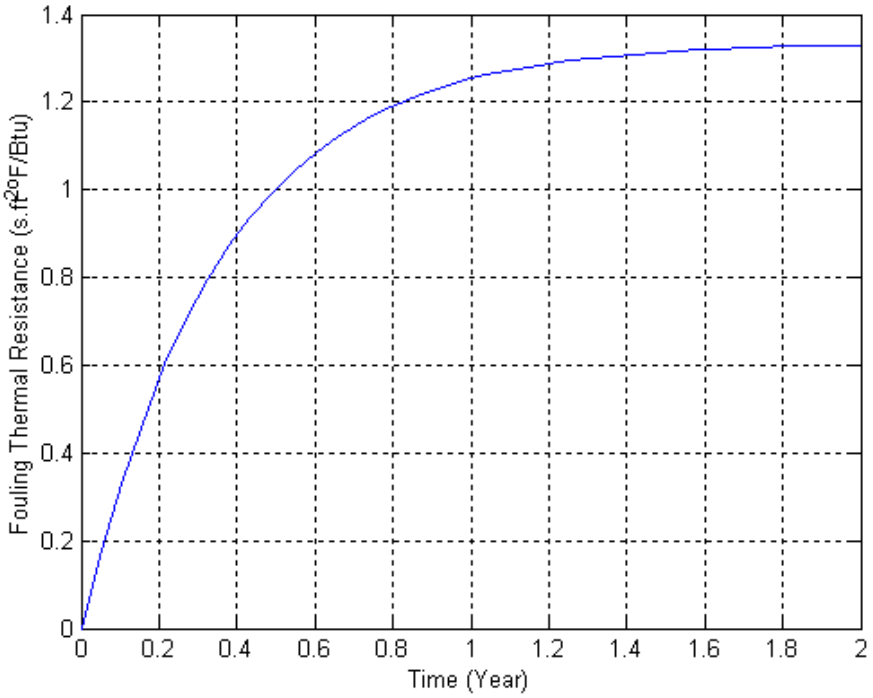

Figure 4.2. Fouling Thermal Resistance Variation versus Time

reduction caused by fouling deposition layer is not considered. This is reasonable since the flow area on the secondary side is relatively larger than on the primary side of UTSG.

Figure 4.3 shows the steam pressure variation versus time. Figure 4.4 presents the average heat flux (on outer tube surface) variation versus time. From the figures, we can see that as the UTSG secondary side tube fouling progresses and the thermal resistance due to fouling increases, both UTSG steam pressure and the average heat flux decrease until the fouling process reaches a steady state, that is, the fouling factor, the steam pressure and heat flux all asymptotically remain constant. From Figures 4.3 and 4.4, we see the following changes at system level as the fouling factor increases and reaches the steady state value of about 1.4 $s^{\bullet}ft^{2\bullet}°F/Btu$.

- The steam pressure decreases from 875 Psia to 798 Psia, indicating a percentage decrease of steam pressure by about 8.8%.

- The average heat flux on the outer tube surface decreases from 30.3 $Btu/(ft^{2\bullet}s)$ to about 27.7 $Btu/(ft^{2\bullet}s)$, indicating a percentage decrease of average heat flux by about 8.6%.

These results show that both the steam pressure and average heat flux have been changed by about the same percentage, nearly 9%, due to the secondary side tube fouling. This decrease in steam pressure is too large in practical plant operation, and

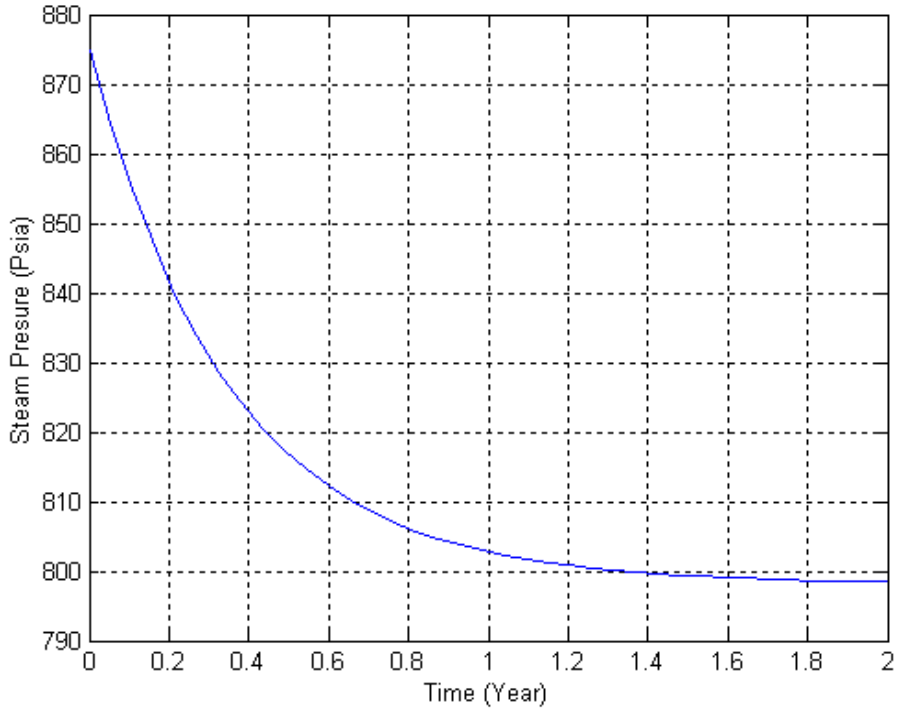

Figure 4.3. Steam Pressure Variation versus Time

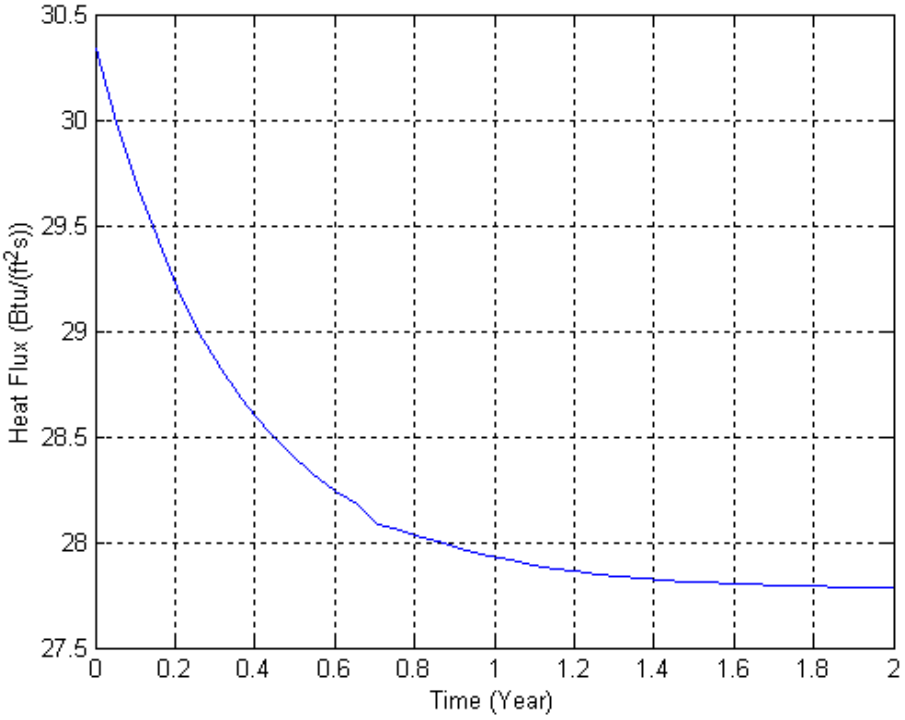

Figure 4.4. Average Heat Flux (on Outer SG Tube Surface) Variation versus Time

results in degraded plant performance and cannot produce the required steam for power generation. Hence, necessary measures, such as UTSG cleaning or improvement of the water chemistry, must be taken to recover the plant performance.

4.3 Remarks

From the above study on simulation of UTSG secondary side fouling and the effects on thermal performance, we can reach the following conclusions:

- Since fouling may involve different kinds of mechanisms simultaneously, there does not exist a generally applicable mathematical model for modeling of fouling involving several fouling mechanisms. For example, to simulate fouling due to corrosion products, we have to study the physical process of corrosion. In up-to-date study, we have only simulated the UTSG particulate fouling. The simulation results are excellent and match with the expected behavior.

- The effect of fouling on UTSG thermal performance can be studied using the previously developed multi-node SIMULINK model if the fouling process can be appropriately simulated by a model. The simulation results can be used for the prediction of UTSG thermal performance and scheduling of the USTG maintenance activities. For example, according to Figure 3.4 we can infer when the steam pressure is supposed to decrease by a certain percentage and we can

decide that proper UTSG maintenance or other actions are needed so as to recover the satisfactory UTSG thermal performance without delay.

Chapter 5

Experimental Study of Particulate Fouling in a Heat Exchanger

5.1 Introduction

In this chapter, we first make a review of experimental study of particulate fouling by earlier investigators. Our goal of this research on fouling is to study the fouling behavior, verify the particulate fouling model through a laboratory experiment and collect the experimental fouling data for monitoring and diagnosis of fouling. In order to accomplish this task, we adapted a previously developed laboratory setup to perform experimental studies of particulate fouling in a small-scale heat exchanger. In this chapter, we present a literature review of experimental studies of particulate fouling, description of the experimental setup, and the experimental results.

5.2 Review of Experimental Study of Particulate Fouling in Heat Exchangers

Several researchers have performed experiments to study the particulate fouling. Here we review some representative work from the literature.

Melo et al (1988) [57] studied particle transport in fouling on copper tubes. They used the material KAOLIN to simulate suspended particles in water. Their fouling

tests were performed in an annular heat exchanger consisting of a 2-meter long external Perspex tube and a removable inner copper tube, which was electrically heated. Water-KAOLIN suspensions were circulated through the annular section at different Reynolds numbers. KAOLIN particles were studied with a laser flow granulometer and a scanning electron microscope (SEM) and the fouling layer was roughly characterized as a thin disc with 16 μm (mean diameter) by 1 μm (mean thickness). SEM visualization of the deposits formed on the copper tube surfaces showed that the particles adhere by their larger faces (the bases of the disc). The thermal conductivity, density, final thickness, mass, and thermal resistance were measured or estimated. The experimental results show that the fouling data fit well into the asymptotical behavior and mass transfer controls the deposition rate when Re < 3900, and the adhesion dominates the process at higher Re values.

Middis et al (1990) [58] performed experimental study on particulate fouling in heat exchangers with enhanced surfaces. In their study, KAOLIN particles in X-2 were chosen as the fouling suspension. They studied the particulate fouling in a plate heat exchanger and a double pipe heat exchanger over a wide range of flow conditions. The fouling experimental results again show that the fouling progression follows a characteristic asymptotic behavior. They also studied the effect of Reynolds number and other factors on fouling behavior, and the conclusions are similar to those reached by

Melo et al [57].

Charmra et al (1993) [59] made a study on the effect of particle size and size distribution on particulate fouling in tubes. In their study, the Wieland NW, Wolverine Korodense, and a plain tube were chosen for testing. Two types of foulants, clay and silt, were used in the tests. The fouling tests were conducted for different concentrations, flow rate, foulant type, and particle diameter. Their experimental results show that the enhanced tubes exhibit higher fouling resistance than the plain tubes; the enhanced and the plain tubes exhibit the same fouling behavior, and the fouling resistance decreases as the concentration decreases for all particle sizes. This is because the deposition rate decreases as the concentration decreases since the deposition rate is proportional to fouling concentration. In addition, as the particle size (diameter) increases, the asymptotic fouling resistance decreases. This is because the particle deposition rate is proportional to $Sc^{-0.57}$, where the Schmidt number Sc is defined as the ratio of the kinematic viscosity over the Brownian diffusivity. Hence smaller particles will have smaller Schmidt numbers and should undergo higher deposition rates (fouling resistances) than larger particles. The experiments also show that the asymptotic fouling resistance, R_f^*, as a function of Reynolds number for the Korodense tube, decreases as the Reynolds number increases. This is because the removal rate is directly proportional to the wall shear stress. Therefore, as the Reynolds number increases, the wall shear stress

increases, which in turn increases the removal rate, and as a result the fouling resistance decreases. Again, the results also show that the fouling resistance decreases as the particle diameter increases. It is also shown that the fouling resistance increases as the particle size decreases. For example in their results, the asymptotic fouling resistance for the 16 μm particles is significantly smaller than that for the 4 μm particles except for the plain tube. This is due to the transition from the diffusion dominant regime to the inertia dominant regime. It is also found that the enhanced tubes (NW and Korodense tubes) have higher asymptotic fouling resistances than the plain tube.

There are other researchers who used other types of material to simulate the fouling particles. Among them, Muller-Steinhagen et al (1988) [60] used Al_2O_3 particles to study particulate fouling in heat exchangers. Basset et al (2000) [61] used the sol-gel method, proposed by Sugimoto et al (1980) [62], to synthesize the simulated magnetite particles to study the fouling of Alloy-800 heat exchanger surfaces by magnetite particles, etc. Turakhia et al (1984) [65] studied measurement and diagnosis of the fouling of heat exchanger surface using the pressure drop method and the overall heat transfer resistance method.

It should be noted that most of the above researchers only used a single tube or even a tube section in their experimental study. Hence it is necessary to use a real heat exchanger to study the particulate fouling behavior.

5.3 Current Experimental Setup for Particulate Fouling Tests

As mentioned above, we want to use a real heat exchanger and perform experiments to study the particulate fouling behavior. For this purpose we have designed and adapted an experimental setup. Figure 5.1 shows the schematic of this setup, and Figure 5.2 shows a photograph of it. In our experiment, we have used KAOLIN clay suspended in water and a small-scale tube-and-shell heat exchanger. The particulate material is the RC-90 KAOLIN from Thiele KAOLIN Company. The particle size is $< 2\ \mu m$ with a percentage of 98.0% and a pH (dry clay tested at 20% solids) of 6.8. The heat exchanger, HT-1-A-CI-2-24, was procured from Mahan's Thermal Products, Inc. It has 31 copper tubes, with shell diameter $2\frac{1}{8}$ inch, tube length 24 inch, and tube outer diameter $1/4$ inch.

As seen in Figures 5.1 and 5.2, the experimental setup consists of a stainless steel water tank, a 2 KW electrical heater, a stainless steel centrifugal pump, a shell-and-tube heat exchanger, two flow-meters measuring the tube-side and shell-side flow rates, four thermocouples measuring the inlet and outlet temperatures of the tube-side and shell-side coolant, and a data acquisition system. The data acquisition system includes two conditioning modules, a connection box, a data acquisition board, and a personal computer. A LabVIEW data acquisition software is used to collect, display, and store

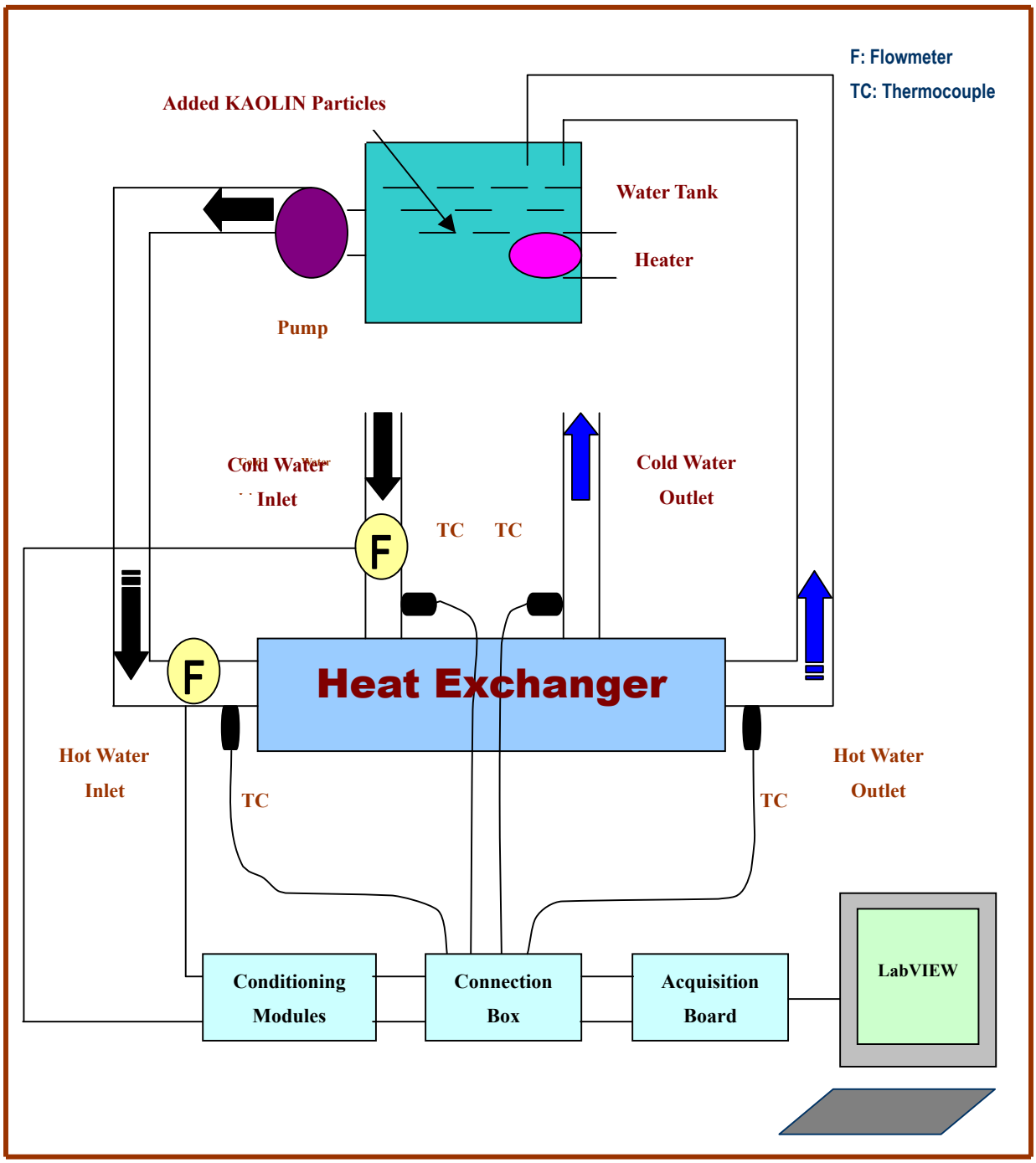

Figure 5.1. Configuration of the Heat Exchanger Experimental Set-up for Particulate Fouling Tests

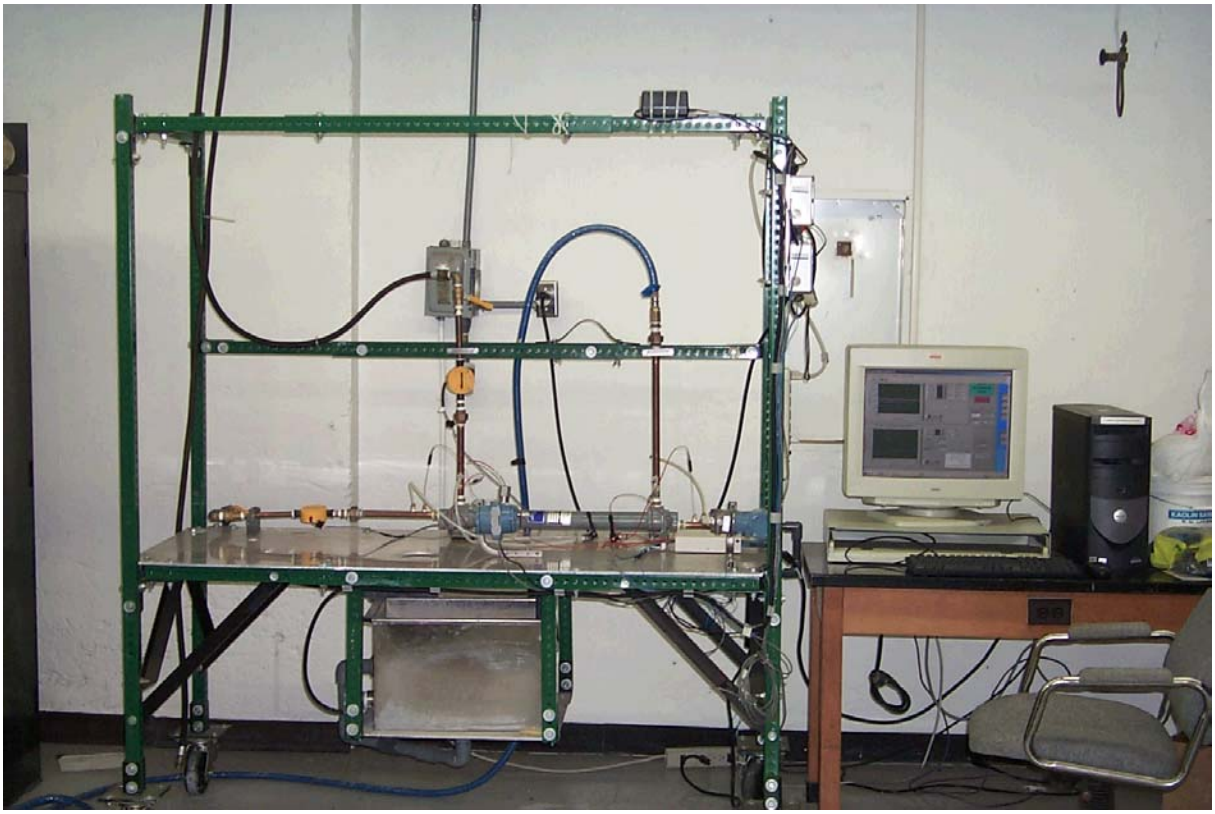

Figure 5.2. An Overview of the Experimental Setup

the experimental data. Water, mixed with KAOLIN particles, is designed to flow through the tube side of the heat exchanger so that it is convenient to remove or wash off the fouling layer after the experiment is completed. Figure 5.2 shows the heat exchanger on the mobile table, water tank (underneath the table), connections to hot and cold water lines, and the data acquisition computer system.

5.4 Calculation of Overall Thermal Resistance and Experimental Results

The effect of the fouling progression can be monitored by continuously evaluating the overall heat transfer thermal resistance (1/UA). From energy balance, we have

$$\dot{Q} = UA\Delta T_{LMTD} = \dot{m}_h C_h \Delta T_h = \dot{m}_c C_c \Delta T_c \qquad (5.1)$$

Where, $\dot{Q}$ is the heat transfer rate;

A is the surface area on which the overall heat transfer coefficient U is based;

ΔT_{LMTD} is the logarithmic mean temperature difference for the heat exchanger and is defined as:

$$\Delta T_{LMTD} = \frac{\Delta t_1 - \Delta t_2}{\ln(\Delta t_1 / \Delta t_2)} \qquad (5.2)$$

For parallel or concurrent flow heat exchangers:

$$\Delta t_1 = t_{h,in} - t_{c,in}\,;\;\; \Delta t_2 = t_{h,out} - t_{c,out}\,. \tag{5.3}$$

For counter flow heat exchangers:

$$\Delta t_1 = t_{h,in} - t_{c,out}\,;\;\; \Delta t_2 = t_{h,out} - t_{c,in}\,. \tag{5.4}$$

As stated above, U is the overall heat transfer coefficient, and A is the heat transfer area, which may slightly change with fouling progress. However, the product UA can be calculated and be thought of as inseparable in terms of the effect of fouling on heat transfer. The inverse of UA is the overall thermal resistance, which increases as the fouling deposition increases.

From Equation (5.1), we can derive the following formula for calculation of the overall thermal resistance:

$$\frac{1}{UA} = \frac{\Delta T_{LMTD}}{\dot{m}_h C_h \Delta T_h} = \frac{\Delta T_{LMTD}}{\dot{m}_c C_c \Delta T_c} \tag{5.5}$$

This overall thermal resistance, 1/(UA), is continuously computed so as to monitor the particulate fouling behavior in the heat exchanger. To determine the overall thermal resistance, we measure the mass flow rate of the cold side or/and the hot side, inlet and outlet temperatures of both the cold side and the hot side, as shown in Figures 5.1 and 5.2. In our calculation of overall thermal resistance, we used the cold-side flow rate and the inlet and outlet temperatures. It should also be noted that in our

experimental design, we have used the parallel flow pattern in the heat exchanger.

In our experiment, initially 70gm KAOLIN particles were added to the water tank then at about 50 hours after the start of the experiment, another 50 gm were added to the tank, which has a dimension of 18" × 12" × 12". This resulted in a fairly high concentration of about 2823 ppm.

The experiment was run for about 170 hours. A MATLAB code is used to process the experimental data and to calculate the overall thermal resistance. The code is given in Appendix D. Figure 5.3 gives the raw signals that were measured and collected during the experiment. Figure 5.4 presents the experimental results of the changes in the overall thermal resistance with time. During the whole experiment, the coolant flows of both the tube-side and the shell-side were basically kept constant.

It should also be indicated that since there is background noise present in the measurements, we used a MATLAB function to filter the computed overall fouling resistance. Thus it looks "smoother" as shown in Figure 5.4.

From Figure 5.4, we see that the overall fouling resistance first increases with time, then at after about 120 hours of running it tends to attain a steady state value. This proves that the overall thermal resistance exhibits an asymptotic behavior even in a real small-scale heat exchanger.

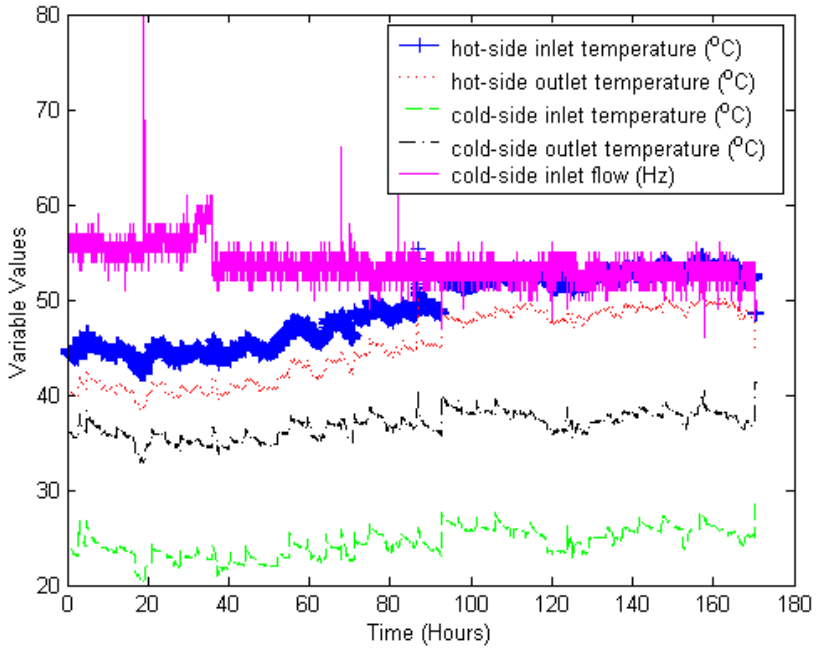

Figure 5.3. Experimental Results—The Measured Raw Signals From the Experiment

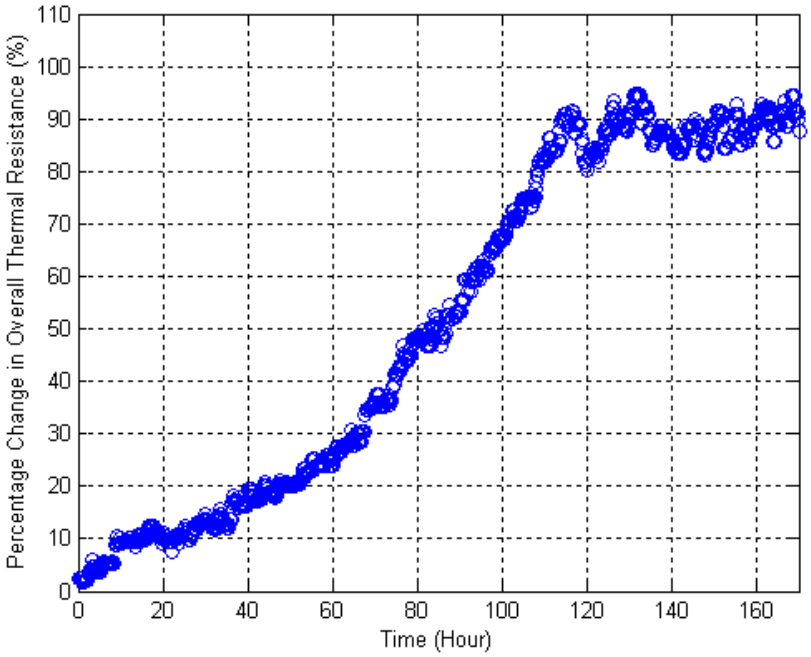

Figure 5.4. Experimental Results—The Overall Thermal Resistance Variation vs. Experimental Running Time

5.5 Overall Thermal Resistance after Removal of the Fouling Deposition Layer

After the experiment was completed, we opened the heat exchanger and used brushes to remove and wash off the fouling layers that attached to the inner surfaces of all the 31 heat exchanger tubes. Then we ran the experiment again for a while and used the same method as above to monitor or track the change in overall thermal resistance of the heat exchanger. The results are shown in Figures 5.5 and 5.6. It should be noted that Figure 5.6 is just a local zoom of Figure 5.5. The objective is to show more clearly the change in the overall thermal resistance of the heat exchanger. From these two figures, we can clearly see that the overall thermal resistance of the heat exchanger after cleaning restores to the overall thermal resistance value of the previous clean state. This confirms that the change in overall thermal resistance of the heat exchanger that we observed during the experiment was really due to the fouling progression. This also indicates that we can successfully monitor the fouling progression in a heat exchanger by tracking the changes in the overall thermal resistance.

5.6 Remarks

From the above experimental study on particulate fouling and its time progression in a small-scale heat exchanger, we make the following observations.

- The particulate fouling in a small-scale heat exchanger still exhibits an asymptotic

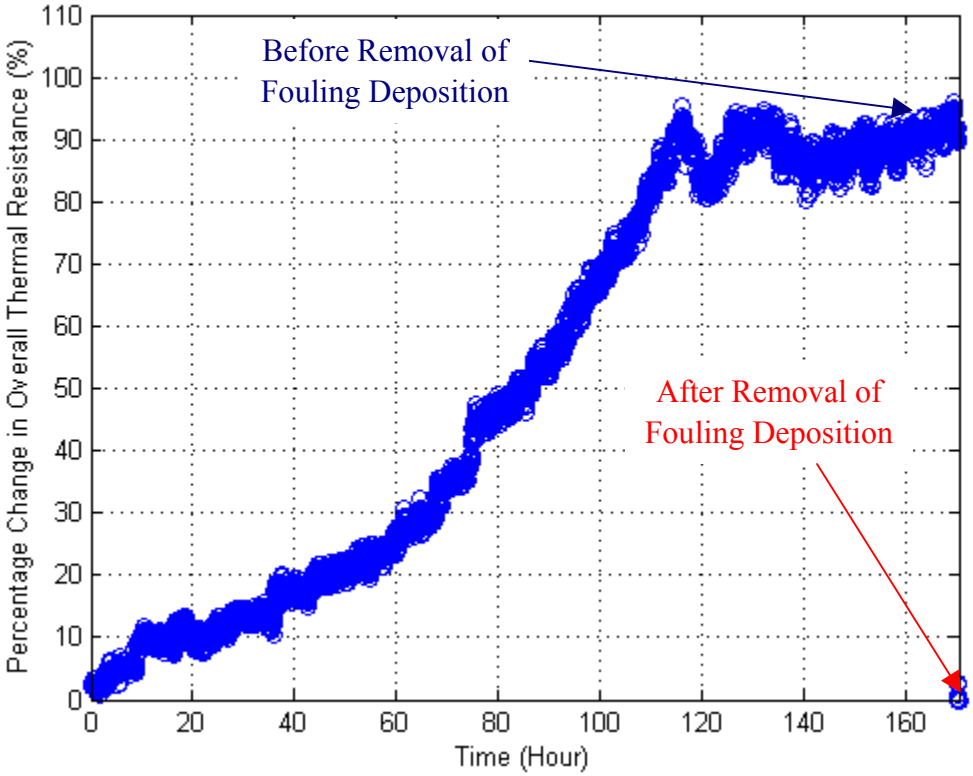

Figure 5.5. Change in Overall Thermal Resistance of the Heat Exchanger before and after Removal of the Fouling Deposition Layers

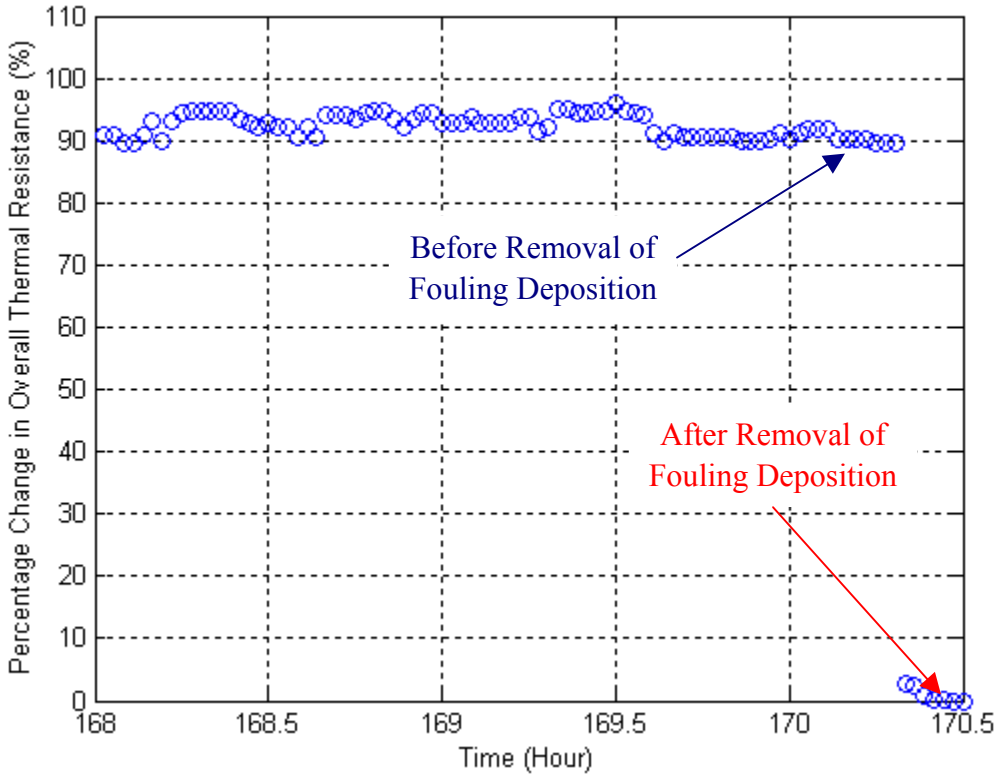

Figure 5.6. Change in Overall Thermal Resistance of the Heat Exchanger before and after Removal of the Fouling Deposition Layers

(A local zoom of Figure 5.5.)

behavior. This agrees with the conclusion from theoretical studies. It should be noted that in Figure 5.3, the overall thermal resistance does not seem to follow a strict exponential trend. This is most likely due to our change (increase) in the fouling particle concentration at about 50 hours after the start of the experiment.

- All the above results show that the experimental methodology and design of the setup for particulate fouling study are correct and successful. It has been demonstrated that the particulate fouling in a heat exchanger can be monitored and diagnosed by tracking the change in the overall thermal resistance.

- The acquired experimental data are useful and can be used for the monitoring and diagnosis of fouling in the heat exchanger using the GMDH modeling techniques. This is discussed in detail in Chapter 6.

Chapter 6

Monitoring and Diagnosis of Fouling Using the GMDH Method

6.1 Introduction

The Group Method of Data Handling (GMDH) method has found wide applications in various areas, such as data mining, forecasting, prediction and system modeling, pattern recognition, and fault detection and isolation (FDI). GMDH is an inductive self-organizing algebraic model since we do not need to know the exact physical model in advance. Instead, GMDH automatically learns the relations that dominate the system variables during the training process. Therefore a good GMDH model can be used to avoid the need for the development of a first-principle model, especially when this model is costly or even impossible to develop for a very complex system. After a reliable GMDH model is developed, it can be then used for FDI or many other purposes as mentioned above.

In later sections of this chapter, we first present a brief introduction to the GMDH approach, then we use the GMDH method and the MATLAB functions previously developed by Ferreira and Upadhyaya (1998) [67] to monitor and diagnose the fouling problems occurring in both a heat exchanger and a steam generator.

6.2 GMDH Methodology

GMDH is a data-driven modeling technique, which uses mathematical functions to characterize the complex nonlinear relationships that are inherent among the given input-output mapping. It uses the following so-called Kolmogorov-Gabor polynomial form to approximate the input-output mapping:

$$y = a_0 + \sum_{i=1}^{n} a_i x_i + \sum_{i=1}^{n}\sum_{j=1}^{n} a_{ij} x_i x_j + \sum_{i=1}^{n}\sum_{j=1}^{n}\sum_{k=1}^{n} a_{ijk} x_i x_j x_k + \ldots \quad (6.1)$$

Where, $\{x_1, x_2, \ldots, x_n\}$ is the input variable vector;

y is the output variable;

$\{a_0, a_i, a_{ij}, \ldots\}$ is the vector of coefficients or weights.

Additional input variables may also be formed from the basic measurements [67].

A polynomial network of GMDH structure with m inputs and k layers is shown in Figure 6.1. The main procedure for GMDH algorithm implementation used for a given set of n observations of m independent variables is described as follows [67-68]:

Step 1:

Subdivide the data into training data set and testing data set and preprocess the

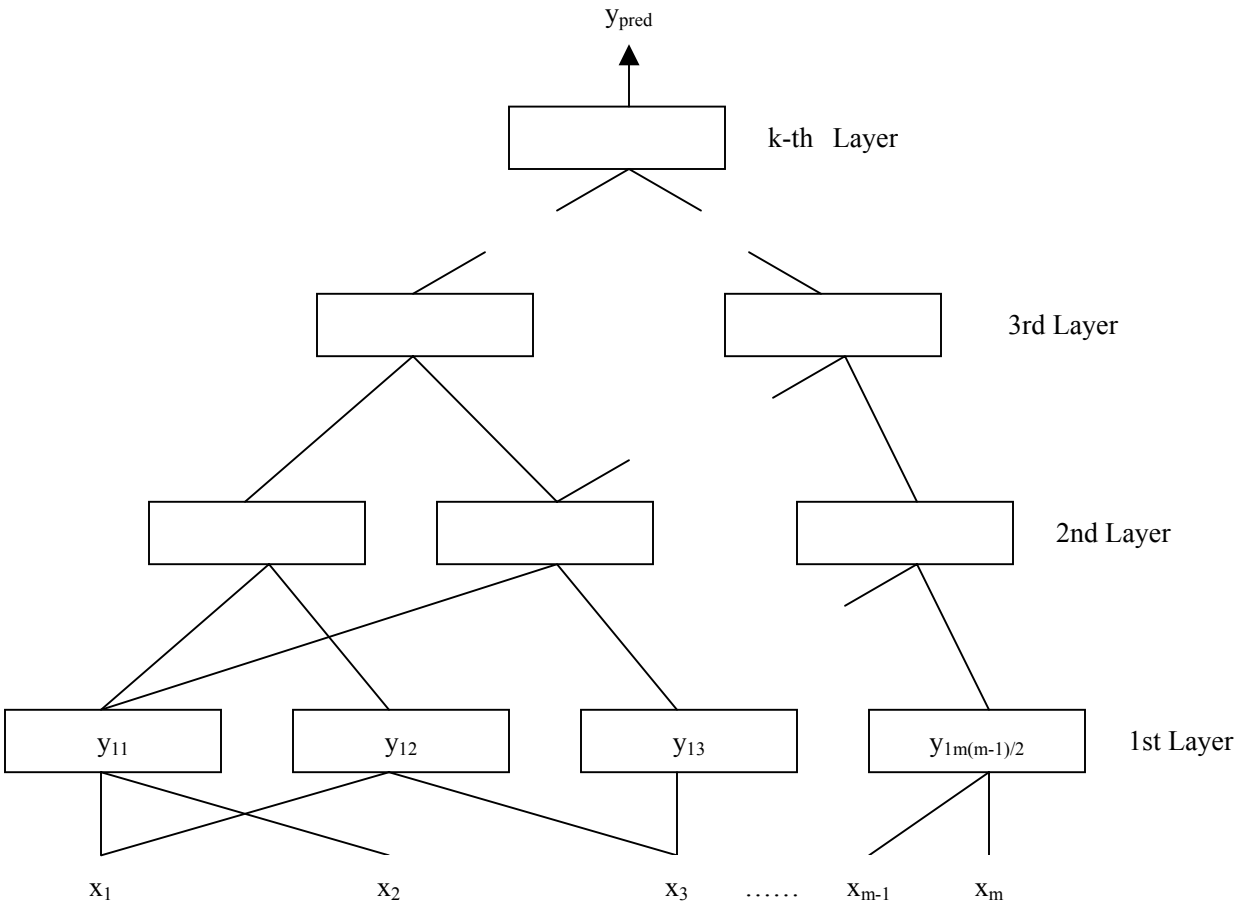

Figure 6.1. The GMDH Network Structure

(From Ref. [67])

data sets by normalizing them.

Step 2:

For each pair of input variables x_i and x_j and associated output y of the training data set, calculate the regression polynomial

$$y = A + Bx_i + Cx_j + Dx_i^2 + Ex_j^2 + Fx_i x_j \qquad (6.2)$$

that best fits the dependent observations y_i in the training set. A total number of $m(m+1)/2$ regression polynomials will be computed from the observations.

Step 3:

For each regression, evaluate the polynomial for all n observations and store these n new observations in a new matrix Z. That is, recalculate current layer's output using all data sets with the parameters generated in step 2, and store these outputs in a new matrix Z as the new input terms for the next layer of the GMDH architecture.

Step 4:

Screening out the least effective variables: First, for each column of the matrix Z, the root mean square error is computed and is given by:

$$r_j^2 = \frac{\sum_{i=1}^{n} \left(y_i - z_{ij}\right)^2}{\sum_{i-1}^{n} y_i^2} \qquad (6.3)$$

Then order the columns of Z according to increasing r_j, and pick those columns of Z that satisfy $r_j < R$ to replace the original columns of X. Here, a cut-off value 'R' needs to be chosen by the user. This means that all the columns of Z satisfying $r_j < R$ are picked to replace the input terms in the previous layer, while all the variables with $r_j > R$ are screened out and are not passed to the next generation of the algorithm.

Step 5:

Testing for optimality: The above procedure is repeated until overfitting starts to occur, which can be checked by cross validation, that is, by plotting the smallest of the r_j's calculated in each generation and comparing it with the smallest r_j's of the previous generation. The process should be stopped when the r_j's begin to increase.

At the completion of GMDH algorithm, all quadratic regression polynomials are stored, and the estimated coefficients for high order polynomial are determined through back tracing the GMDH architecture until the original variables ($x_1, x_2, \ldots, x_n$) is reached. Then we can use this GMDH model to make new predictions of y.

More details of GMDH algorithm and its implementation are given by Ferreira and Upadhyaya (1998) [67], Lu (2001) [68], Ivakhnenko (1995) [69] and Kondo (2003) [70]. In the following sections of this chapter, we will use the MATLAB functions GMDH_PBK, ANNt_PBK, etc., developed by Ferreira and Upadhyaya (1998) [67], to monitor fouling degradation in both HX and UTSG systems.

6.3 Data Generation

To monitor and diagnose degradations including fouling in a heat exchanger or UTSG, it is first necessary to generate data for the development of good data-driven models. In order to generate data, an appropriately developed first-principle model is essential.

In our study, for the heat exchanger, we use the energy (heat) balance equations, as defined by Equations (5.1) - (5.3) for the case of parallel flow, to generate the normal data. The MATLAB code is given in Appendix E. The experimental data, characterizing the progress of fouling in a heat exchanger, were collected from the experimental setup and is used for monitoring and diagnosis of fouling in the heat exchanger using GMDH method. When generating normal data for HX, the coolant flow on both the tube-side and the shell-side were kept constant as was the case during the experiment, and only the inlet temperatures of both sides were chosen as the forcing

(input) variables.

For the UTSG, we have already developed a good model in Chapter 3. We have used this SIMULINK model to generate both normal data and the data with the presence of fouling, which is assumed to progress with time as given in Figures 4.1 and 4.2. These data are used for monitoring and diagnosis of fouling in a steam generator using the GMDH method. When generating the normal data, both the tube-side inlet temperature and the number of heat transfer tubes were chosen as forcing variables; and an additional fouling thermal resistance was added when generating data for fouling.

It should be noted that when generating the data, all the input forcing variables should cover the entire desired space. Otherwise, a good data-driven model cannot be properly developed.

6.4 Monitoring and Diagnosis of Fouling in the Heat Exchanger

Now that both the normal data and data with fouling are available, we first use the GMDH method to develop a data-driven model and then use the model to monitor and diagnose the fouling progress. The MATLAB code for monitoring and diagnosis of fouling in the heat exchanger is given in Appendix F.

The procedure is first to establish a data-driven model using the normal data, then

use this model and the faulty data, i.e. the experimental data characterizing the fouling progress, to make predictions and estimate residual of the outlet temperatures of both the tube-side and the shell-side.

Figure 6.2 gives the hot-side or the tube-side outlet temperature data used for training and the GMDH predicted values; Figure 6.3 presents the hot-side or the tube-side outlet temperature data used for testing and the GMDH predicted values. We see from these two figures that they both agree with each other very well.

After development of the GMDH model, we use the experimental data and the model to make new predictions. Figure 6.4 gives the GMDH predictions of the hot-side outlet temperature of the heat exchanger versus the real experimental data of the same variable. Figure 6.5 presents the estimate residual. From Figure 6.4 and Figure 6.5, we can see that at the initial stage of the experiment, the predicted value and the measurements are almost equal to each other because there is little fouling at the early stage. Then as the fouling progress and gradually increases, the residual also increases. When finally the fouling reaches the asymptotical value and keeps basically constant, the residual also follows the same trend, coming to a steady-state value.

Comparing Figure 6.5 with Figure 5.14, it is interesting to note that the GMDH

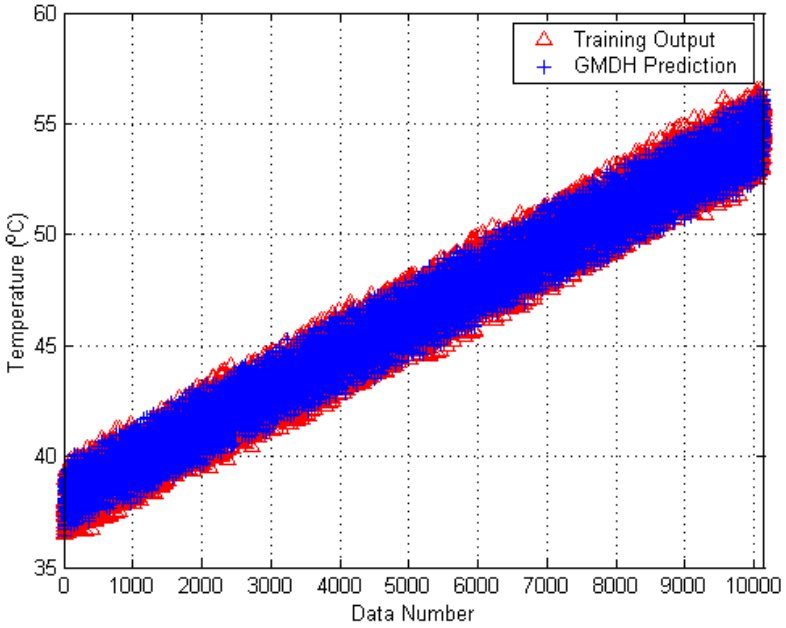

Figure 6.2. The Training Output and the GMDH Predicted Values of the Tube-side/Hot-side Outlet Temperature

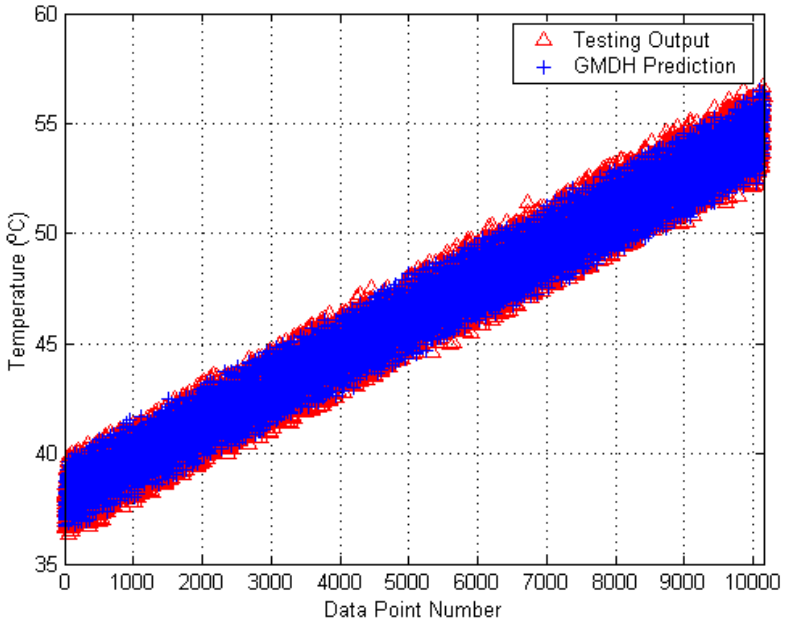

Figure 6.3. The Testing Output and the GMDH Predicted Values of the Tube-side/Hot-side Outlet Temperature

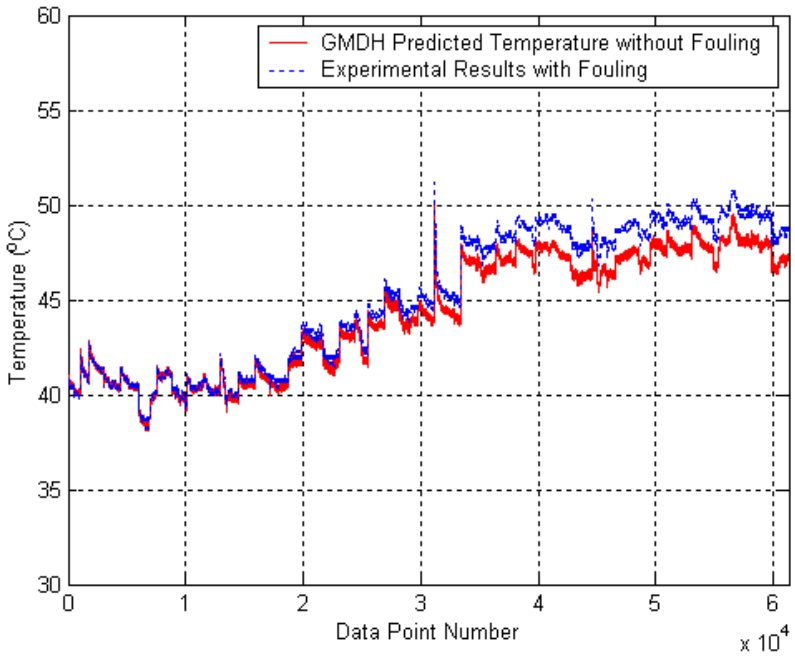

Figure 6.4. The GMDH Predictions of the Hot-side Outlet Temperatures of the Heat Exchanger versus the Real Experimental Data

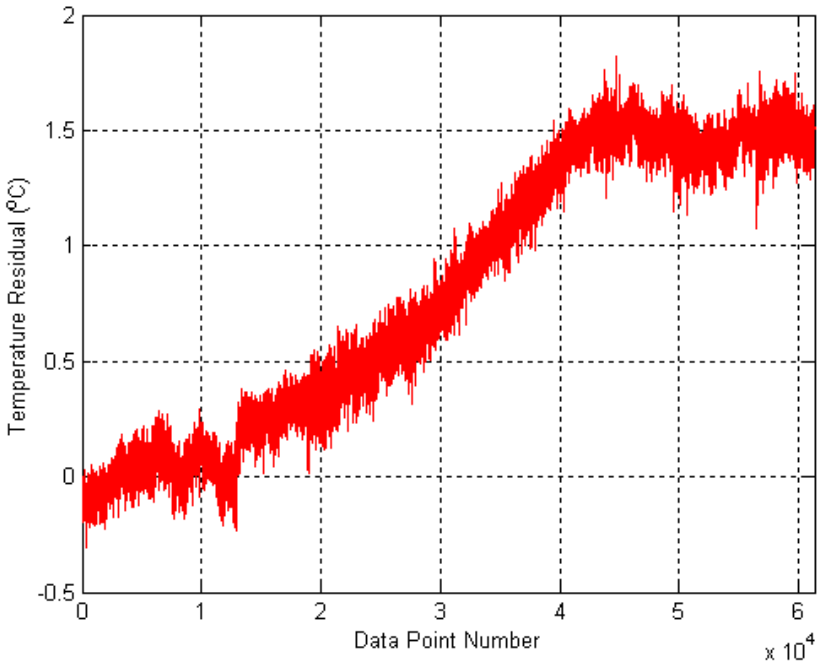

Figure 6.5. The Residual between the GMDH Predictions of the Hot-side Outlet Temperatures of the Heat Exchanger and the Real Experimental Data

estimation residuals follow the same behavior as the overall thermal resistance as a function of experimental running time.

Figure 6.6 gives the cold-side or the shell-side outlet temperature used for training and the GMDH predicted values; Figure 6.7 presents the cold-side outlet temperature used for testing and the GMDH predicted values. Also we can see from these two figures that they both agree with each other very well.

Then we use the experimental data and the developed GMDH model to make new predictions. Figure 6.8 gives the GMDH predictions of the cold-side outlet temperature of the heat exchanger versus the real experimental data of the same variable. Figure 6.9 shows the residuals. Again from Figures 6.8 and 6.9, we can see that at the initial stages of the experiment, the predicted values and the measurements agree very well with each other because there is very little fouling at the early stage. Then as the fouling progresses and gradually increases, the residual also increases. Finally the fouling reaches an asymptotical value and keeps almost constant, the residual also follows the same tendency and finally attains a steady state.

Comparing Figure 6.9 with Figure 5.14, again we find that the GMDH estimation residual follows the same behavior as the overall thermal resistance as a function of experimental running time.

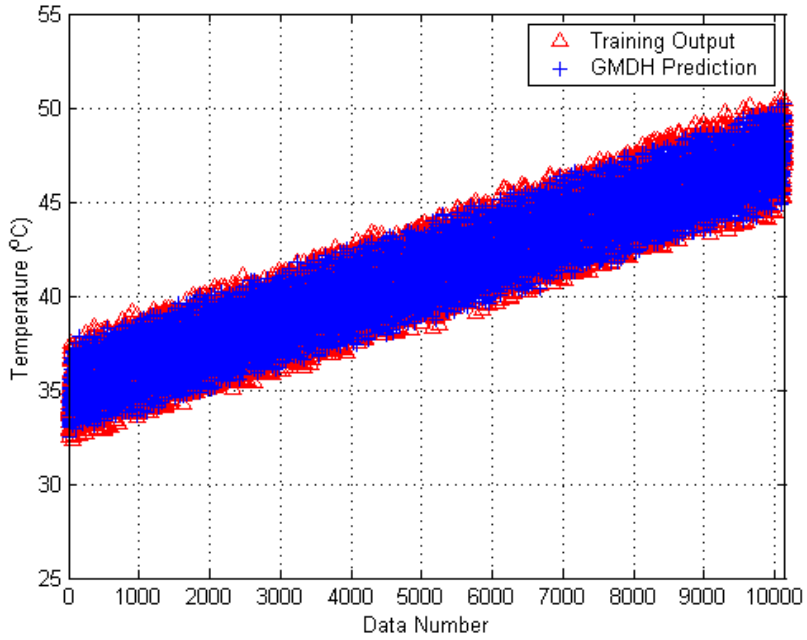

Figure 6.6. The Training Output and the GMDH Predicted Values of the Shell-side/Cold-side Outlet Temperature

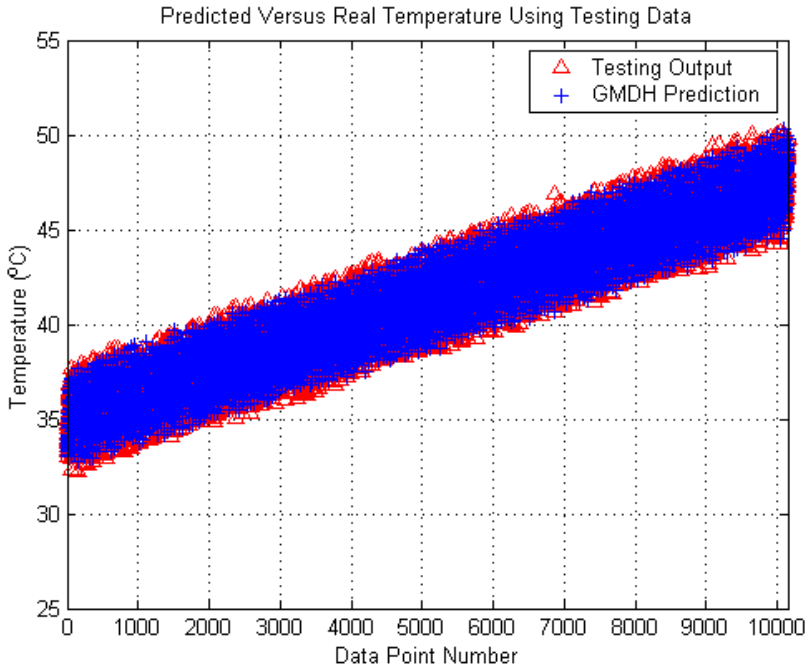

Figure 6.7. The Testing Output and the GMDH Predicted Values of the Shell-side/Cold-side Outlet Temperature

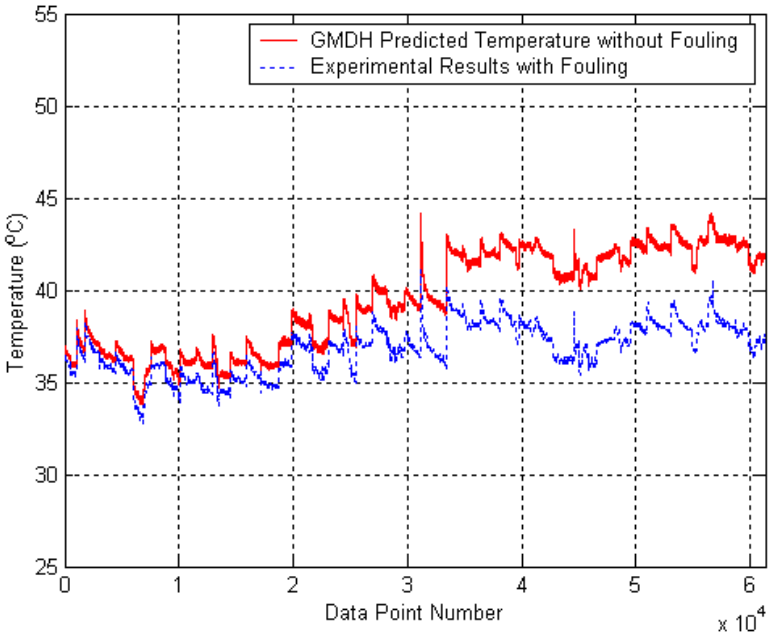

Figure 6.8. The GMDH Predictions of the Cold-side Outlet Temperatures of the Heat Exchanger versus the Real Experimental Data

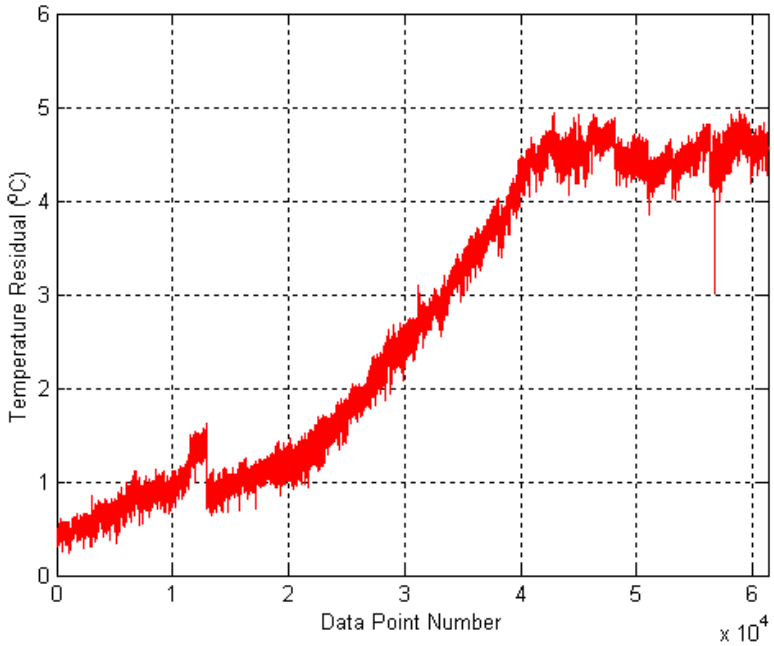

Figure 6.9. The Residual between the GMDH Predictions of the Cold-side Outlet Temperatures of the Heat Exchanger and the Real Experimental Data

These results suggest that we can easily use the residual trending given in Figures 6.4-6.5 and Figures 6.8-6.9 to monitor and diagnose the fouling problem that is occurring in a heat exchanger.

6.5 Monitoring and Diagnosis of Fouling in the Steam Generator

With both the normal data and data with fouling generated using the developed UTSG SIMULINK model, we first use the GMDH method to develop a data-driven model and then use the model to monitor and diagnose the fouling progress. The MATLAB code for monitoring and diagnosis of fouling in the heat exchanger is given in Appendix G.

The procedure is the same as that used above for the heat exchanger. That is, first we establish a data-driven model using the normal data. Then we use this model and the faulty data, that is, with the fouling progression, to make predictions and estimate residuals of the steam pressure. In our study, the hot-leg temperature and the number of tubes are used as the inputs for predicting steam pressure.

Figure 6.10 gives the data for UTSG steam pressure used for training and the GMDH predicted values; Figure 6.11 presents the steam pressure data used for testing and the GMDH predicted values. We see from these two figures that they both agree with each other very well.

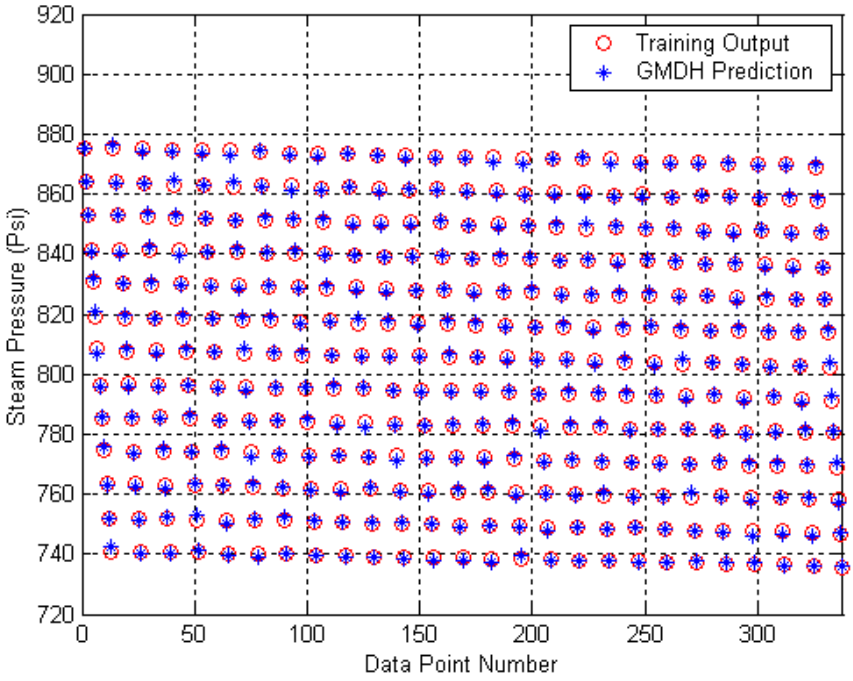

Figure 6.10. The Training Steam Pressure and the GMDH Predicted Values

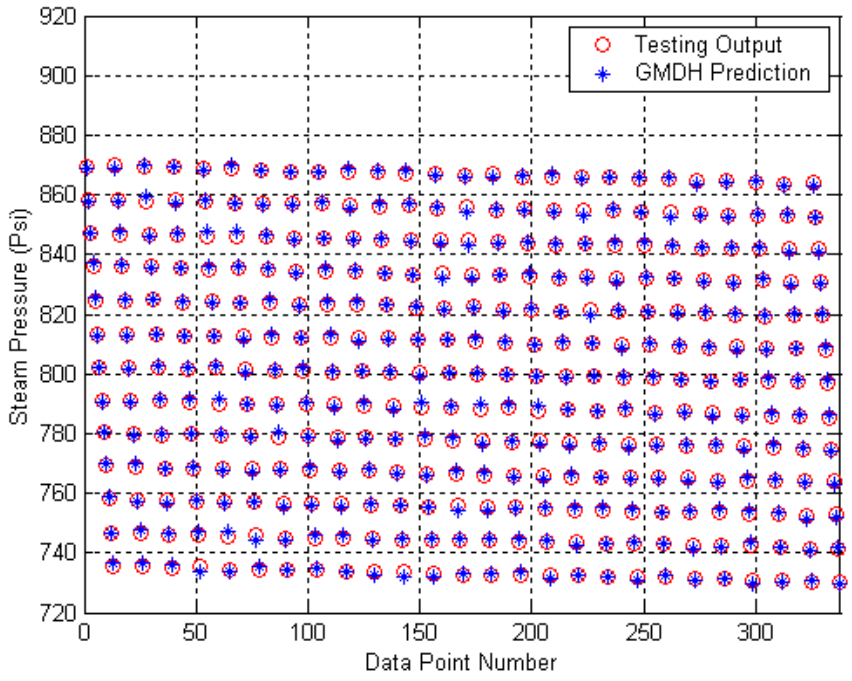

Figure 6.11. The Testing Steam Pressure and the GMDH Predicted Values

After the development of the GMDH model, now we use the experimental data and the model to make new predictions. Figure 6.12 gives the GMDH predictions of the UTSG steam pressure versus the simulation results from the UTSG SIMULINK model. Figure 6.13 shows the residuals. It should be noted that the steam pressure is evaluated with different UTSG hot-side inlet temperatures. Therefore we see that there are different curve blocks in Figure 6.12. The predictions of the steam pressure with a single fixed hot-side inlet temperature are shown in Figures 6.14 and 6.15. From Figures 6.12 - 6.15, we can see that for both cases, at the initial stage of the simulated fouling progress, the estimated residual is comparatively small since there is not much fouling. Then as the fouling progresses and gradually increases, the residual also becomes larger. While finally the fouling reaches the asymptotic value and keeps constant, the residual also follows the same trend and becomes asymptotically constant.

Comparing Figures 6.12 - 6.15 with Figures 4.1 - 4.2, we again notice that the GMDH estimation residual follows the same behavior as the fouling progression with time.

Again these results suggest that we can effectively use the residual trend as given in Figures 6.12 - 6.15 to monitor and diagnose the fouling problem that is occurring in a steam generator.

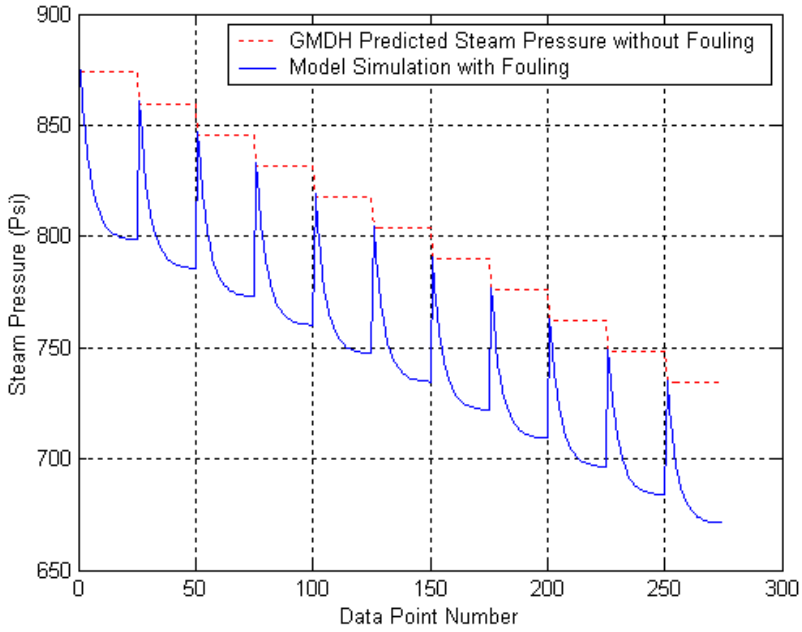

Figure 6.12. The GMDH Predictions of the UTSG Steam Pressure versus the Simulations of the UTSG SIMULINK Model (with Different Hot-side Inlet Temperature)

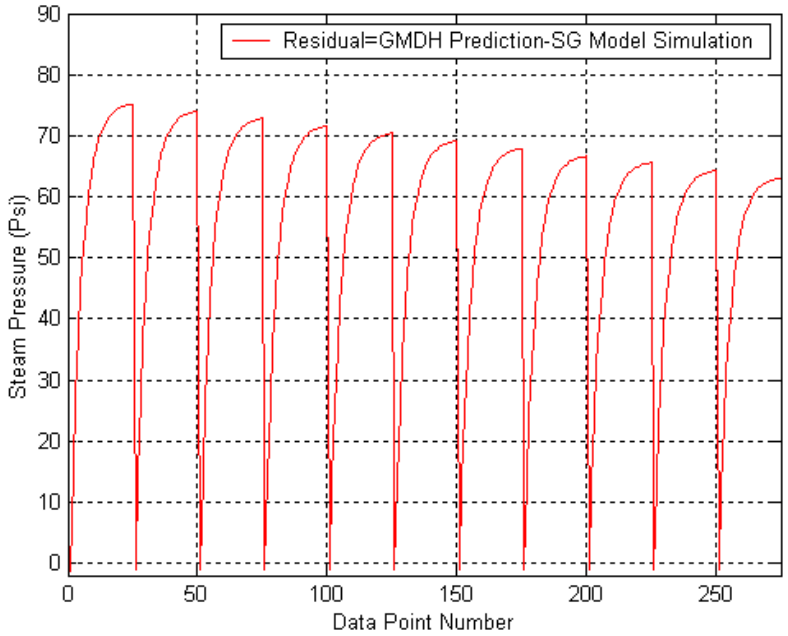

Figure 6.13. The Residual Between the GMDH Predictions of the UTSG Steam Pressure and the Simulations of the UTSG SIMULINK Model (with Different Hot-side Inlet Temperature)

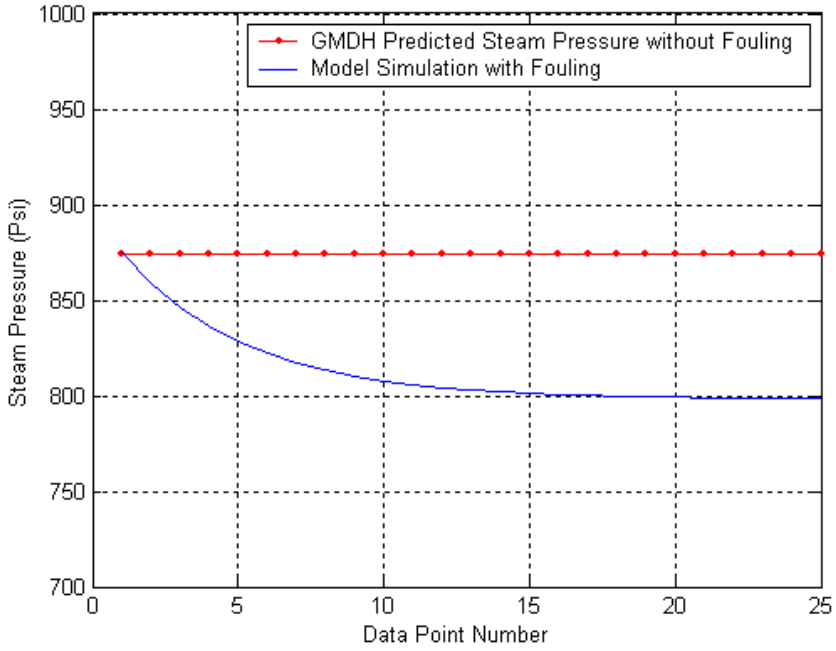

Figure 6.14. The GMDH Predictions of the UTSG Steam Pressure versus the Simulations of the UTSG SIMULINK Model (with a Single Hot-side Inlet Temperature)

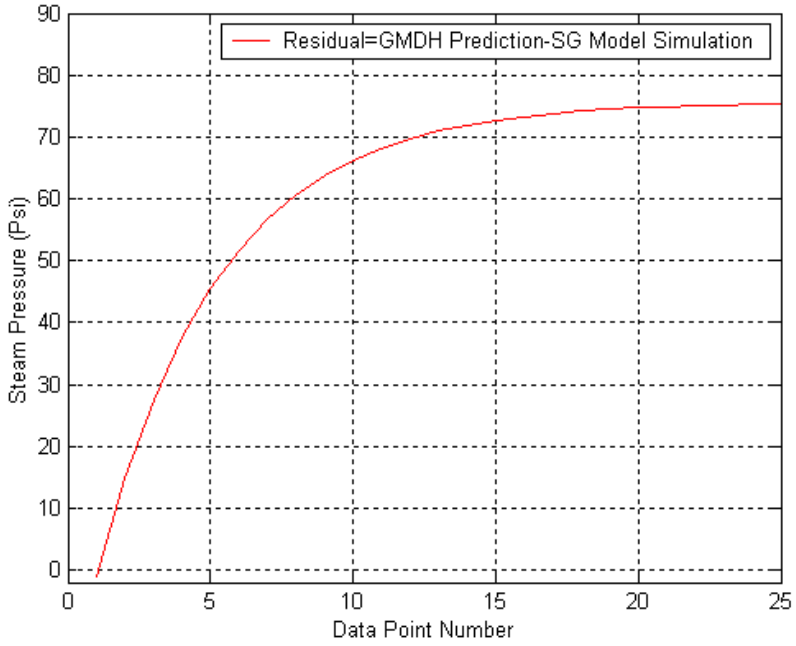

Figure 6.15. The Residual Between the GMDH Predictions of the UTSG Steam Pressure and the Simulations of the UTSG SIMULINK Model (with a Single Hot-side Inlet Temperature)

It should be indicated that we can also use the appropriately developed GMDH model to make predictions of the UTSG steam pressure as a function of other variable, such as the decreasing number of heat transfer tubes, as shown in Figures 6.16 and 6.17. This is possible since we include the number of tubes as the forcing variable when we develop the GMDH model. As seen from Figures 6.16 and 6.17, the GMDH prediction error is very small compared with the simulation results from the UTSG SIMULINK model. This shows that we can also use the GMDH model to monitor the UTSG performance degradation due to other defects such as the decreased number of heat transfer tubes.

6.6 Remarks

In this Chapter, we have used the first-principle models to generate data for development of the corresponding GMDH models for the heat exchanger and the UTSG. Then these models are used to make predictions and the corresponding estimates of the residuals. It should be emphasized that for the heat exchanger we have used the experimental data collected from the experimental setup. All the above results demonstrate that GMDH method can be successfully applied for monitoring and diagnosis of the fouling progression or other degradations that may occur in both heat exchangers and steam generators, as long as adequate data are available and the GMDH model is properly developed.

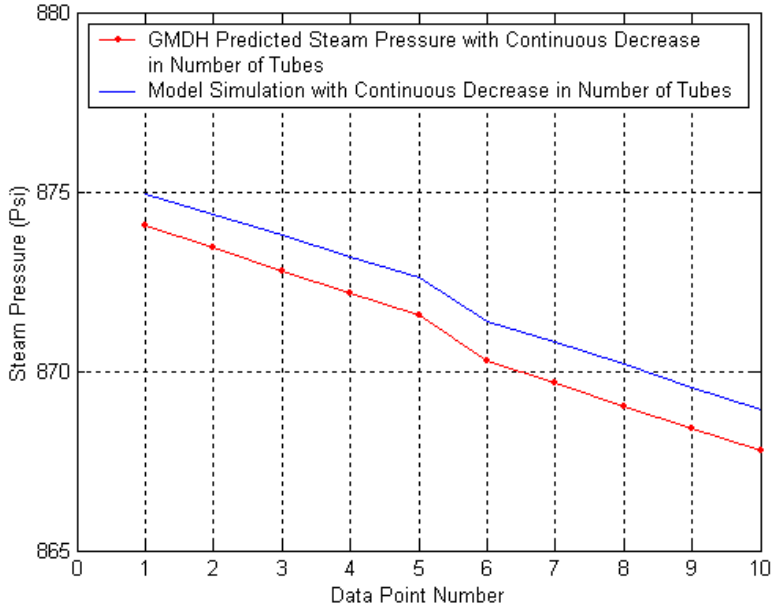

Figure 6.16. The GMDH Predictions of the UTSG Steam Pressure versus the Simulations of the UTSG SIMULINK Model (with Decreasing Number of Heat Transfer Tubes)

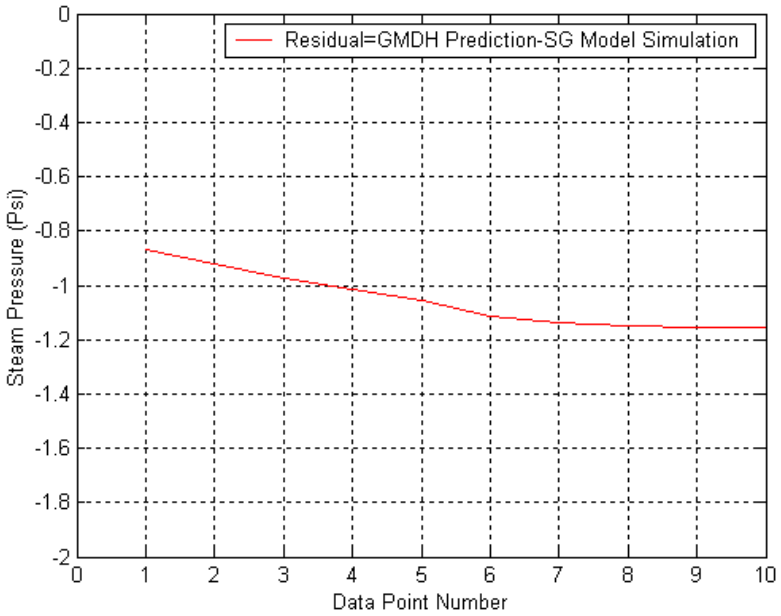

Figure 6.17. The Residual Between the GMDH Predictions of the UTSG Steam Pressure and the Simulations of the UTSG SIMULINK Model (with Decreasing Number of Heat Transfer Tubes)

Chapter 7

Summary, Conclusions, and Recommendations for Future Research

7.1 Summary

In this thesis research, first a comprehensive literature study was made on the types and mechanisms of steam generator and heat exchanger degradation. A literature review of fouling, including the definition, types, theoretical modeling and experimental studies was also performed. Reviews of the basics of corrosion, including corrosion mechanisms, types, important contributing variables, corrosion control, corrosion monitoring are presented in this thesis. A brief review of the steam generator program guidelines that are implemented in order to maintain the integrity of SGs is also included.

Based on an existing UTSG model, we have derived the mathematical equations using the moving-boundary method and the related conservation laws. The goal is to improve the UTSG model and enhance the capability by increasing the axial nodes along the heat transfer tubes. Thus we can study the effect of various defects on UTSG thermal performance, especially the effect of fouling at different axial location of the tubes. The multi-node UTSG model equations are then implemented under MATLAB SIMULINK. This SIMULINK model is used to simulate the dynamics and the

responses of UTSG to different types of degradations.

A literature study of the particulate fouling modeling has shown that the particulate fouling progression follows an exponential behavior. Hence, to verify the theoretical model for fouling and to collect experimental data for fouling monitoring and diagnosis, we have modified and used an existing experimental setup, so as to simulate the fouling progression in a real small-scale heat exchanger, by adding KAOLIN particles in the tube-side fluid.

The research has integrated the GMDH method, and both the model-generated data and the experimental data to monitor and diagnose fouling and its progression both in the heat exchanger and in the UTSG. During the study, the UTSG SIMULINK model is used to generate both the normal data and the data characterizing fouling. A first-principle model is developed and is used to generate only the normal data for the heat exchanger, since the fouling data collected from the experimental setup are available.

7.2 Conclusions

The major contributions of this research include the successful development of a multi-node UTSG SIMULINK model, experimental study of the fouling progression in a heat exchanger using a laboratory setup, and monitoring and diagnosis of the fouling

problem using the GMDH method. Through the study of this research, we can reach the following major conclusions.

- The comprehensive literature study shows that corrosion and fouling are among the most important factors that contribute to the system-level degradations of heat exchangers and steam generators, and that the particulate fouling is the most common type of fouling and follows an exponential law.

- Based on an existing model, a multi-nodal UTSG first-principle model has been successfully developed and implemented under MATLAB SIMULINK in a very easy and reliable fashion. The simulation results of the UTSG dynamics and responses to various defects or faults have illustrated the high fidelity of this model. Compared with the previous model, the new model is more versatile for simulation studies, and can be used to simulate the effect of fouling at different axial locations along the heat transfer tubes.

- A successful experimental study of fouling progression in a heat exchanger has been made. The experimental results show that the particulate fouling progression in even a real small-scale heat exchanger follows an asymptotic behavior. The experimental outcomes also show that we can monitor the particulate fouling by tracking the overall thermal resistance of the heat exchanger.

Real experimental fouling data have also been collected from the laboratory setup and can be used for further study of degradation monitoring of the heat exchangers.

- The GMDH method has been successfully used to monitor the fouling problem in both a heat exchanger and a steam generator. The results show that the GMDH method can be successfully used to monitor and diagnose the fouling progression or possibly other degradations that may occur in both heat exchangers and UTSGs, if adequate data are available and the GMDH model is properly developed. The GMDH model based on first-principle model data is capable of predicting operational variables of both HX and UTSG.

7.3 Recommendations for Future Research

Based on the experience and results of this research, the following recommendations are made for further research.

- The UTSG model can be further improved by enhancing its capability so that it can be used to simulate the effects of more possible defects or degradations, such as tube thinning, tube leakage due to corrosion cracking, etc.

- Using the same method and procedures that have been shown to be valid and

successful by the current experimental results, more detailed and systematic experimental studies of fouling may be planned and performed to further verify the theoretical model for fouling, and to investigate the effects of various variables or factors on the fouling progression. These variables may include the concentration of the particles in the bulk flow, flow rate, temperature, pH value, size of particles, etc. Moreover, the pressure drop across the fouled heat exchanger tubes can be continuously measured during the experiment in order to demonstrate whether the fouling in a heat exchanger can be also monitored and diagnosed by continuously tracking this pressure drop.

- In this research, we have only used the real data characterizing the fouling progression, collected from our experimental setup. All the other data are generated from first-principle models. If available, normal and off-normal plant operational data for USTGs and heat exchangers should be used to perform more complete FDI studies using the GMDH method or other methods. In addition, more degradation modes should be included in the FDI study.

References

References

1. B. R. Upadhyaya, J. W. Hines et al, *Automated Monitoring and Diagnostics of the Integrity of Nuclear Plant Steam generators*, Transactions of the American Nuclear Society Annual Meeting, pp. 188-189, June 2002.

2. B. R. Upadhyaya, J. W. Hines et al, *On-Line Monitoring and Diagnostics of the Integrity of Nuclear Plant Steam Generators and Heat Exchangers*, Semi-Annual Report, Report No. DE-FG07-01ID14114/UTNE-01, December 2001.

3. B. R. Upadhyaya, J. W. Hines et al, *On-Line Monitoring and Diagnostics of the Integrity of Nuclear Plant Steam Generators and Heat Exchangers*, Annual Report, Report No. DE-FG07-01ID14114/UTNE-02, June 2002.

4. B. R. Upadhyaya, J. W. Hines et al, *On-Line Monitoring and Diagnostics of the Integrity of Nuclear Plant Steam Generators and Heat Exchangers*, Semi-Annual Report, Report No. DE-FG07-01ID14114/UTNE-03, December 2002.

5. B. R. Upadhyaya, J. W. Hines et al, *On-Line Monitoring and Diagnostics of the Integrity of Nuclear Plant Steam Generators and Heat Exchangers*, Annual Report, Report No. DE-FG07-01ID14114/UTNE-04, June 2003.

6. http://www.domeng.com/

7. C. M. Allison et al, *SCDAP/RELAP5/MOD2 Code Manual*, U.S. Nuclear Regulatory Commission, Office of Nuclear Regulatory Research, Division of Systems Research, EG&G Idaho, 1989.

8. J. M. Putney et al, *Assessment of PWR Steam Generator Modeling in RELAP5/MOD2*, U.S. Nuclear Regulatory Commission, 1993.

9. SCDAP/RELAP5 Development Team, *SCDAP/RELAP5/MOD3.2 Code Manual*, U.S. Nuclear Regulatory Commission, Office of Nuclear Regulatory Research, Division of Systems Technology, SCDAP/RELAP5 Development Team, 1998.

10. M. Naghedolfeizi and B. R. Upadhyaya, *Dynamic Modeling of a Pressurized Water Reactor Plant for Diagnostics and Control*, Research Report, DOE/NE/88ER12824-02, June 1991.

11. P. E. MacDonald, V. N. Shah, L. W. Ward, and P. G. Ellison, *Steam Generator Tube Failures*, NUREG/CR-6365, 1996.

12. K. C. Wade, *Steam Generator Degradation and its Impact on Continued Operation of Pressurized Water Reactors in the United States*, Energy Information Administration/ Electric Power Monthly, August 1995.

13. http://domino.pall.com/www/weblib.nsf/pub/80EC605D2451474E852567EF0053F173?opendocument

14. http://www.cpe.surrey.ac.uk/dptri/hms/fouling.htm

15. M. Naghedolfeizi, *A Life Assessment Methodology for Heat Exchanger and Steam Generator Tubing*, A dissertation presented for the Doctor of Philosophy Degree, The University of Tennessee, Knoxville, 1994.

16. D. Q. Kern and R. E. Seaton, *A Theoretical Analysis of Thermal Surface Fouling*, British Chemical Engineering, Vol. 4, No. 5, pp. 258-262, 1959.

17. S. K. Beal, *Particulate Fouling of Heat Exchangers*, Proceeding of the Engineering Foundation Conference, White Harie, PA, October 31 - November 5, 1982.

18. C. I. Hussain, I. H. Newson, and T.R. Bott, *Diffusion Controlled Deposition of Particulate Matter from Flowing Slurries*, Proceeding of the Eighth International Heat Transfer Conference, San Francisco, 1986.

19. H. Muller-Stehinhagen, F. Reif, N. Epstein, and A.P. Watkinson, *Influence of Operating Conditions on Particulate Fouling*, Canadian Journal of Chemical Engineering, Vol. 66, pp. 42-50, February 1988.

20. Y. Mussalli et al, *Effects of Fouling and Corrosion on Heat Transfer,* American Society of Mechanical Engineers, Htd, Vol. 50, 1985.

21. R. L. Watts and L. O. Levine, *Monitoring Technology Trends with Patent Data: Fouling of Heat Exchangers - A Case Study*, Presented at the 22nd National Heat Transfer Conference and Exhibition, Niagara Falls, New York, August 1984.

22. J. Taborek, T. Aoku, R. B. Ritter, J.W. Paeln, and J.G. Knudsen, *Fouling: the Major Unresolved Problem in Heat Transfer*, Chemical Engineering Progress, Vol. 68, No. 2,

pp. 59-67, February 1972.

23. H. Muller-Steinhagen, and R. Bloch, *Particulate Fouling in Heat Exchangers*, Transcripts of Institute of Professional Engineers, New Zealand, EMC Eng-Sec., Vol. 15, No. 3, pp. 109-118, November 1988.

24. A. K. Gupta and T. W. Jackson, *On the Mechanism of Particle Deposition through Boundary Layers in a Heat Exchanger System*, Presented at the American Institute of Aeronautic and Astronautics, 24th Aerospace Sciences Meeting, Reno, Nevada, January 1986.

25. J. G. Knudsen, *Coping with Cooling Water Fouling in Tubular Heat Exchangers*, AIChE Symposium Series, Vol. 85, No. 269, pp. 1-12, 1989.

26. P. G. Papavergos and A. B. Hadley, *Particle Deposition Behavior from Turbulent Flows*, Chemical Engineering Research, Vol. 62, pp. 275-295, September 1984.

27. F. B. Incropera and D. P. DeWitt, *Fundamentals of Heat and Mass Transfer*, 4th Edition, John Wiley, New York, 1996.

28. J. P. Holman, *Heat Transfer*, 5th Edition, McGraw-Hill, New York, 1981.

29. M. G. Fontana and N. D. Greene, *Corrosion Engineering*, 2nd ed., McGraw-Hill, New York, 1978.

30. A. Stutzmann et al, *French Experience on OD-IGA/SCC and Fouling of SG Tubes*, Nuclear Energy, Vol. 41, No. 2, pp. 137-144, April 2002.

31. J. R. Davis et al, *Corrosion—Understanding the Basics*, ASM International, 2000.

32. P. Marcus et al, *Corrosion Mechanisms in Theory and Practice*, Marcel Dekker, 1995.

33. T. Kuppan, *Heat Exchanger Design Handbook*, Marcel Dekker, New York, 2000.

34. C.F. Britton et al, *Effective Corrosion Monitoring*, NACE, Material Performance, April 1988.

35. C. Wood, *On Chemistry and Corrosion at Nuclear Power Plants*, Nuclear News, October 2002.

36. J. Gorman, *Survey of PWR Water Chemistry*, NUREG/CR-5116, 1989.

37. *Water Chemistry and Corrosion Problems in Nuclear Power Plants*, Proceedings of an International Symposium on Water Chemistry and Corrosion Problems of Nuclear Reactor Systems and Components Organized by IAEA, 1982.

38. NEI 97-06 (Rev 1), *Steam Generator Program Guidelines*, January 2001.

39. *PWR Steam Generator Examination Guidelines*, EPRI Report TR-107569**.**

40. *PWR Primary-to-Secondary Leak Guidelines*, EPRI Report TR-104788**.**

41. *PWR Secondary Water Chemistry Guidelines*, EPRI Report TR-102134**.**

42. *PWR Primary Water Chemistry Guidelines*, EPRI Report TR-105714**.**

43. *Steam Generator Integrity Assessment Guideline*, EPRI Report TR-107621.

44. *PWR Steam Generator Tube Plug Assessment Document*, EPRI Report TR-109495.

45. EPRI *PWR Sleeving Assessment Document*, EPRI Report TR-105962.

46. EPRI NP-7552 *Heat Exchanger Performance Monitoring Guidelines*, December 1991.

47. Y. Liner et al, *Simulation of Magnetite Particulate Fouling in Nuclear Steam Generators*, Chalk River Laboratories, AECL Research, Ontario, Canada, 1992.

48. C. W. Turner et al, *Modeling Magnetite Particle Deposition in Nuclear Steam Generators and Comparisons with Plant Data*, Presented at the Second International Steam Generator and Heat Exchanger Conference, Toronto, Canada, 1994.

49. J. W. Cleaver et al, *The Effect of Re-entrainment on Particle Deposition*, Chemical Engineering and Science, Vol. 31, pp. 147-151, 1976.

50. B. D. Bowen et al, *Fine Particle Deposition in Smooth Parallel-Plate Channel*, J. Colloid Interf. Sci., Vol. 72, pp. 81-97, 1979.

51. E. Ruckenstein et al, Rate of Deposition of Browning Particle under the Action of London and Double-layer Forces, J. Chem. Soc., Far. Trans., II, Vol. 69, pp. 1522-1536, 1973.

52. J. W. Cleaver et al, *A Sub Layer Model for the Deposition of Particles from a Turbulent Flow*, Chemical Engineering and Science, Vol. 30, pp. 983-992, 1975.

53. Y. Asakura et al, *Iron Oxide Deposition on Heated Surfaces in Pressurized Boiling Water*, Nucl. Sci. and Eng., Vol 72, pp. 117-120, 1979.

54. G. S. McNab et al, *Thermophoresis in Liquids*, J. Colloid Interf. Sci., 44, pp. 339-346, 1973.

55. S. Kakac et al, *Heat Exchanger: Thermal-Hydraulic Fundamentals and Design*, Hemisphere Publishing Corporation, 1980.

56. http://www.tranterphe.com/phe/PDFs/SC-TD-017.pdf

57. L. F. Melo et al, *Particle Transport in Fouling Caused by KAOLIN-Water Suspensions on Copper Tubes*, Canadian Journal of Chemical Engineering, Volume 66, pp. 36-41, February 1988.

58. J. Middis et al, *Particulate Fouling in Heat Exchangers with Enhanced Surfaces*, 18th Australasian Chemical Engineering Conference, Auckland, New Zealand, pp. 1053-1061, 1990.

59. L. M. Chamra et al, *Effect of Particle Size and Size Distribution on Particulate Fouling in Enhanced Tubes*, Enhanced Heat Transfer, Vol. 1, No. 1, pp. 65-75, 1993.

60. H. Muller-Steinhagen et al, *Particulate Fouling in Heat Exchangers*, Transactions of EMCh, Vol. 15, No. 3, pp. 109-118, November 1988.

61. M. Basset et al, *The Fouling of Alloy-800 Heat Exchange Surfaces by Magnetite Particles*, Canadian Journal of Chemical Engineering, Vol. 78, February 2000.

62. T. Sugimoto et al, *Formation of Uniform Spherical Magnetite Particles by Crystallization from Ferrous Hydroxide Gels*, Journal of Colloid and Interface Science, Vol. 74, No. 1, pp. 227-243, March 1980.

63. C. W. Turner et al, *Deposition of Magnetite Particles from Flowing Suspensions under Flow-Boiling and Single-Phase Forced-Convective Heat Transfer*, Canadian Journal of Chemical Engineering, Vol. 78, pp. 1065-1072, December 2000.

64. H. Muller-Steinhagen et al, *Influence of Operating Conditions on Particulate Fouling*, Canadian Journal of Chemical Engineering, Vol. 66, pp. 42-50, February 1988.

65. M. Turakhia et al, *Fouling of Heat Exchanger Surface: Measurement and Diagnosis*, Heat Transfer Engineering, Vol. 5, No. 1–2, pp. 93–101, 1984.

66. H. Muller-Steinhagen, *Cooling-Water Fouling in Heat Exchangers*, Advances in Heat Transfer, Vol. 33, Academic Press, pp. 415-491, 1999.

67. B. R. Upadhyaya and P. B. Ferreira, *Detection and Isolation of Incipient Faults in Processing Components*, UTNE/FR/98-05, Nuclear Engineering Department, The University of Tennessee, December 1998.

68. B. Lu, *Incipient FDI algorithm for Steam Generator System in a Nuclear Power Plant*, A Thesis Presented for the Master of Science Degree, The University of Tennessee, Knoxville, September 2001.

69. A. G. Ivakhnenko et al, *The Review of Problems Solvable by Algorithms of the Group Method of Data Handling (GMDH)*, Pattern Recognition and Image Analysis, Vol. 5, No. 4, 1995.

70. T. Kondo et al, *GMDH-type Neural Networks and Their Application to the Medical Image Recognition of the Lungs*, Proceeding of the 38th SICE Annual Conference, International Paper, 1999.

Appendices

Appendix A

Derivation of the Equations for UTSG Lumped Primary Coolant Nodes

In this appendix, we will derive the describing equations for the U-tube primary-side lumped coolant nodes based on mass balance and energy balance.

Node 1 (PRL1):

Mass balance: $\frac{dM_{p1}}{dt} = W_{pi} - W_{p1}$

Or: $\rho_{p1} A_p \frac{dL_{s1}}{dt} = W_{pi} - W_{p1}$

Where, we assume that the coolant densities in all the nodes of the primary side are all equal, which is ρ_{pi}.

Energy balance: $\frac{d}{dt}(M_{p1} C_{p1} T_{p1}) = W_{pi} C_{p1} T_{pi} - W_{p1} C_{p1} T_{p1} - U_{pm1} S_{pm1} (T_{p1} - T_{m1})$

Or: $\frac{d}{dt}(\rho_{pi} A_p L_{s1} C_{p1} T_{p1}) = W_{pi} C_{p1} T_{pi} - W_{p1} C_{p1} T_{p1} + U_{pm1} S_{pm1} (T_{m1} - T_{p1})$

$$\rho_{pi} A_p C_{p1} (L_{s1} \frac{dT_{p1}}{dt} + T_{p1} \frac{dL_{s1}}{dt}) = W_{pi} C_{p1} T_{pi} - W_{p1} C_{p1} T_{p1} + U_{pm1} S_{pm1} (T_{m1} - T_{p1})$$

Using the mass balance equation, hence we have:

$$\rho_{pi} A_p C_{p1} L_{s1} \frac{dT_{p1}}{dt} + C_{p1} T_{p1} (W_{pi} - W_{p1}) = W_{pi} C_{p1} T_{pi} - W_{p1} C_{p1} T_{p1} + U_{pm1} S_{pm1} (T_{m1} - T_{p1})$$

$$\frac{dT_{p1}}{dt} = \frac{W_{pi}}{\rho_{pi} A_p L_{s1}} (T_{pi} - T_{p1}) + \frac{U_{pm1} S_{pm1}}{M_{p1} C_{p1}} (T_{m1} - T_{p1})$$

Similarly we can derive the equations for other primary coolant nodes.

Node 2 (PRL2):

Mass balance: $\frac{dM_{p2}}{dt} = W_{p1} - W_{p2}$

Or: $\frac{d}{dt}(\rho_{pi} A_p L_{s2}) = W_{p1} - W_{p2}$

Where, $L_{s2} = \frac{1}{3}(L_0 - L_{s1})$

Hence we have:

$$-\frac{1}{3}\rho_{pi} A_p \frac{dL_{s1}}{dt} = W_{pi} - \rho_{pi} A_p \frac{dL_{s1}}{dt} - W_{p2}$$

$$W_{p2} = W_{pi} - \frac{2\rho_{pi} A_p}{3}\frac{dL_{s1}}{dt}$$

Energy balance:

$$\frac{d}{dt}(M_{p2} C_{p2} T_{p2}) = W_{p1} C_{p2} T_{p1} - W_{p2} C_{p2} T_{p2} - U_{pm2} S_{pm2}(T_{p2} - T_{m2})$$

Using the mass balance equation, hence we have:

$$\rho_{pi} A_p C_{p2}(L_{s2}\frac{dT_{p2}}{dt} - \frac{1}{3}T_{p2}\frac{dL_{s1}}{dt}) = (W_{pi} - \rho_{pi} A_p \frac{dL_{s1}}{dt})C_{p2} T_{p1}$$
$$-(W_{pi} - \frac{2\rho_{pi} A_p}{3}\frac{dL_{s1}}{dt})C_{p2} T_{p2} - U_{pm2} S_{pm2}(T_{p2} - T_{m2})$$

$$\frac{dT_{p2}}{dt} = \frac{W_{pi}}{\rho_{pi} A_p L_{s2}}(T_{p1} - T_{p2}) + \frac{U_{pm2} S_{pm2}}{M_{p2} C_{p2}}(T_{m2} - T_{p2}) + \frac{T_{p2} - T_{p1}}{L_{s2}}\frac{dL_{s1}}{dt}$$

Node 3 (PRL3):

Mass balance: $\frac{dM_{p3}}{dt} = W_{p2} - W_{p3}$

Or: $\frac{d}{dt}(\rho_{pi} A_p L_{s2}) = W_{pi} - \frac{2\rho_{pi} A_p}{3}\frac{dL_{s1}}{dt} - W_{p3}$

Hence we have:

$$-\frac{1}{3}\rho_{pi}A_p\frac{dL_{s1}}{dt}=W_{pi}-\frac{2}{3}\rho_{p1}A_p\frac{dL_{s1}}{dt}-W_{p3}$$

$$W_{p3}=W_{pi}-\frac{\rho_{pi}A_p}{3}\frac{dL_{s1}}{dt}$$

Energy balance:

$$\frac{d}{dt}(M_{p3}C_{p3}T_{p3})=W_{p2}C_{p3}T_{p2}-W_{p3}C_{p3}T_{p3}-U_{pm3}S_{pm3}(T_{p3}-T_{m3})$$

Using the mass balance equation, hence we have:

$$\rho_{pi}A_pC_{p3}(L_{s2}\frac{dT_{p3}}{dt}-\frac{1}{3}T_{p3}\frac{dL_{s1}}{dt})=(W_{pi}-\frac{2}{3}\rho_{pi}A_p\frac{dL_{s1}}{dt})C_{p3}T_{p2}$$
$$-(W_{pi}-\frac{\rho_{pi}A_p}{3}\frac{dL_{s1}}{dt})C_{p3}T_{p3}-U_{pm3}S_{pm3}(T_{p3}-T_{m3})$$

$$\frac{dT_{p3}}{dt}=\frac{W_{pi}}{\rho_{pi}A_pL_{s2}}(T_{p2}-T_{p3})+\frac{U_{pm3}S_{pm3}}{M_{p3}C_{p3}}(T_{m3}-T_{p3})+\frac{2(T_{p3}-T_{p2})}{3L_{s2}}\frac{dL_{s1}}{dt}$$

Node 4 (PRL4):

Mass balance: $\frac{dM_{p4}}{dt}=W_{p3}-W_{p4}$

Or: $\frac{d}{dt}(\rho_{pi}A_pL_{s2})=W_{pi}-\frac{\rho_{pi}A_p}{3}\frac{dL_{s1}}{dt}-W_{p4}$

Hence we have:

$$-\frac{1}{3}\rho_{pi}A_p\frac{dL_{s1}}{dt}=W_{pi}-\frac{1}{3}\rho_{p1}A_p\frac{dL_{s1}}{dt}-W_{p4}$$

$$W_{p4}=W_{pi}$$

Energy balance:

$$\frac{d}{dt}(M_{p4}C_{p4}T_{p4}) = W_{p3}C_{p4}T_{p3} - W_{p4}C_{p4}T_{p4} - U_{pm4}S_{pm4}(T_{p4} - T_{m4})$$

Using the mass balance equation, hence we have:

$$\rho_{pi}A_pC_{p4}(L_{s2}\frac{dT_{p4}}{dt} - \frac{1}{3}T_{p4}\frac{dL_{s1}}{dt}) = (W_{pi} - \frac{1}{3}\rho_{pi}A_p\frac{dL_{s1}}{dt})C_{p4}T_{p3} - W_{pi}C_{p4}T_{p4} - U_{pm4}S_{pm4}(T_{p4} - T_{m4})$$

$$\frac{dT_{p4}}{dt} = \frac{W_{pi}}{\rho_{pi}A_pL_{s2}}(T_{p3} - T_{p4}) + \frac{U_{pm4}S_{pm4}}{M_{p4}C_{p4}}(T_{m4} - T_{p4}) + \frac{T_{p4} - T_{p3}}{3L_{s2}}\frac{dL_{s1}}{dt}$$

Node 5 (PRL5):

Mass balance: $\frac{dM_{p5}}{dt} = W_{p4} - W_{p5}$

Or: $\frac{d}{dt}(\rho_{pi}A_pL_{s2}) = W_{p4} - W_{p5}$

Hence we have:

$$-\frac{1}{3}\rho_{pi}A_p\frac{dL_{s1}}{dt} = W_{pi} - W_{p5}$$

$$W_{p5} = W_{pi} + \frac{1}{3}\rho_{pi}A_p\frac{dL_{s1}}{dt}$$

Energy balance:

$$\frac{d}{dt}(M_{p5}C_{p5}T_{p5}) = W_{p4}C_{p5}T_{p4} - W_{p5}C_{p5}T_{p5} - U_{pm5}S_{pm5}(T_{p5} - T_{m5})$$

Using the mass balance equation, hence we have:

$$\rho_{pi}A_pC_{p5}(L_{s2}\frac{dT_{p5}}{dt} - \frac{1}{3}T_{p5}\frac{dL_{s1}}{dt}) = W_{pi}C_{p5}T_{p4} - (W_{pi} + \frac{1}{3}\rho_{pi}A_p\frac{dL_{s1}}{dt})C_{p5}T_{p5} - U_{pm5}S_{pm5}(T_{p5} - T_{m5})$$

$$\frac{dT_{p5}}{dt} = \frac{W_{pi}}{\rho_{pi} A_p L_{s2}}(T_{p4} - T_{p5}) + \frac{U_{pm5} S_{pm5}}{M_{p5} C_{p5}}(T_{m5} - T_{p5})$$

Node 6 (PRL6):

Mass balance: $\frac{dM_{p6}}{dt} = W_{p5} - W_{p6}$

Or: $\frac{d}{dt}(\rho_{pi} A_p L_{s2}) = W_{p5} - W_{p6}$

Hence we have:

$$-\frac{1}{3}\rho_{pi} A_p \frac{dL_{s1}}{dt} = W_{pi} + \frac{1}{3}\rho_{pi} A_p \frac{dL_{s1}}{dt} - W_{p6}$$

$$W_{p6} = W_{pi} + \frac{2}{3}\rho_{pi} A_p \frac{dL_{s1}}{dt}$$

Energy balance:

$$\frac{d}{dt}(M_{p6} C_{p6} T_{p6}) = W_{p5} C_{p6} T_{p5} - W_{p6} C_{p6} T_{p6} - U_{pm6} S_{pm6}(T_{p6} - T_{m6})$$

Using the mass balance equation, hence we have:

$$\rho_{pi} A_p C_{p6}(L_{s2}\frac{dT_{p6}}{dt} - \frac{1}{3}T_{p6}\frac{dL_{s1}}{dt}) = (W_{pi} + \frac{1}{3}\rho_{pi} A_p \frac{dL_{s1}}{dt})C_{p6} T_{p5}$$
$$- (W_{pi} + \frac{2}{3}\rho_{pi} A_p \frac{dL_{s1}}{dt})C_{p6} T_{p6} - U_{pm6} S_{pm6}(T_{p6} - T_{m6})$$

$$\frac{dT_{p6}}{dt} = \frac{W_{pi}}{\rho_{pi} A_p L_{s2}}(T_{p5} - T_{p6}) + \frac{U_{pm6} S_{pm6}}{M_{p6} C_{p6}}(T_{m6} - T_{p6}) + \frac{T_{p5} - T_{p6}}{3L_{s2}}\frac{dL_{s1}}{dt}$$

Node 7 (PRL7):

Mass balance: $\frac{dM_{p7}}{dt} = W_{p6} - W_{p7}$

Or: $\frac{d}{dt}(\rho_{pi} A_p L_{s2}) = W_{p6} - W_{p7}$

Hence we have:

$$-\frac{1}{3}\rho_{pi}A_p\frac{dL_{s1}}{dt}=W_{pi}+\frac{2}{3}\rho_{pi}A_p\frac{dL_{s1}}{dt}-W_{p6}$$

$$W_{p6}=W_{pi}+\rho_{pi}A_p\frac{dL_{s1}}{dt}$$

Energy balance:

$$\frac{d}{dt}(M_{p7}C_{p7}T_{p7})=W_{p6}C_{p7}T_{p6}-W_{p7}C_{p7}T_{p7}-U_{pm7}S_{pm7}(T_{p7}-T_{m7})$$

Using the mass balance equation, hence we have:

$$\rho_{pi}A_pC_{p7}(L_{s2}\frac{dT_{p7}}{dt}-\frac{1}{3}T_{p7}\frac{dL_{s1}}{dt})=(W_{pi}+\frac{2}{3}\rho_{pi}A_p\frac{dL_{s1}}{dt})C_{p7}T_{p6}$$
$$-(W_{pi}+\rho_{pi}A_p\frac{dL_{s1}}{dt})C_{p7}T_{p7}-U_{pm7}S_{pm7}(T_{p7}-T_{m7})$$

$$\frac{dT_{p7}}{dt}=\frac{W_{pi}}{\rho_{pi}A_pL_{s2}}(T_{p6}-T_{p7})+\frac{U_{pm7}S_{pm7}}{M_{p7}C_{p7}}(T_{m7}-T_{p7})+\frac{2(T_{p6}-T_{p7})}{3L_{s2}}\frac{dL_{s1}}{dt}$$

Node 8 (PRL8):

Mass balance: $\frac{dM_{p8}}{dt}=W_{p7}-W_{p8}$

Or: $\frac{d}{dt}(\rho_{pi}A_pL_{s1})=W_{p7}-W_{p8}$

Hence we have:

$$\rho_{pi}A_p\frac{dL_{s1}}{dt}=W_{pi}+\rho_{pi}A_p\frac{dL_{s1}}{dt}-W_{p8}$$

$$W_{p8}=W_{pi}$$

Energy balance:

$$\frac{d}{dt}(M_{p8}C_{p8}T_{p8})=W_{p7}C_{p8}T_{p7}-W_{p8}C_{p8}T_{p8}-U_{pm8}S_{pm8}(T_{p8}-T_{m8})$$

Using the mass balance equation, hence we have:

$$\rho_{pi} A_p C_{p8} (L_{s1} \frac{dT_{p8}}{dt} + T_{p8} \frac{dL_{s1}}{dt}) = (W_{pi} + \rho_{pi} A_p \frac{dL_{s1}}{dt}) C_{p8} T_{p7} - W_{pi} C_{p8} T_{p8} - U_{pm8} S_{pm8} (T_{p8} - T_{m8})$$

$$\frac{dT_{p8}}{dt} = \frac{W_{pi}}{\rho_{pi} A_p L_{s1}} (T_{p7} - T_{p8}) + \frac{U_{pm8} S_{pm8}}{M_{p8} C_{p8}} (T_{m8} - T_{p8}) + \frac{T_{p7} - T_{p8}}{L_{s1}} \frac{dL_{s1}}{dt}$$

Appendix B

Derivation of the Equations for UTSG Tube Wall Lumped Metal Nodes

In this appendix, we will derive the describing equations for the U-tube wall lumped metal nodes based on energy balance.

Node 1 (MTL1):

Energy balance:

$$\frac{d}{dt}(M_{m1}C_mT_{m1}) = U_{pm1}S_{pm1}(T_{p1}-T_{m1}) - U_{ms1}S_{ms1}(T_{m1}-T_{s1}) + \rho_m A_m C_m \frac{T_{m1}+T_{m2}}{2}\cdot\frac{dL_{s1}}{dt}$$

Where, $M_{m1} = \rho_m A_m L_{s1}$ and $T_{s1} = \frac{T_d + T_{sat}}{2}$. Hence we have:

$$M_{m1}C_m\frac{dT_{m1}}{dt} + \rho_m A_m C_m T_{m1}\frac{dL_{s1}}{dt} = U_{pm1}S_{pm1}(T_{p1}-T_{m1}) - U_{ms1}S_{ms1}(T_{m1}-T_{s1}) + \rho_m A_m C_m \frac{T_{m1}+T_{m2}}{2}\cdot\frac{dL_{s1}}{dt}$$

$$\frac{dT_{m1}}{dt} = \frac{U_{pm1}S_{pm1}}{M_{m1}C_m}T_{p1} - \frac{U_{pm1}S_{pm1}+U_{ms1}S_{ms1}}{M_{m1}C_m}T_{m1} + \frac{U_{ms1}S_{ms1}}{M_{m1}C_m}\cdot\frac{T_d+T_{sat}}{2} + \frac{T_{m2}-T_{m1}}{2L_{s1}}\cdot\frac{dL_{s1}}{dt}$$

Similarly we can derive the energy balance equations for other tube-wall nodes.

Node 2 (MTL2):

Energy balance:

$$\frac{d}{dt}(M_{m2}C_mT_{m2}) = U_{pm2}S_{pm2}(T_{p2}-T_{m2}) - U_{ms2}S_{ms2}(T_{m2}-T_{sat}) - \rho_m A_m C_m \frac{T_{m1}+T_{m2}}{2}\cdot\frac{dL_{s1}}{dt} + \rho_m A_m C_m \frac{T_{m2}+T_{m3}}{2}\cdot\frac{2}{3}\frac{dL_{s1}}{dt}$$

Where, $M_{m2} = \rho_m A_m \frac{L_0 - L_{s1}}{3}$. Hence we can reach:

$$\frac{dT_{m2}}{dt}=\frac{U_{pm2}S_{pm2}}{M_{m2}C_m}(T_{p2}-T_{m2})-\frac{U_{ms2}S_{ms2}}{M_{m2}C_m}(T_{m2}-T_{sat})+\frac{T_{m2}+2T_{m3}-3T_{m1}}{2(L_0-L_{s1})}\cdot\frac{dL_{s1}}{dt}$$

Node 3 (MTL3):

Energy balance:

$$\frac{d}{dt}(M_{m3}C_mT_{m3})=U_{pm3}S_{pm3}(T_{p3}-T_{m3})-U_{ms3}S_{ms3}(T_{m3}-T_{sat})$$
$$-\rho_mA_mC_m\frac{T_{m2}+T_{m3}}{2}\cdot\frac{2}{3}\frac{dL_{s1}}{dt}+\rho_mA_mC_m\frac{T_{m3}+T_{m4}}{2}\cdot\frac{1}{3}\frac{dL_{s1}}{dt}$$

Where, $M_{m3}=\rho_mA_m\frac{L_0-L_{s1}}{3}$. Hence we can reach:

$$\frac{dT_{m3}}{dt}=\frac{U_{pm3}S_{pm3}}{M_{m3}C_m}(T_{p3}-T_{m3})-\frac{U_{ms3}S_{ms3}}{M_{m3}C_m}(T_{m3}-T_{sat})+\frac{T_{m3}+T_{m4}-2T_{m2}}{2(L_0-L_{s1})}\cdot\frac{dL_{s1}}{dt}$$

Node 4 (MTL4):

Energy balance:

$$\frac{d}{dt}(M_{m4}C_mT_{m4})=U_{pm4}S_{pm4}(T_{p4}-T_{m4})-U_{ms4}S_{ms4}(T_{m4}-T_{sat})-\rho_mA_mC_m\frac{T_{m3}+T_{m4}}{2}\cdot\frac{1}{3}\frac{dL_{s1}}{dt}$$

Where, $M_{m4}=\rho_mA_m\frac{L_0-L_{s1}}{3}$. Hence we can reach:

$$\frac{dT_{m4}}{dt}=\frac{U_{pm4}S_{pm4}}{M_{m4}C_m}(T_{p4}-T_{m4})-\frac{U_{ms4}S_{ms4}}{M_{m4}C_m}(T_{m4}-T_{sat})+\frac{T_{m4}-T_{m3}}{2(L_0-L_{s1})}\cdot\frac{dL_{s1}}{dt}$$

Node 5 (MTL5):

Energy balance:

$$\frac{d}{dt}(M_{m5}C_mT_{m5})=U_{pm5}S_{pm5}(T_{p5}-T_{m5})-U_{ms5}S_{ms5}(T_{m5}-T_{sat})-\rho_mA_mC_m\frac{T_{m5}+T_{m6}}{2}\cdot\frac{1}{3}\frac{dL_{s1}}{dt}$$

$$\frac{dT_{m5}}{dt}=\frac{U_{pm5}S_{pm5}}{M_{m5}C_m}(T_{p5}-T_{m5})-\frac{U_{ms5}S_{ms5}}{M_{m5}C_m}(T_{m5}-T_{sat})+\frac{T_{m5}-T_{m6}}{2(L_0-L_{s1})}\cdot\frac{dL_{s1}}{dt}$$

Where, $M_{m5} = \rho_m A_m \frac{L_0 - L_{s1}}{3}$. Hence we can reach:

Node 6 (MTL6):

Energy balance:

$$\frac{d}{dt}(M_{m6} C_m T_{m6}) = U_{pm6} S_{pm6} (T_{p6} - T_{m6}) - U_{ms6} S_{ms6} (T_{m6} - T_{sat}) + \rho_m A_m C_m \frac{T_{m5} + T_{m6}}{2} \cdot \frac{1}{3} \frac{dL_{s1}}{dt} - \rho_m A_m C_m \frac{T_{m6} + T_{m7}}{2} \cdot \frac{2}{3} \frac{dL_{s1}}{dt}$$

Where, $M_{m6} = \rho_m A_m \frac{L_0 - L_{s1}}{3}$. Hence we can reach:

$$\frac{dT_{m6}}{dt} = \frac{U_{pm6} S_{pm6}}{M_{m6} C_m} (T_{p6} - T_{m6}) - \frac{U_{ms6} S_{ms6}}{M_{m6} C_m} (T_{m6} - T_{sat}) + \frac{T_{m5} + T_{m6} - 2T_{m7}}{2(L_0 - L_{s1})} \cdot \frac{dL_{s1}}{dt}$$

Node 7 (MTL7):

Energy balance:

$$\frac{d}{dt}(M_{m7} C_m T_{m7}) = U_{pm7} S_{pm7} (T_{p7} - T_{m7}) - U_{ms7} S_{ms7} (T_{m7} - T_{sat}) + \rho_m A_m C_m \frac{T_{m6} + T_{m7}}{2} \cdot \frac{2}{3} \frac{dL_{s1}}{dt} - \rho_m A_m C_m \frac{T_{m7} + T_{m8}}{2} \cdot \frac{dL_{s1}}{dt}$$

Where, $M_{m7} = \rho_m A_m \frac{L_0 - L_{s1}}{3}$. Hence we can reach:

$$\frac{dT_{m7}}{dt} = \frac{U_{pm7} S_{pm7}}{M_{m7} C_m} (T_{p7} - T_{m7}) - \frac{U_{ms7} S_{ms7}}{M_{m7} C_m} (T_{m7} - T_{sat}) + \frac{2T_{m6} + T_{m7} - 3T_{m8}}{2(L_0 - L_{s1})} \cdot \frac{dL_{s1}}{dt}$$

Node 8 (MTL8):

Energy balance:

$$\frac{d}{dt}(M_{m8} C_m T_{m8}) = U_{pm8} S_{pm8} (T_{p8} - T_{m8}) - U_{ms8} S_{ms8} (T_{m8} - T_{s1}) + \rho_m A_m C_m \frac{T_{m7} + T_{m8}}{2} \cdot \frac{dL_{s1}}{dt}$$

Where, $M_{m8} = \rho_m A_m L_{s1}$ and $T_{s1} = \frac{T_d + T_{sat}}{2}$. Hence we have:

$$\frac{dT_{m8}}{dt} = \frac{U_{pm8} S_{pm8}}{M_{m8} C_m}(T_{p8} - T_{m8}) - \frac{U_{ms8} S_{ms8}}{M_{m8} C_m}(T_{m8} - \frac{T_d + T_{sat}}{2}) + \frac{T_{m7} - T_{m8}}{2L_{s1}} \cdot \frac{dL_{s1}}{dt}$$

Appendix C

The MATLAB Code for UTSG Particulate Fouling Model

```
%    A Code for Modeling the Particulate Fouling
%    on UTSG Tube Secondary Side (Outer Surface)
Time=[0:24*3600:2*365*24*3600];
Cc=2.3e-10;
Rou=(DENSw+DENSb10+DENSb20+DENSb30)/4*16.03;
Roup=5.2*1e3;% Kg/m^3
dp=0.6*1e-6;% m
Kin_vis=1e-6;% m^2/sec
K_fluid=0.5;% W/mK
K_d=0.02;% W/mK
Hc=(2*0.87603+6*1.87)/8*20441.748028009; % W/(m^2K)
Rou_d=Roup/2; % Kg/m^3
Tou_w=0.5;
Tsat=X1+K5*P0+256;
Tm_ave=(Tm10+Tm20+Tm30+Tm40+Tm50+Tm60+Tm70+Tm80)/8.+256;
Ts=Tm_ave;
Tl_ave=(Td0+256+Tsat)/2;
Tb=Tl_ave;
U_star=(Tou_w/Rou)^0.5;
Tp_star=1/18*Roup/Rou*(U_star*dp/Kin_vis)^2;
Kb=1.38e23;%J/K
T=273.15;
D=Kb*T/(3*pi*Kin_vis*Rou*dp);
Sc=Kin_vis/D;
Kd=Sc^(-2/3)*U_star/11.9;
Ki=1/500*(U_star*Tp_star/5.23*Rou/Roup)*exp(0.48*Tp_star);
q=28*0.2931/(0.348^2);% ??
Hfg=Hfg*1054.8/0.4536; % J/Kg
Kb=0.05*q/(Hfg*Rou);
Kthh=-0.26*Hc*Kin_vis*(Ts-Tb)/((2*K_fluid+K_d)*Tb)/6;
K0=1.9;% m/s
Ea=42000;% KJ/Kmol
R=8.314;% KJ/(K.Kmol)
```

```
Ka=K0*exp(-Ea/(R*Ts));
Kt=Kd+Ki+Kb+Kthh;
K=(1/Kt+1/Ka)^-1;
aa=7e-11;
M=(K*Cc*Rou*Kin_vis/(aa*U_star^2))*(1-exp(-aa*U_star^2*Time/Kin_vis));
Rf=M*0.2048/(K_d*Rou_d)/(0.000160497032*0.06243);
Time=Time/(24*3600*365);
figure(1)
plot(Time,M,'b');
title('Deposit Mass Variation versus Time')
xlabel('Time (Year)')
ylabel('Deposit Mass per Unit Area (Kg/m^2)')
figure(2)
plot(Time,Rf,'m');
title('Fouling Thermal Resistance versus Time')
xlabel('Time (Year)')
ylabel('Fouling Thermal Resistance (s.ft^2^oF/Btu)')
```

Appendix D

The MATLAB Code Used to Process the Fouling Experimental Data and Calculate the Overall Thermal Resistance

```
clear all
clf

load HX_EXP_DATA
load fouling_removal

[m n]=size(fouling_removal);
ar=fouling_removal(3:m,:);
a=[aa' ar']';
[m n]=size(a);
a=a(1:100:m,:);

deltat_hot=a(:,1)-a(:,3);
deltat_cold=a(:,2)-a(:,4);
deltat_cold0=a(:,4)-a(:,3);
deltat_hot0=a(:,1)-a(:,2);
[m n]=size(a);
m_hot(1:m,1)=146;
m_cold=a(:,6);
Inv_U=(deltat_hot-deltat_cold)./m_cold./deltat_cold0./log(deltat_hot./deltat_cold);
%
[mm nn]=size(a);
x1=(1:mm)./3600*100;
Inv_U_percent=(Inv_U(1:mm)-.015)./0.015*100;
data=[a Inv_U_percent];
data1=medfilt1(data,7);
save data_HX_FILT data1
figure(1)
plot(x1,Inv_U_percent,'bo');
AXIS([0 max(x1) 0 110])
xlabel('Time (Hour)')
```

```
ylabel('Overall Thermal Resistance Percentage Change (%)')
title('HX Overall Thermal Resistance versus Experimental Duration')
figure(2)
[mm nn]=size(x1);
yy1=medfilt1(Inv_U_percent,7);
xx=x1(1,2:nn)';
yy=yy1(2:nn);
plot(xx,yy,'bo');
AXIS([0 max(xx) 0 110])
xlabel('Time (Hour)')
ylabel('Percentage Change in Overall Thermal Resistance (%)')
title('HX Overall Thermal Resistence Change versus Experimental Duration')
grid
figure(3)
[mm nn]=size(a);
x1=(1:mm)./3600*100;
plot(x1,a(:,1),'b'); hold on
plot(x1,a(:,2),'r'); hold on
plot(x1,a(:,3),'g'); hold on
plot(x1,a(:,4),'k'); hold on
plot(x1,a(:,5),'c'); hold on
plot(x1,a(:,6),'m'); hold on
hold off
legend('hot-side inlet temp.','hot-side outlet temp.','cold-side inlet temp.','cold-side outlet temp.','hot-side inlet flow','cold-side inlet flow')
xlabel('Time (Hours)')
ylabel('Variable Values')
title('The Raw Signals versus Time')
```

Appendix E

The MATLAB Code Used to Generate Normal Data for Heat Exchanger

```
%% Heat exchanger GMDH data generation model (normal data)
clear all
clf

UA=1/0.015;
k=1.168;
m_h=147;
m_c=54;
C_c=1;
C_h=1;
mc_c=m_c*C_c;
mc_h=m_h*C_h*k;
T_hin=40:0.1:60;
T_cin=20:0.1:30;

for ii=1:length(T_hin)
for jj=1:90
T_hout0(ii,jj)=T_hin(ii)*(1-0.01*jj);
end
end

for ii=1:length(T_cin)
for jj=1:180
T_cout0(ii,jj)=T_cin(ii)*(1+0.01*jj);
end
end
[m1 n1]=size(T_hout0);
[m2 n2]=size(T_cout0);

for i=1:length(T_hin)
      for j=1:length(T_cin)
            dd0=160;
            for jj=1:n1
```

```
            for kk=1:n2
                ka=T_hout0(i,jj)-T_cout0(j,kk);
            if(ka>0)
                ke=(T_hin(i)-T_cin(j))/ka;
            if (ke~=1)
            aa=UA*(T_hin(i)-T_cin(j)-T_hout0(i,jj)+T_cout0(j,kk))/log(ke);
            cc=mc_c*(T_cout0(j,kk)-T_cin(j));
            hh=mc_h*(-T_hout0(i,jj)+T_hin(i));
            tt=abs(aa-cc);
            ss=abs(aa-hh);
            dd=tt+ss;
            if (dd<=dd0)
                dd0=dd;
                mm=jj;
                nn=kk;
            end
            end
            end
            end
            end
            T_hout(i,j)=T_hout0(i,mm);
            T_cout(i,j)=T_cout0(j,nn);
        end
end

figure(1)
surf(T_cin,T_hin,T_hout)
xlabel('Tcin')
ylabel('Thin')
zlabel('Thout')
title('The Hot-side Outlet Temperature (generated data by model)')
figure(2)
surf(T_cin,T_hin,T_cout)
xlabel('Tcin')
ylabel('Thin')
zlabel('Tcout')
title('The Cold-side Outlet Temperature (generated data by model)')
save data_HX_Temp T_cin T_hin T_cout T_hout
%
[mt1,nt1]=size(T_hin);
```

```
[mt2,nt2]=size(T_cin);
[mt3,nt3]=size(T_hout);
[mt4,nt4]=size(T_cout);

for i=1:nt1
for j=1:nt2
TT_hin((i-1)*nt2+j)=T_hin(i);
TT_cin((i-1)*nt2+j)=T_cin(j);
TT_hout((i-1)*nt2+j)=T_hout(i,j);
TT_cout((i-1)*nt2+j)=T_cout(i,j);
end
end
save data_HX_TT TT_cin TT_hin TT_cout TT_hout
```

Appendix F

The MATLAB Code for Monitoring and Diagnosis of Fouling in the Heat Exchanger Using GMDH Method

```
%% THe MATLAB Code for GMDH Monitoring of Heat Exchanger fouling
clear all
clf
load data_HX_FILT
data=data1;
[m,n]=size(data);
aa=10;
data_exp=[data(1:aa:m,1) data(1:aa:m,3) data(1:aa:m,2) data(1:aa:m,4)];
%plot(data_exp)
load data_HX_TT
% Divide the transient data into traning set and test set.
% Odd data comprise the training set
% Even data comprise the testing set
data=[TT_hin' TT_cin' TT_hout' TT_cout'];
[m,n]=size(data);
data=data+data.*0.05.*rand(m,4);
save ddd data data_exp
[m,n]=size(data);
ind1=find(rem([1:m],2)==1);
ind2=find(rem([1:m],2)~=1);
Train_data=data(ind1,:);
Test_data=data(ind2,:);
[trndata,mean_val,std_val]=zscore2(Train_data);
[testdata,mean_val,std_val]=zscore2(Test_data,mean_val,std_val);
[pred_data,mean_val,std_val]=zscore2(data_exp,mean_val,std_val);
%%%%%%%%%%%%%%%%%%%%%%%%%%%%%%%%%%%%%%%%
% Establising the outlet temperatures as function of inlet temperatures          %
%%%%%%%%%%%%%%%%%%%%%%%%%%%%%%%%%%%%%%%%
global JobCounter MaxPower;
TrainInputData=trndata(:,1:2);
TrainOutputData=trndata(:,3);
```

```
TestInputData=testdata(:,1:2);
TestOutputData=testdata(:,3);
pred_inputdata=pred_data(:,1:2);
cc=size(TrainInputData,2);
if (cc==2)
    TrainInputData=[TrainInputData,TrainInputData(:,1).*TrainInputData(:,2)];
    TestInputData=[TestInputData,TestInputData(:,1).*TestInputData(:,2)];
    pred_inputdata=[pred_inputdata,pred_inputdata(:,1).*pred_inputdata(:,2)];
end
% creating the complete database
x_alldata = [TrainInputData ; TestInputData];
y_alldata = [TrainOutputData ; TestOutputData];
MaxPower = 11;
for JobCounter=1:2^MaxPower-1;
    [Layer,LayerOrder,Coef]
GMDH_PBK(TrainInputData,TrainOutputData,TestInputData,TestOutputData);
    y_pred = ANNt_PBK(x_alldata,Layer,LayerOrder,Coef);
    y_pred1 = unscore(y_pred,mean_val(3),std_val(3));
    error=y_alldata-y_pred; % ytest-yptest;
    MSE=mean((error).^2)
    y_pred = ANNt_PBK(TrainInputData,Layer,LayerOrder,Coef);
    y_pred1 =unscore(y_pred,mean_val(3),std_val(3));
    figure(1);
    TrainOutputData1=unscore(TrainOutputData,mean_val(3),std_val(3));
    bb=[1:length(TrainOutputData1)];
    plot(bb,TrainOutputData1,'ro')
    grid
    axis([0 max(bb) 0 70]);
    hold
    plot(bb,y_pred1,'b')
    hold
    xlabel('Data Number')
    ylabel ('Temperature')
    legend('Training Output','GMDH Prediction')
    hold off
    figure(2)
    TestOutputData1=unscore(TestOutputData,mean_val(3),std_val(3));
    bb=[1:length(TestOutputData1)];
    plot(bb,TestOutputData1,'ro')
    grid
```

```
    axis([0 max(bb) 0 70]);
    hold
    y_pred_test = ANNt_PBK(TestInputData,Layer,LayerOrder,Coef);
    y_pred_test1 =unscore(y_pred_test,mean_val(3),std_val(3));
    plot(bb,y_pred_test1,'b')
    hold
    xlabel('Data Point Number')
    ylabel ('Temperature')
    title ('Predicted Versus Real Temperature Using Testing Data')
    legend('Testing Output','GMDH Prediction')
    hold off
    error=TestOutputData-y_pred_test ;
    MSE1=mean((error).^2)
    figure(3)
    err=abs(TrainOutputData-y_pred)./TrainOutputData*100;
    plot(err)
    grid
    axis([0 length(err) 1.2*min(err) 1.2*max(err)]);
    xlabel('Data Point Number')
    ylabel ('Error(%)')
    title('Temperature - Percentage of Error between Prediction and Training Data')
    if(MSE<=4e-2 & MSE1<=4e-2)
      JC1_best=JobCounter
    break
    end
end
  y_pred = ANNt_PBK(pred_inputdata,Layer,LayerOrder,Coef);
  y_pred1 =unscore(y_pred,mean_val(3),std_val(3));
  res=data_exp(:,3)-y_pred1;
  size(res)
  figure(4)
  bb=[1:length(y_pred1)];
  plot(y_pred1,'r')
  grid
  axis([0 length(y_pred1) -10 70]);
  hold on
  plot(data_exp(:,3),'b')
  hold on
  plot(res,'g')
  xlabel('Data Point Number')
```

```
 ylabel ('Temperature (C)')
 title ('The Heat Exchanger Hot-side Outlet Temperature')
 legend('GMDH Predicted Temperature without Fouling', 'Experimental Results with
Fouling','Residual=Measurement-Prediction')
 hold off
 figure(9)
 plot(res,'r')
 grid
 axis([0 length(res) -0.5 2])
 xlabel('Data Point Number')
 ylabel ('Temperature Residual (C)')
 title ('Residual of the Heat Exchanger Hot-side Outlet Temperature')
%%%%%%%%%%%%%%%%%%%%%%%%%%
clear all
load ddd
[m,n]=size(data);
ind1=find(rem([1:m],2)==1);
ind2=find(rem([1:m],2)~=1);
Train_data=data(ind1,:);
Test_data=data(ind2,:);
[trndata,mean_val,std_val]=zscore2(Train_data);
[testdata,mean_val,std_val]=zscore2(Test_data,mean_val,std_val);
[pred_data,mean_val,std_val]=zscore2(data_exp,mean_val,std_val);
global JobCounter MaxPower;
TrainInputData=trndata(:,1:2);
TrainOutputData=trndata(:,4);
TestInputData=testdata(:,1:2);
TestOutputData=testdata(:,4);
pred_inputdata=pred_data(:,1:2);
cc=size(TrainInputData,2);
if (cc==2)
    TrainInputData=[TrainInputData,TrainInputData(:,1).*TrainInputData(:,2)];
    TestInputData=[TestInputData,TestInputData(:,1).*TestInputData(:,2)];
    pred_inputdata=[pred_inputdata,pred_inputdata(:,1).*pred_inputdata(:,2)];
end
x_alldata = [TrainInputData ; TestInputData];
y_alldata = [TrainOutputData ; TestOutputData];
MaxPower = 11;
for JobCounter=1:2^MaxPower-1
    [Layer,LayerOrder,Coef]=
```

```
GMDH_PBK(TrainInputData,TrainOutputData,TestInputData,TestOutputData);
    y_pred = ANNt_PBK(x_alldata,Layer,LayerOrder,Coef);
    y_pred1 = unscore(y_pred,mean_val(4),std_val(4));
    error=y_alldata-y_pred;
    MSE=mean((error).^2)
    y_pred = ANNt_PBK(TrainInputData,Layer,LayerOrder,Coef);
    y_pred1 =unscore(y_pred,mean_val(4),std_val(4));
    figure(5);
    grid
    TrainOutputData1=unscore(TrainOutputData,mean_val(4),std_val(4));
    bb=[1:length(TrainOutputData1)];
    plot(bb,TrainOutputData1,'ro')
    grid
    axis([0 max(bb) 0 70]);
    hold
    plot(bb,y_pred1,'b')
    hold
    xlabel('Data Number')
    ylabel ('Temperature')
    legend('Training Output','GMDH Prediction')
    hold off
    figure(6)
    TestOutputData1=unscore(TestOutputData,mean_val(4),std_val(4));
    bb=[1:length(TestOutputData1)];
    plot(bb,TestOutputData1,'ro')
    grid
    axis([0 max(bb) 0 70]);
    hold
    y_pred_test = ANNt_PBK(TestInputData,Layer,LayerOrder,Coef);
    y_pred_test1 =unscore(y_pred_test,mean_val(4),std_val(4));
    plot(bb,y_pred_test1,'b')
    hold
    xlabel('Data Point Number')
    ylabel ('Temperature')
    title ('Predicted Versus Real Temperature Using Testing Data')
    legend('Testing Output','GMDH Prediction')
    hold off
    error=TestOutputData-y_pred_test ;
    MSE1=mean((error).^2)
    err=abs(TrainOutputData-y_pred)./TrainOutputData*100;
```

```
    figure(7)
    plot(err)
    grid
    axis([0 length(err) 1.2*min(err) 1.2*max(err)]);
    xlabel('Data Point Number')
    ylabel ('Error(%)')
    title('Temperature - Percentage of Error between Prediction and Training Data')
    if(MSE<=4e-2 & MSE1<=4e-2)
     JC2_best=JobCounter
    break
    end
end
 y_pred = ANNt_PBK(pred_inputdata,Layer,LayerOrder,Coef);
 y_pred1 =unscore(y_pred,mean_val(4),std_val(4));
 res=data_exp(:,4)-y_pred1;
 size(res)
 figure(8)
 plot(y_pred1,'r')
 axis([0 length(res) -10 60]);
 grid
 hold on
 plot(data_exp(:,4),'b')
 hold on
 plot(res,'g')
 xlabel('Data Point Number')
 ylabel ('Temperature (C)')
 title ('The Heat Exchanger Cold-side Outlet Temperature')
 legend('GMDH Predicted Temperature without Fouling', 'Experimental Results with
Fouling','Residual=Measurement-Prediction')
 hold off
 figure(10)
 plot(abs(res),'r')
 axis([0 length(res) 0 6]);
 grid
 xlabel('Data Point Number')
 ylabel ('Temperature Residual (C)')
 title ('Absolute Residual of the Heat Exchanger Cold-side Outlet Temperature')
```

Appendix G

The MATLAB Code for Monitoring and Diagnosis of Fouling in the Steam Generator Using GMDH Method

```
% THe MATLAB Code for GMDH monitoring of UTSG fouling
clear all
clf
load data_SG_fouling
ind=find(N_tube==3388);
data_exp=[Tpi_s(ind) N_tube(ind) P_s(ind)];
%data_exp=data_exp(1:25,:);
figure(50)
plot(RRf(1:25))
grid
title('Fouling Thermal Resistance')
xlabel('Data Point Number')
ylabel('Fouling Thermal Resistance (s.ft^2^oF/Btu)')

load data_SG_normal
% Divide the transient data into traning set and test set.
% Odd data comprise the training set
% Even data comprise the testing set

data=[Tpi_s N_tube P_s];
[m,n]=size(data);
data=data+data.*0.001.*rand(m,3);
%save ddd data data_exp
[m,n]=size(data);
ind1=find(rem([1:m],2)==1);
ind2=find(rem([1:m],2)~=1);
Train_data=data(ind1,:);
Test_data=data(ind2,:);
[trndata,mean_val,std_val]=zscore2(Train_data);
[testdata,mean_val,std_val]=zscore2(Test_data,mean_val,std_val);
[pred_data,mean_val,std_val]=zscore2(data_exp,mean_val,std_val);
```

```
global JobCounter MaxPower;
TrainInputData=trndata(:,1:2);
TrainOutputData=trndata(:,3);
TestInputData=testdata(:,1:2);
TestOutputData=testdata(:,3);
pred_inputdata=pred_data(:,1:2);
cc=size(TrainInputData,2);
if (cc==2)
    TrainInputData=[TrainInputData,TrainInputData(:,1).*TrainInputData(:,2)];
    TestInputData=[TestInputData,TestInputData(:,1).*TestInputData(:,2)];
    pred_inputdata=[pred_inputdata,pred_inputdata(:,1).*pred_inputdata(:,2)];
end
% creating the complete database
x_alldata = [TrainInputData ; TestInputData];
y_alldata = [TrainOutputData ; TestOutputData];
MaxPower = 11;
for JobCounter=1:2^MaxPower-1;
    [Layer,LayerOrder,Coef] =
GMDH_PBK(TrainInputData,TrainOutputData,TestInputData,TestOutputData);
    y_pred = ANNt_PBK(x_alldata,Layer,LayerOrder,Coef);
    y_pred1 = unscore(y_pred,mean_val(3),std_val(3));
    error=y_alldata-y_pred;
    MSE=mean((error).^2)
    y_pred = ANNt_PBK(TrainInputData,Layer,LayerOrder,Coef);
    y_pred1 =unscore(y_pred,mean_val(3),std_val(3));
    figure(1);
    TrainOutputData1=unscore(TrainOutputData,mean_val(3),std_val(3));
    bb=[1:length(TrainOutputData1)];
    plot(bb,TrainOutputData1,'ro')
    grid
    axis([0 max(bb) 720 920]);
    hold on
    plot(bb,y_pred1,'b')
    hold on
    xlabel('Data Point Number')
    ylabel ('Steam Pressure (Psi)')
    legend('Training Output','GMDH Prediction')
    hold off
    figure(2)
    TestOutputData1=unscore(TestOutputData,mean_val(3),std_val(3));
```

```
    bb=[1:length(TestOutputData1)];
    plot(bb,TestOutputData1,'ro')
    grid
    axis([0 max(bb) 720 920]);
    hold on
    y_pred_test = ANNt_PBK(TestInputData,Layer,LayerOrder,Coef);
    y_pred_test1 =unscore(y_pred_test,mean_val(3),std_val(3));
    plot(bb,y_pred_test1,'b')
    hold on
    xlabel('Data Point Number')
    ylabel ('Steam Pressure (Psi)')
    title ('Predicted Versus Real Steam Pressure Using Testing Data')
    legend('Testing Output','GMDH Prediction')
    hold off

    error=TestOutputData-y_pred_test ;
    MSE1=mean((error).^2)

    figure(3)
    err=abs(TrainOutputData-y_pred)./TrainOutputData*100;
    plot(err)
    grid
    axis([0 length(err) 1.2*min(err) 1.2*max(err)]);
    xlabel('Data Point Number')
    ylabel ('Error(%)')
    title('Steam Pressure - Percentage of Error between Prediction and Training Data')
    if(MSE<=4e-2 & MSE1<=4e-2)
      JC1_best=JobCounter
    break
    end
end

 y_pred = ANNt_PBK(pred_inputdata,Layer,LayerOrder,Coef);
 y_pred1 =unscore(y_pred,mean_val(3),std_val(3));
 res=y_pred1-data_exp(:,3);
 size(res);
 figure(4)
 bb=[1:length(y_pred1)];
 plot(y_pred1,'r')
 grid
```

```
  axis([0 length(y_pred1) -40 1000]);
  hold on
  plot(data_exp(:,3),'b')
  hold on
  plot(res,'g')
  xlabel('Data Point Number')
  ylabel ('Steam Pressure (Psi)')
  title ('Steam Pressure')
  legend('GMDH Predicted Steam Pressure without Fouling', 'Model Simulation with
Fouling','Residual=GMDH Prediction-SG Model Simulation')
  hold off
  figure(5)
  plot(res,'r')
  grid
  axis([0 length(res) -2 90])
  xlabel('Data Point Number')
  ylabel ('Steam Pressure (Psi)')
  title ('Residual of the Steam Pressure')
  legend('Residual=GMDH Prediction-SG Model Simulation')
%%%%%%%%%%%%%%%%%%%%%%%%%%%%%%%%%%%%
clear all
load data_SG_fouling
ind=find(RRf==0);
data_exp=[Tpi_s(ind) N_tube(ind) P_s(ind)];
indd=find(data_exp(:,1)==592.5);
data_exp=data_exp(indd,:);

load data_SG_normal
% Divide the transient data into traning set and test set.
% Odd data comprise the training set
% Even data comprise the testing set
%ind=find(N_tube==3388);
data=[Tpi_s N_tube P_s];
[m,n]=size(data);
data=data+data.*0.001.*rand(m,3);
%save ddd data data_exp
[m,n]=size(data);
ind1=find(rem([1:m],2)==1);
ind2=find(rem([1:m],2)~=1);
Train_data=data(ind1,:);
```

```
Test_data=data(ind2,:);
[trndata,mean_val,std_val]=zscore2(Train_data);
[testdata,mean_val,std_val]=zscore2(Test_data,mean_val,std_val);
[pred_data,mean_val,std_val]=zscore2(data_exp,mean_val,std_val);
global JobCounter MaxPower;
TrainInputData=trndata(:,1:2);
TrainOutputData=trndata(:,3);
TestInputData=testdata(:,1:2);
TestOutputData=testdata(:,3);
pred_inputdata=pred_data(:,1:2);
cc=size(TrainInputData,2);
if (cc==2)
    TrainInputData=[TrainInputData,TrainInputData(:,1).*TrainInputData(:,2)];
    TestInputData=[TestInputData,TestInputData(:,1).*TestInputData(:,2)];
    pred_inputdata=[pred_inputdata,pred_inputdata(:,1).*pred_inputdata(:,2)];
end
% creating the complete database
x_alldata = [TrainInputData ; TestInputData];
y_alldata = [TrainOutputData ; TestOutputData];
MaxPower = 11;
for JobCounter=1:2^MaxPower-1;
    [Layer,LayerOrder,Coef] =
GMDH_PBK(TrainInputData,TrainOutputData,TestInputData,TestOutputData);
    y_pred = ANNt_PBK(x_alldata,Layer,LayerOrder,Coef);
    y_pred1 = unscore(y_pred,mean_val(3),std_val(3));
    error=y_alldata-y_pred;
    MSE=mean((error).^2)
    y_pred = ANNt_PBK(TrainInputData,Layer,LayerOrder,Coef);
    y_pred1 =unscore(y_pred,mean_val(3),std_val(3));
    figure(6);
    TrainOutputData1=unscore(TrainOutputData,mean_val(3),std_val(3));
    bb=[1:length(TrainOutputData1)];
    plot(bb,TrainOutputData1,'ro')
    grid
    axis([0 max(bb) 720 920]);
    hold on
    plot(bb,y_pred1,'b')
    hold on
    xlabel('Data Point Number')
    ylabel ('Steam Pressure (Psi)')
```

```
    legend('Training Output','GMDH Prediction')
    hold off
    figure(7)
    TestOutputData1=unscore(TestOutputData,mean_val(3),std_val(3));
    bb=[1:length(TestOutputData1)];
    plot(bb,TestOutputData1,'ro')
    grid
    axis([0 max(bb) 720 920]);
    hold on
    y_pred_test = ANNt_PBK(TestInputData,Layer,LayerOrder,Coef);
    y_pred_test1 =unscore(y_pred_test,mean_val(3),std_val(3));
    plot(bb,y_pred_test1,'b')
    hold on
    xlabel('Data Point Number')
    ylabel ('Steam Pressure (Psi)')
    title ('Predicted Versus Real Steam Pressure Using Testing Data')
    legend('Testing Output','GMDH Prediction')
    hold off
    error=TestOutputData-y_pred_test ;
    MSE1=mean((error).^2)
    figure(8)
    err=abs(TrainOutputData-y_pred)./TrainOutputData*100;
    plot(err)
    grid
    axis([0 length(err) 1.2*min(err) 1.2*max(err)]);
    xlabel('Data Point Number')
    ylabel ('Error(%)')
    title('Steam Pressure - Percentage of Error between Prediction and Training Data')
    if(MSE<=4e-2 & MSE1<=4e-2)
    JC1_best=JobCounter
    break
    end
end
 y_pred = ANNt_PBK(pred_inputdata,Layer,LayerOrder,Coef);
 y_pred1 =unscore(y_pred,mean_val(3),std_val(3));
 res=y_pred1-data_exp(:,3);
 size(res);
 figure(9)
 bb=[1:length(y_pred1)];
 plot(y_pred1,'r')
```

```
grid
axis([0 length(y_pred1) -40 1000]);
hold on
plot(data_exp(:,3),'b')
hold on
plot(res,'g')
xlabel('Data Point Number')
ylabel ('Steam Pressure (Psi)')
title ('Steam Pressure')
legend('GMDH Predicted Steam Pressure with Continuous Decrease in Number of Tubes', 'Model Simulation with Continuous Decrease in Number of Tubes','Residual=GMDH Prediction-SG Model Simulation')
hold off
figure(10)
plot(res,'r')
grid
axis([0 length(res) -6 0])
xlabel('Data Point Number')
ylabel ('Steam Pressure (Psi)')
title ('Residual of the Steam Pressure')
legend('Residual=GMDH Prediction-SG Model Simulation')
```

Vita

Xuedong Huang was born in Suining, Sichuan Province, China on June 2, 1967. In 1982 he moved to Dazhou in the same province and graduated from the high school in 1984. Then he entered the Energy and Power Engineering Department of Xi'an Jiao Tong University, and majored in Nuclear Engineering. He received the BS degree in July 1988. Then he continued his graduate studies there and received the MS degree in 1991. Following the graduation, he joined the Nuclear Power Institute of China and worked there mainly on reliability engineering, maintainability engineering, and probabilistic risk assessment for ten years. In April 1998, he went to GRS Germany as a visiting scholar and worked there for six months. In July 2001, he entered the Master of Science program of Nuclear Engineering Department at the University of Tennessee, Knoxville. He is currently a graduate research assistant at UTK-NE and working on a DOE-NEER project. During this thesis study, he has published three papers in scientific society meetings.